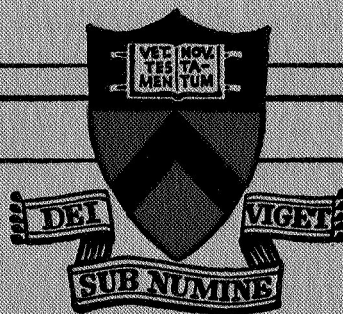


Prepared for  
National Aeronautics  
and Space Administration

PULSED ELECTROMAGNETIC GAS ACCELERATION  
NGL 31-001-005  
Supplement No. 7

14th Semi-annual Progress Report  
1 January 1969 to 30 June 1969

Report 634m



CASE FILE  
COPY

PRINCETON UNIVERSITY  
DEPARTMENT OF  
AEROSPACE AND MECHANICAL SCIENCES

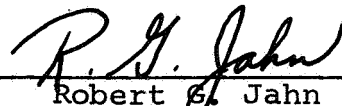
Prepared for  
National Aeronautics  
and Space Administration

PULSED ELECTROMAGNETIC GAS ACCELERATION  
NGL 31-001-005  
Supplement No. 7

14th Semi-annual Progress Report  
1 January 1969 to 30 June 1969

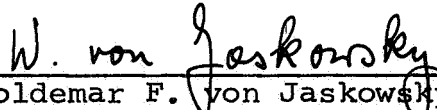
Report 634m

Prepared by:



Robert G. Jahn  
Professor  
and Research Leader

and:



Woldemar F. von Jaskowsky  
Senior Research Engineer  
and Lecturer

Reproduction, translation, publication, use and disposal in  
whole, or in part, by or for the United States Government is  
permitted.

July 1969

School of Engineering and Applied Science  
Department of Aerospace and Mechanical Sciences  
Guggenheim Aerospace Propulsion Laboratories  
PRINCETON UNIVERSITY  
Princeton, New Jersey

## ABSTRACT

Attempts have been made to determine the velocity field in the outflow from a quasi-steady coaxial accelerator by three methods: (a) biased double electrostatic probes to monitor times-of-flight of characteristic portions of the exhaust pulse; (b) gridded ion energy analyzers; and (c)  $\vec{u} \times \vec{B}$  probes. The last has so far yielded little coherent information, but the first two agree on the following picture of the exhaust velocity profile: The initial burst of "snowplowed" plasma is followed, after a brief transition period, by a region of uniform flow of duration corresponding to the driving-current pulse length, and of substantially greater velocity than that of the initiation burst. Hence, this quasi-steady portion of the exhaust pulse tends to telescope into the snowplow region ahead of it, and the entire pulse shortens in flight.

Extension of previous studies on the portion of high-current discharges near anode surfaces continue to indicate the disproportionately large influence of this region on overall discharge characteristics, such as terminal voltage and current density distribution. Similar studies near the cathode indicate that the relative importance of this region depends strongly on discharge geometry. In quasi-steady discharges, a "cathode jet" can be identified, and the current flow fields near it mapped.

Laser probing of the quasi-steady flow in a parallel-plate accelerator permits estimates of the ionic species composition of various portions of the flow, and gives some hint of nonequilibrium excitation and population inversion in certain regimes.

Progress continues on the design, construction, and testing of a 160-kJ capacitor line which will permit operation of various quasi-steady accelerators for pulse times two orders of magnitude greater than previously possible, and which will also provide a multiple pulse capability.

## TABLE OF CONTENTS

	Page
Title Page. . . . .	i
Abstract. . . . .	ii
Table of Contents . . . . .	iii
List of Illustrations . . . . .	iv
Current Student Participation . . . . .	vi
 I. INTRODUCTION. . . . .	 1
II. VELOCITY FIELD DETERMINATION IN QUASI-STEADY ACCELERATORS. . . . .	2
A. Biased Double Electrostatic Probes. . . . .	2
B. Electrostatic Ion Energy Analyzers. . . . .	13
C. $\vec{u} \times \vec{B}$ Probes. . . . .	23
III. ANODE PROCESSES IN HIGH-CURRENT DISCHARGES. . . . .	25
IV. CATHODE JET STUDIES IN A PARALLEL-PLATE GEOMETRY . . . . .	41
V. RADIATIVE PROCESSES IN QUASI-STEADY DISCHARGES . . . . .	54
VI. A 160-KILOJOULE PULSE-FORMING NETWORK FOR QUASI-STEADY ACCELERATORS . . . . .	72
PROJECT REFERENCES. . . . .	78
GENERAL REFERENCES. . . . .	87
APPENDIX A: Semi-annual Statement of Expenditures. . . . .	89



# LIST OF ILLUSTRATIONS

Figure		Page
1	Concentric velocity probe. . . . .	3
2	Diagram of concentric velocity probe circuit .	5
3	Parallel-plate velocity probe. . . . .	6
4	Concentric and parallel-plate probe responses.	8
5	Trajectories of plasma signatures. . . . .	9
6	Convective fluctuations. . . . .	11
7	Experimental velocity profile. . . . .	12
8	Ion probe. . . . .	14
9	Floating potential probe . . . . .	16
10	Circuit for ion probe. . . . .	17
11	Collector current $j_p$ at 9 in. from anode 1 in. off $\phi$ . . . . .	18
12	Ion current $j_+$ at different axial positions. .	20
13	Trajectories of ion current signatures . . . .	21
14	Maximum ion current and ion density on $\phi$ . . .	22
15	Progress of bifurcating current sheet in 100 $\mu$ argon . . . . .	26
16	Oscillograms of current waveform and inner divider voltage. . . . .	27
17	Voltage distribution across chamber at 1 in. radius. . . . .	30
18	Potential distribution across discharge chamber at $r = 1$ ". . . . .	32
19	Arc voltages for different anode insulation. .	33
20	Parallel-plate accelerator . . . . .	35
21	Inner divider records for anode insulation . .	36
22	Resistive voltage drop at 2 $\mu$ sec in parallel-plate accelerator. . . . .	37
23	Inner divider records for cathode insulation .	39
24	Schematic diagram of parallel-plate accel- erator modified for cathode jet studies. . . .	42
25	Probe positioning. . . . .	43
26	Contours of constant magnetic field strength .	46

# LIST OF ILLUSTRATIONS-contd.

Figure		Page
27	Transverse current density $j_y$ . . . . .	47
28	Streamwise current density $j_x$ . . . . .	48
29	Comparison of streamwise and transverse current density. . . . .	49
30	Transverse electric field $E_y$ . . . . .	51
31	Streamwise electron velocity . . . . .	52
32	Enclosed current contours in parallel-plate accelerator . . . . .	55
33	Schematic of experimental apparatus. . . . .	57
34	Intensity of spontaneous emission. . . . .	60
35	Intensity of discharge modified laser output .	61
36	Gain coefficient $\alpha$ for 50 mT ambient argon. .	63
37	Gain coefficient $\alpha$ for 100 mT ambient argon .	64
38	Gain coefficient $\alpha$ for 200 mT ambient argon .	65
39	Spectrograms of 120 kA x 20 $\mu$ sec discharge . .	70
40	Schematic of pulse-forming network . . . . .	73
41	Partial view of pulse-forming network. . . . .	75
42	View of 130 m $\Omega$ electrolytic resistor . . . . .	76

# CURRENT STUDENT PARTICIPATION

<u>Student</u>	<u>Period</u>	<u>Degree</u>	<u>Thesis Topic</u>
BOYLE, Michael J.	1968-1969	B.S.E. Cand.	Plasma Velocity Measurements with Electric Probes
BRUCKNER, Adam P.	1966-	Ph.D. Cand.	Radiation Studies of Gas Accelerating Discharges
CORY, John S.	1969-	Ph.D. Cand.	Velocity Field Determinations in Quasi-steady Accelerators
DI CAPUA, Marco S.	1966-	Ph.D. Cand.	Current-voltage Characteristics of High-current Discharges
OBERTH, Ronald C.	1966-	Ph.D. Cand.	Current Sheet Anode Foot Phenomena
SPRENGEL, Uwe W.	1968-1969	Visiting Scholar	Ion Velocity Measurement in MPD Discharges
TURCHI, Peter J.	1963-	Ph.D. Cand.	Unsteady Plasma Diagnostics

## I. INTRODUCTION

The last three semi-annual reports<sup>56,61,75</sup> have concentrated on the research results from our larger, quasi-steady facilities, somewhat to the exclusion of many of the smaller-scale supporting experiments. While the former continue to yield substantial and exciting information, it seems appropriate in this report to catch up a bit on some of the equally informative work in progress on related topics covered by this program. For this purpose we shall first describe as an example of our instrumentation development a sequence of studies of various methods for determination of velocity fields in plasma streams. Next are presented accounts of research on the near-electrode regions of high-current discharges--both at the anode and cathode--and their influence on the overall discharge behavior. Then follows a description of a program to relate various optical properties of accelerating discharges to their interior details, with particular reference to nonequilibrium population densities and the implications of this to frozen flow losses. Finally, we review the progress on the construction of a 160-kJ capacitor line which will power many of our quasi-steady accelerators in the future.



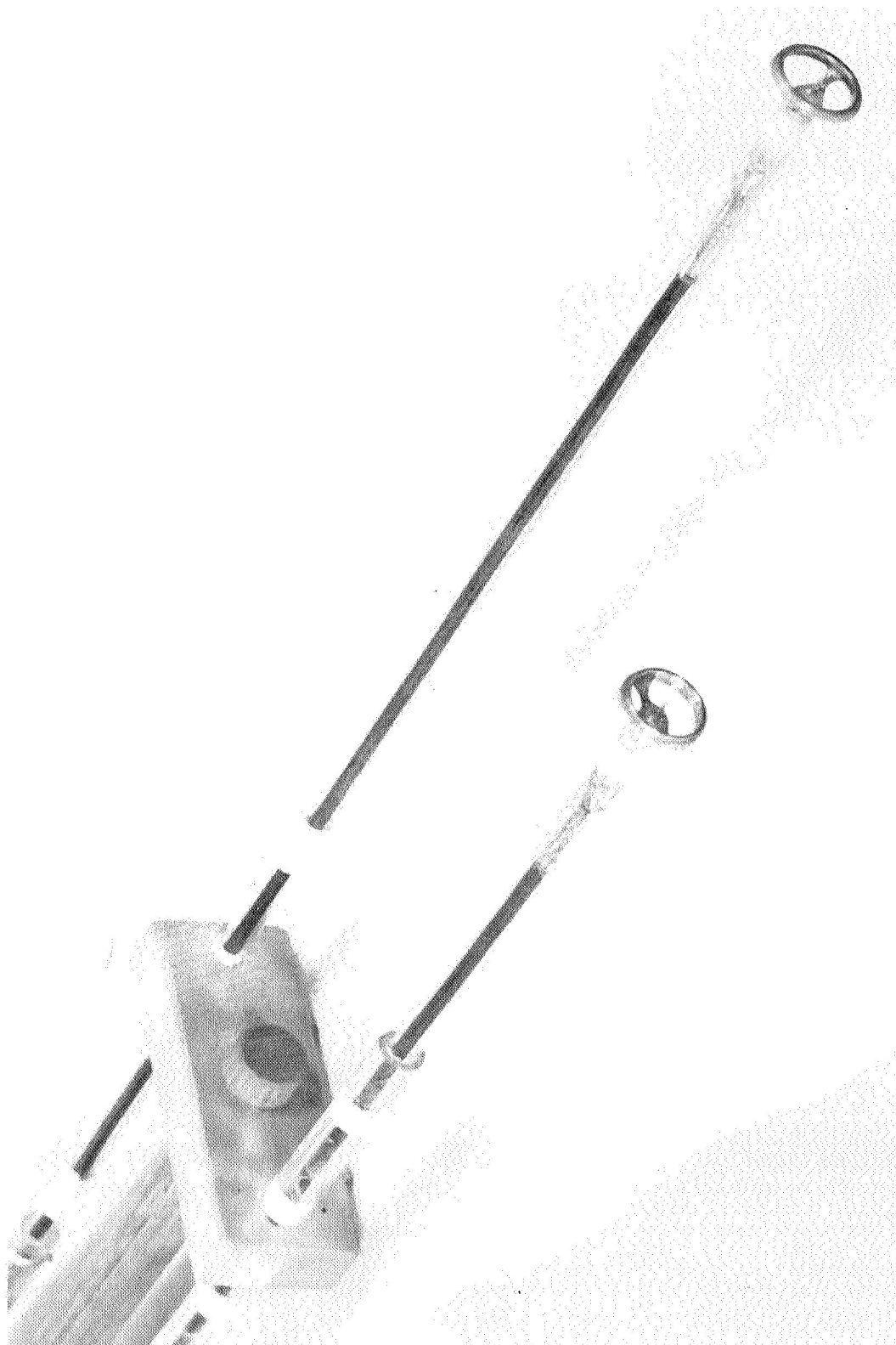
## II. VELOCITY FIELD DETERMINATIONS IN QUASI-STEADY ACCELERATORS

During the present period, a major effort has been undertaken to develop serviceable devices for monitoring the patterns of plasma flow velocity which exist in the discharge and outflow from quasi-steady accelerators. Even in steady flow devices, such as MPD arcs, this is a difficult measurement to achieve with any precision, and in this particular case, the transient nature of our experiments does not work in our favor. For example, the Doppler shift techniques which have proven marginally useful in steady flow arcs, are eliminated here because of inadequate exposure time to obtain the desired spectral resolution. However, of the three electromagnetic techniques which we have attempted, two now show some promise of serviceability for such velocity field measurements:

### A. Biased Double Electrostatic Probes — Boyle

The first approach to the velocity field measurement involves the application of two sets of biased double probes, oriented transversely to the flow, and displaced axially by a known dimension. In their proper domain of operation, such probes conduct an ion saturation current proportional to the local ion density, and hence respond to small intrinsic fluctuations in the plasma stream. Comparison of times-of-arrival of these characteristic fluctuations at the two axial positions then yields ion streaming velocities.

Two geometries of probe have been employed. A coaxial version, shown in Fig. 1, has an outer conductor



CONCENTRIC VELOCITY PROBE

FIGURE 1  
AP25 P300

1.0 cm in diameter and an inner electrode 0.1 cm in diameter, both 0.3 cm in axial width. These are directly attached to a 50 ohm coaxial cable, via which they are connected to the biasing and measurement circuits shown in Fig. 2. In operation the probe and its charged capacitor are isolated from the charging circuit via a triple pole switch. An isolation transformer is necessary to protect the oscilloscope from the main discharge. Frequency response of this circuit was checked with a square wave generator, and the transformer terminators adjusted for no overshoot, 4  $\mu$ sec rise time, and minimum inductance droop.

Although this coaxial probe configuration minimizes electromagnetic pickup, this advantage is overbalanced by a tendency for the probes to short themselves after a few shots, via some degradation of the insulation on the outer probe support structure, and by the partial obstruction the leading probe introduces into the flow over the trailing probe. These difficulties are avoided by conversion to a parallel-plate probe geometry, with the added benefit of a simpler signal interpretation for the equal electrode areas. As shown in Fig. 3, these probes consist of two composite parallel plates, each involving three conducting brass surfaces separated by insulating areas of epoxy. All three plates are maintained at the same bias potential although only the center conducting surfaces are used to extract the signal, thereby minimizing leading edge and field-fringing effects. The supporting structures leave the parallel plates at right angles from the rear of the probe and combine approximately 3 cm away to reduce the flow obstruction and inductive pickup. The biasing and signal leads are led back in 50 ohm coaxial cables through a shielded glass tubing and out of the vacuum tank in Tygon tubing. The circuitry

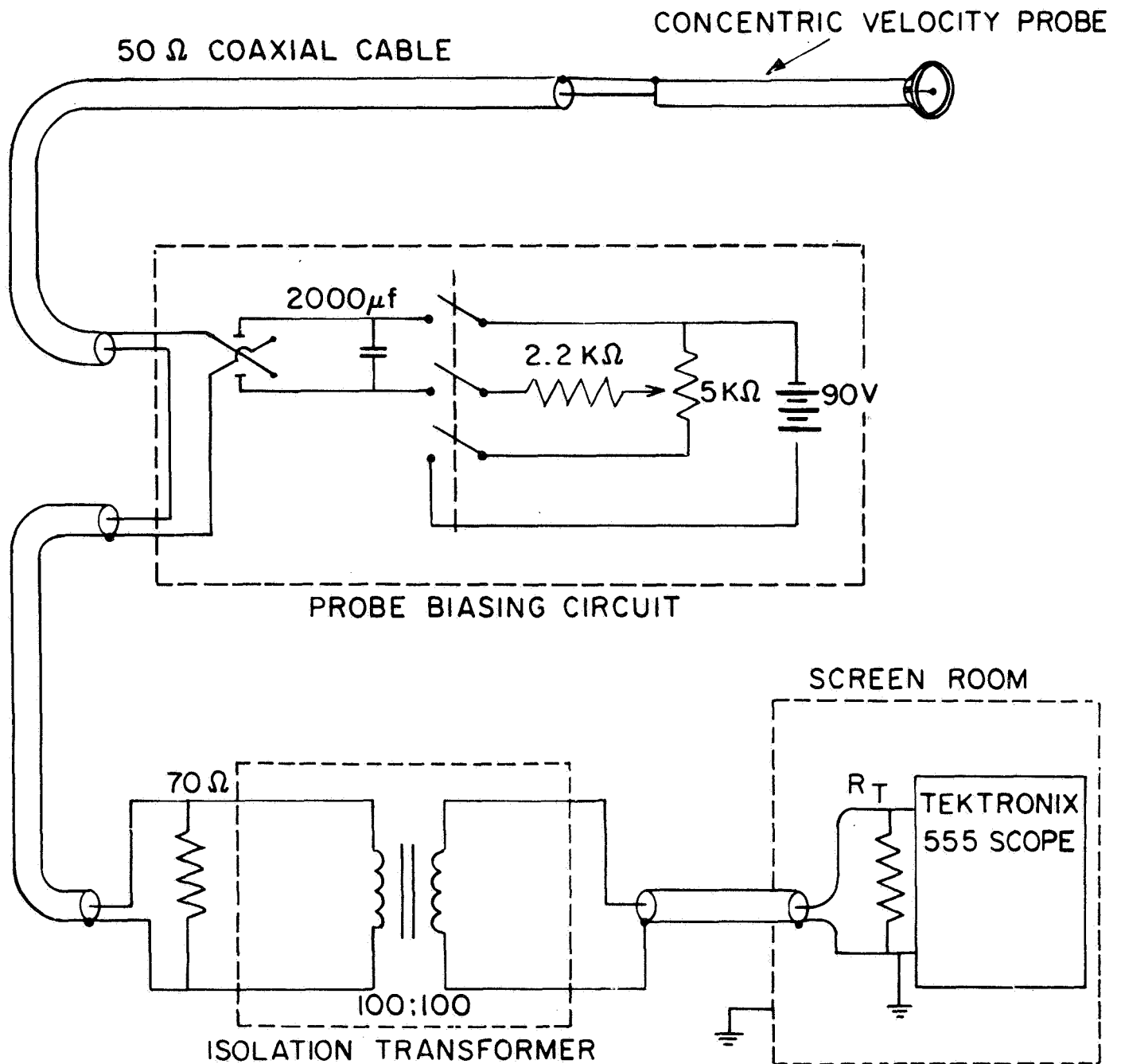
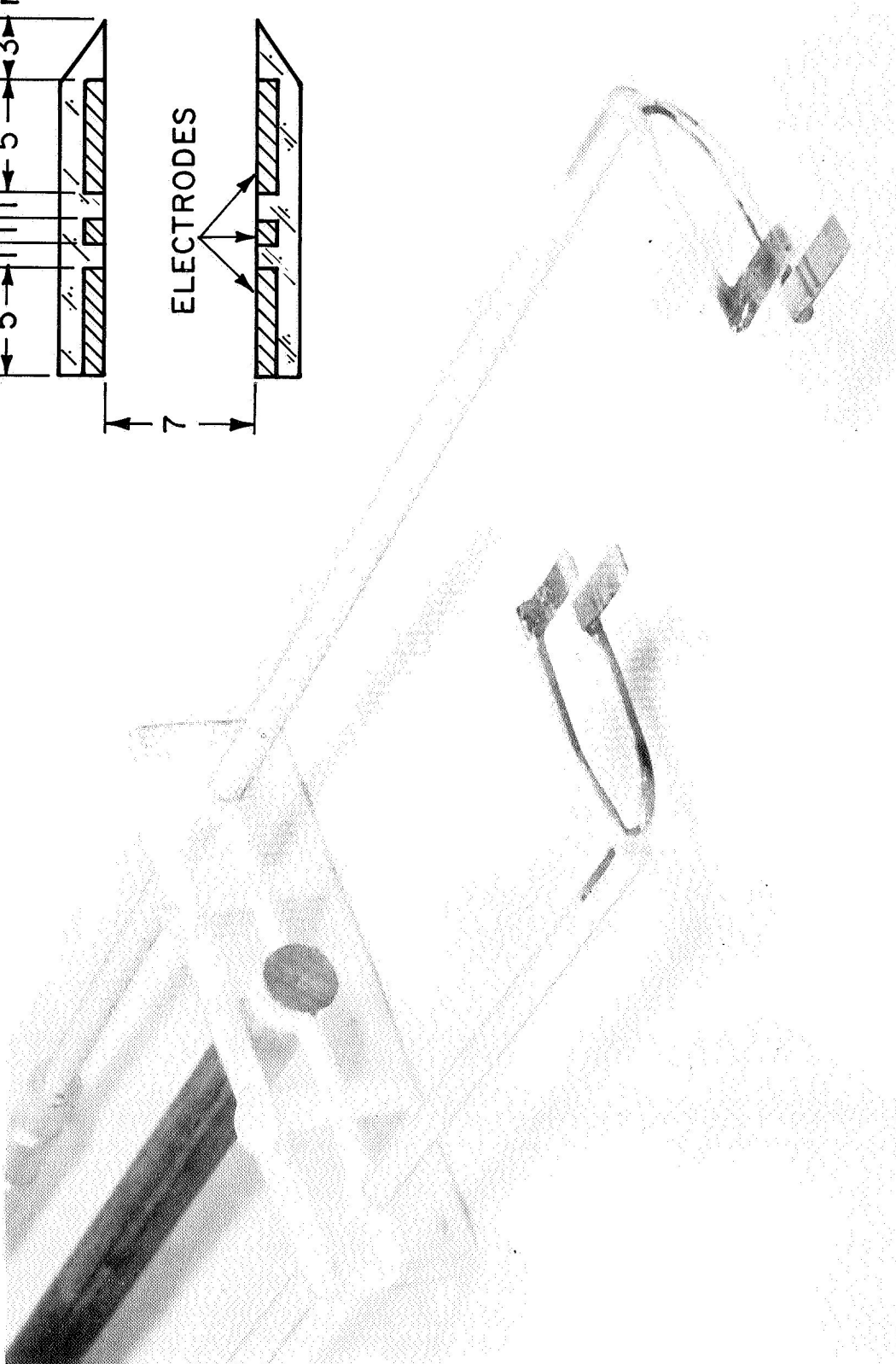
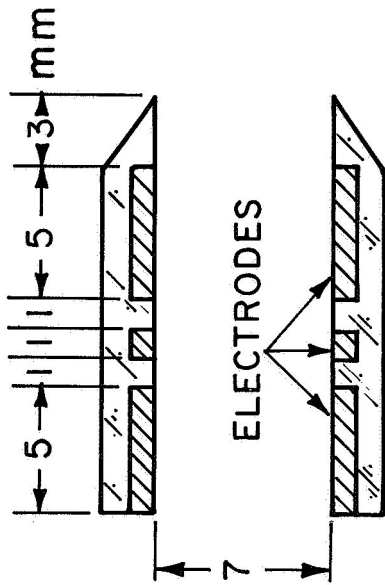


DIAGRAM OF CONCENTRIC VELOCITY PROBE CIRCUIT





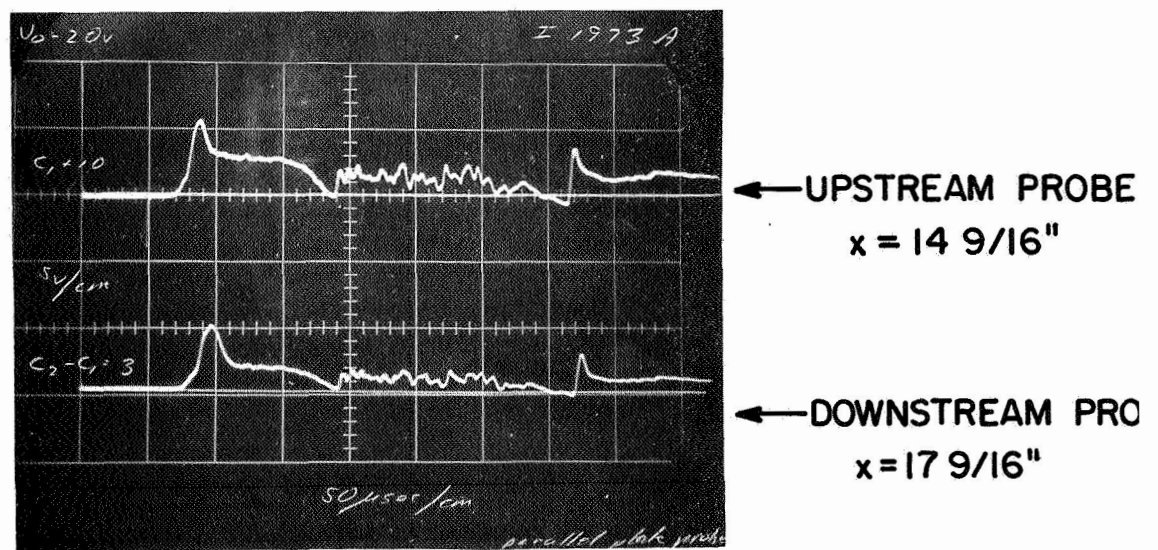
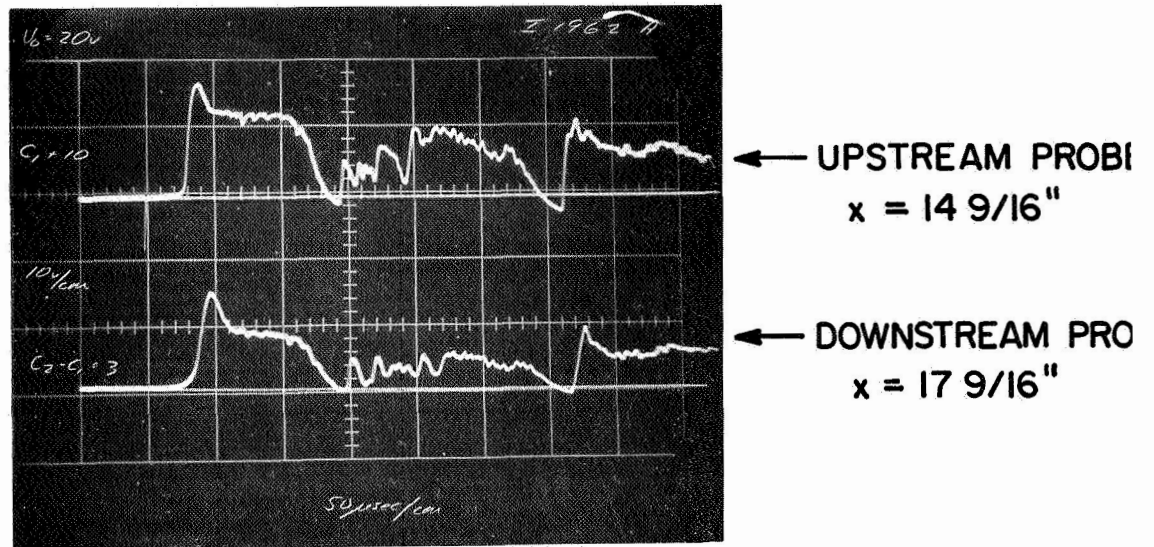
PARALLEL PLATE VELOCITY PROBE

FIGURE 3  
AP25 P301

is the same as used with the concentric probes, with the addition of two capacitors which separately maintain the compensating conducting surfaces at the same bias potential as that of the middle signal surfaces.

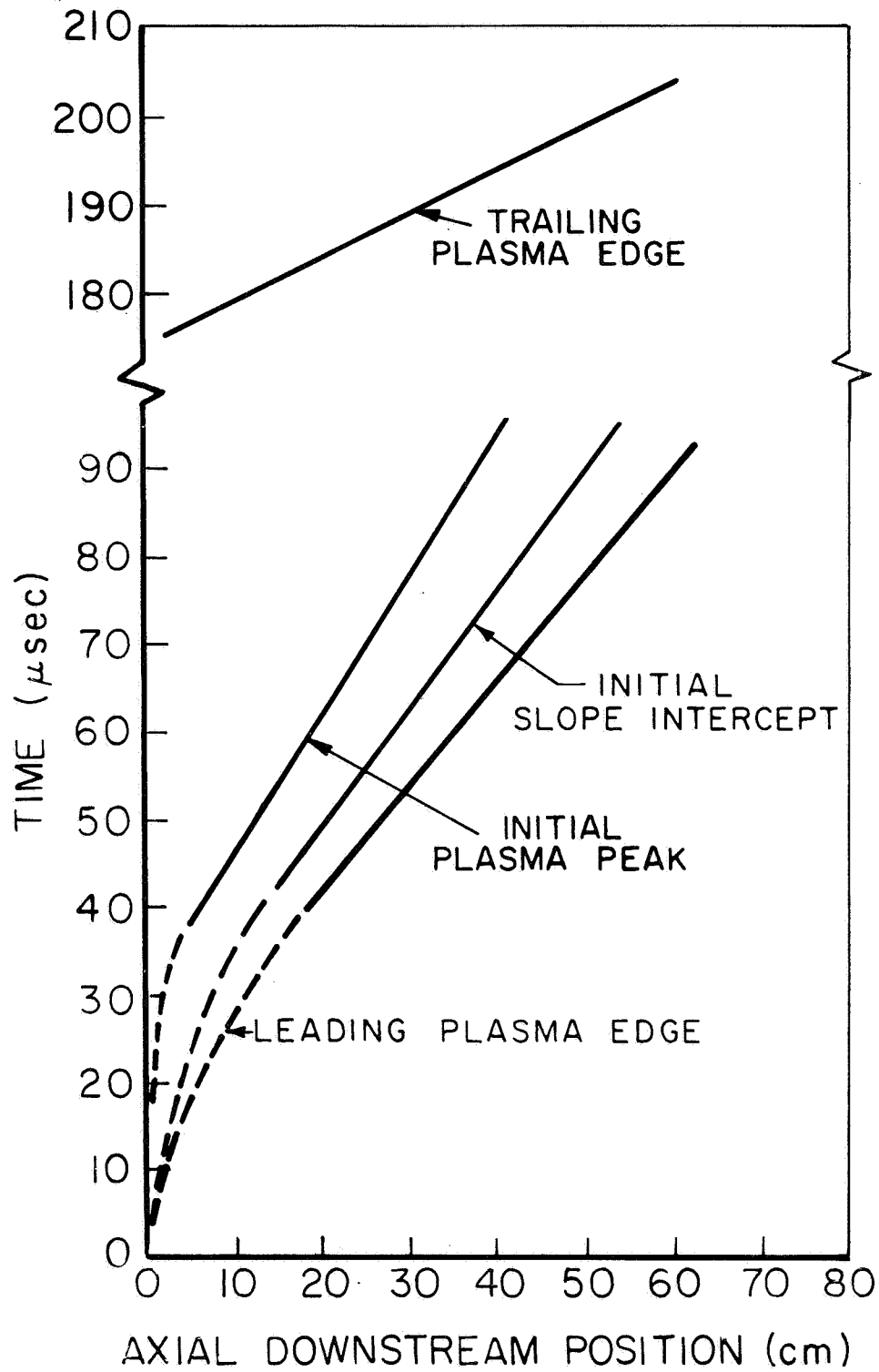
Figure 4 displays responses of pairs of probes of both types, at the same position in a given flow. Clearly, there is little to choose between them in terms of the character of the signature, and hence the bulk of the studies to date have used the somewhat more convenient parallel-plate arrangement.

The traces of Fig. 4 actually cover nearly three half cycles of the driving-current waveform. Note that the first and third pulses, for which the normal central cathode polarity of the accelerator prevails, are quite similar; the reverse polarity pulse yields a badly distorted waveform. Confining attention to the normal pulses, these may be considered to consist of a succession of characteristic signals, associated with successive phases of the flow: a sharp leading edge and initial peak, associated with the passage of the initial snowplowed plasma; a declining phase related to the transition of the flow; a plateau indicative of the quasi-steady region, and a fall off at pulse reversal. Relying on shot-to-shot reproducibility of the accelerator, one can readily plot time of arrival of various portions of the signature vs. axial position and thereby extract velocity histories. Figure 5 presents such data for the initial signal edge, the first peak, and the trailing edge, from which terminal velocities of 0.8, 0.6, and  $2.2 \times 10^4$  m/sec, respectively, are extracted. Some indication of the acceleration profile can also be derived from these, particularly the initial slope intercept data, which shows velocity growing for some 5 - 10 cm downstream of the



## CONCENTRIC AND PARALLEL PLATE PROBE RESPONSES

FIGURE 4  
 AP25 P 263



TRAJECTORIES OF PLASMA SIGNATURES

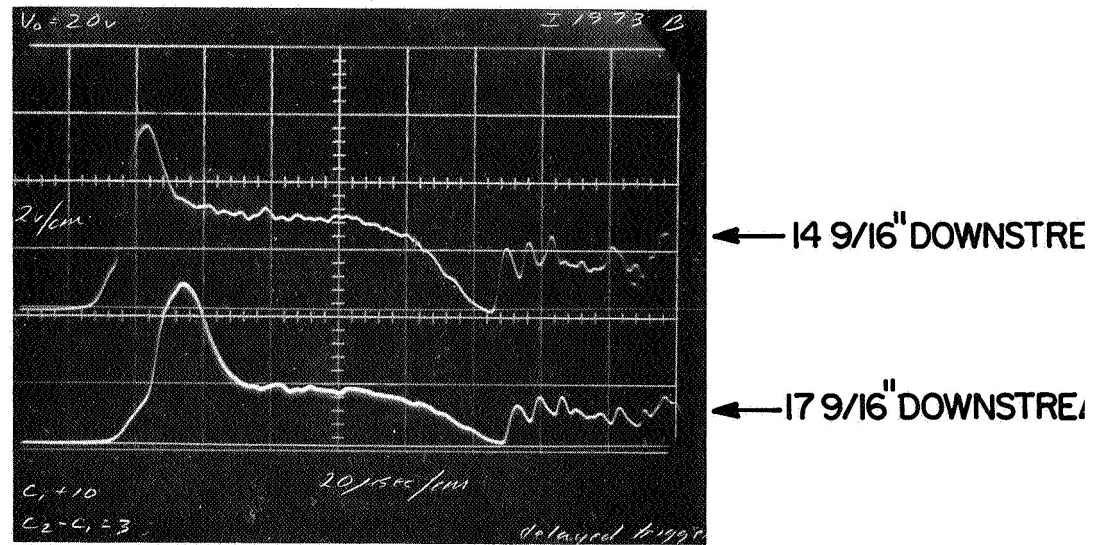


anode plane, consistent with the known extension of the discharge current.<sup>76,80,75</sup>

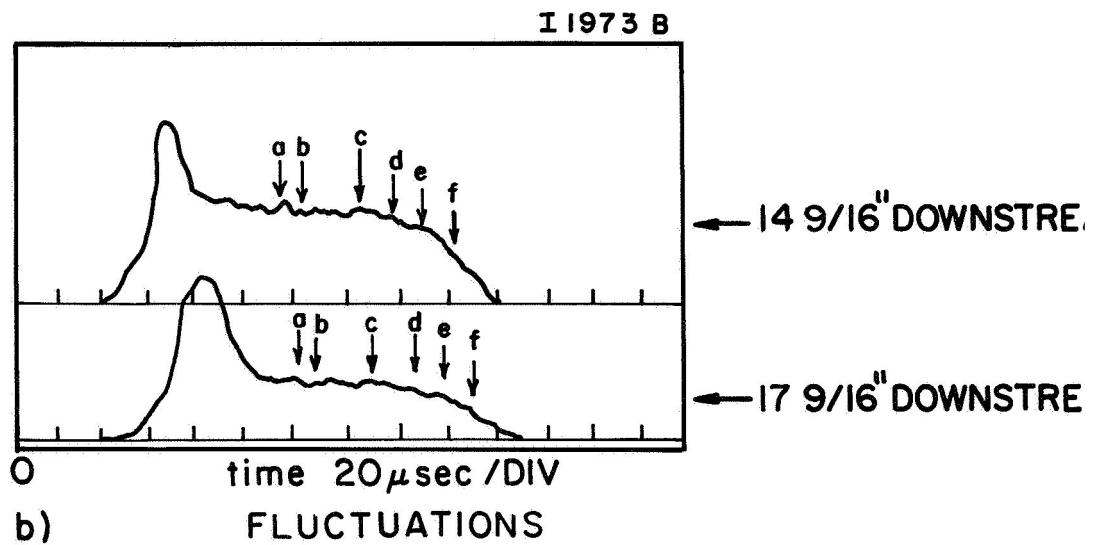
This comparatively high velocity of the trailing edge of the plasma pulse is provocative, particularly since this would seem to bear on the quasi-steady portion of the flow. Attention was thus focused on the fine-scale comparison of signals from two probes displaced axially 3 in., with particular reference to small characteristic fluctuations in the quasi-steady plateau portion of the signatures. Typical traces are shown in Fig. 6 with a schematic, annotated copy below. Each of the lettered elements can be identified in each trace, and thereby a virtually continuous record of velocity in this regime is available. The result is again striking: namely, the flow velocity in this quasi-steady portion, like the trailing edge, is substantially higher than that of the initial plasma burst, specifically about  $2.5 \times 10^4$  m/sec compared to 0.8 m/sec. Figure 7 is an attempt to display the velocity profile along the plasma pulse, compared to its local density.

The results of these experiments, described in detail in Ref. 82, are far from complete, but nevertheless provide convincing semi-quantitative evidence that the quasi-steady portion of the operation is highly effective at accelerating the injected gas flow, even more so than the classical snowplow initiation phase. The numerical magnitude of the quasi-steady velocities found by this technique are in good agreement with those predicted for steady MPD operation at this current and mass flow,<sup>76</sup> giving further assurance that the accelerator is functioning in the proper electromagnetic fashion.

Experiments are currently in progress to refine this



a) EXPERIMENTAL TRACE



b) FLUCTUATIONS

## CONVECTIVE FLUCTUATIONS

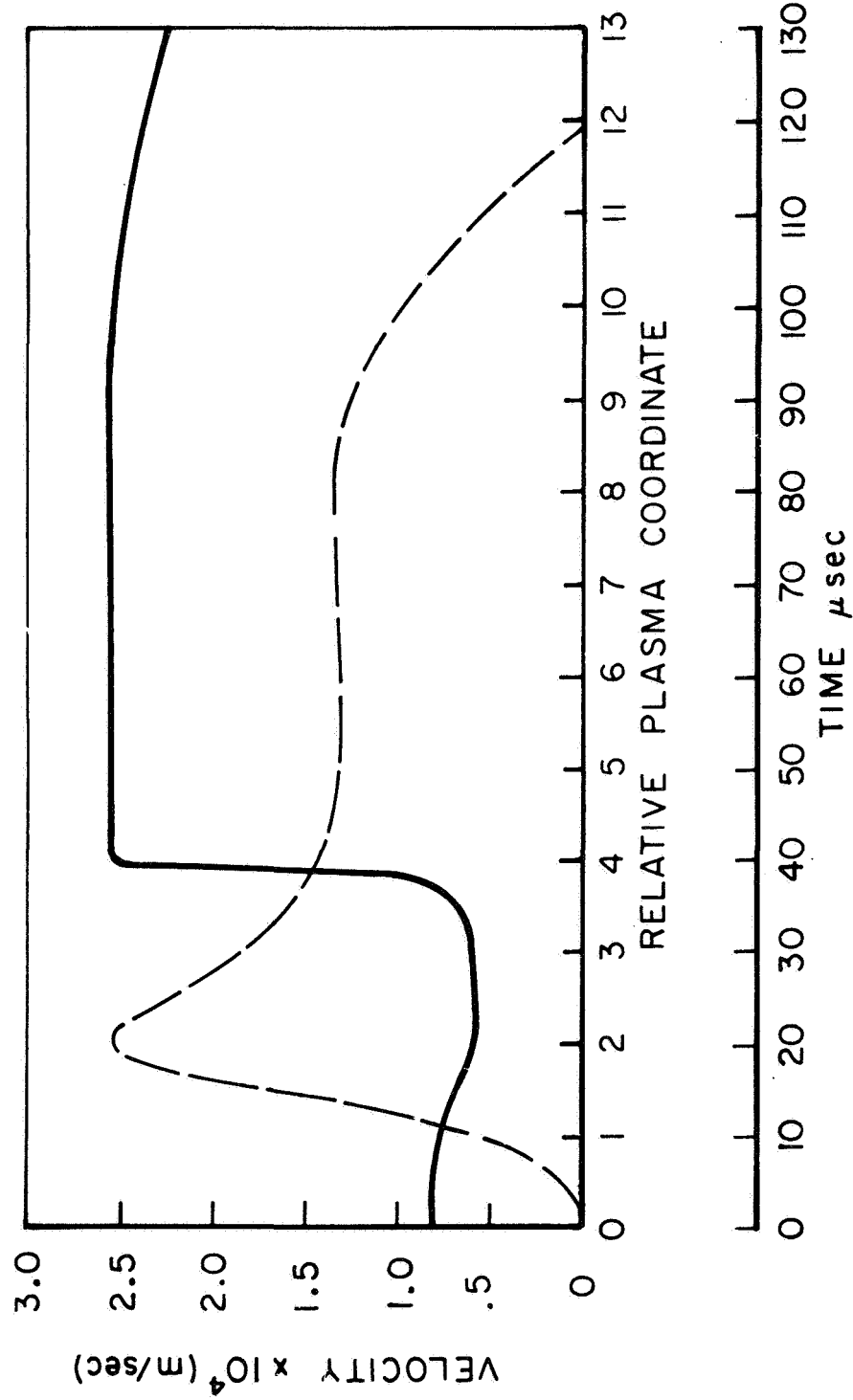


FIGURE 7  
AP 25-4507

EXPERIMENTAL VELOCITY PROFILE  
AXIAL POSITION 14 9/16"

technique, including attempts to impose more precise markers on the flow by an auxiliary upstream spark or other electromagnetic method. When completely serviceable, the probes will be employed for a systematic mapping of the full velocity fields for a variety of accelerator conditions.

#### B. Electrostatic Ion Energy Analyzers - Sprengel

A second method of determining ion velocities in the flow invokes a negatively biased Faraday cup which repels all electrons and collects only ions. The total ion current can then be transcribed to ion velocity if the ion density, charge number per ion, and effective collection area of the probe are known. The velocity distribution of the ions can be studied with somewhat more sophisticated gridded probes<sup>A-1</sup> which record the ion flux as a function of an applied potential barrier. In either case it is critical to maintain the proper relation of the dimensions of the plasma sheaths on the various electrodes, i.e., the Debye length, to the grid spacing and mesh. For example, we initially attempted to achieve ion energy measurements with the gridded probe sketched in Fig. 8. However, in the flow regions of prime interest, the ion density turned out to be much higher than expected with the result that the grid-collector gap became space-charge saturated and incapable of selecting the proper ion flux over the desired potential range. The probe was useful, however, in monitoring total ion flux, as discussed later.

Another requirement for application of such probes is a knowledge of plasma potential throughout the field, which can be computed from measurements of floating potential, corrected by reasonable estimates of the local electron



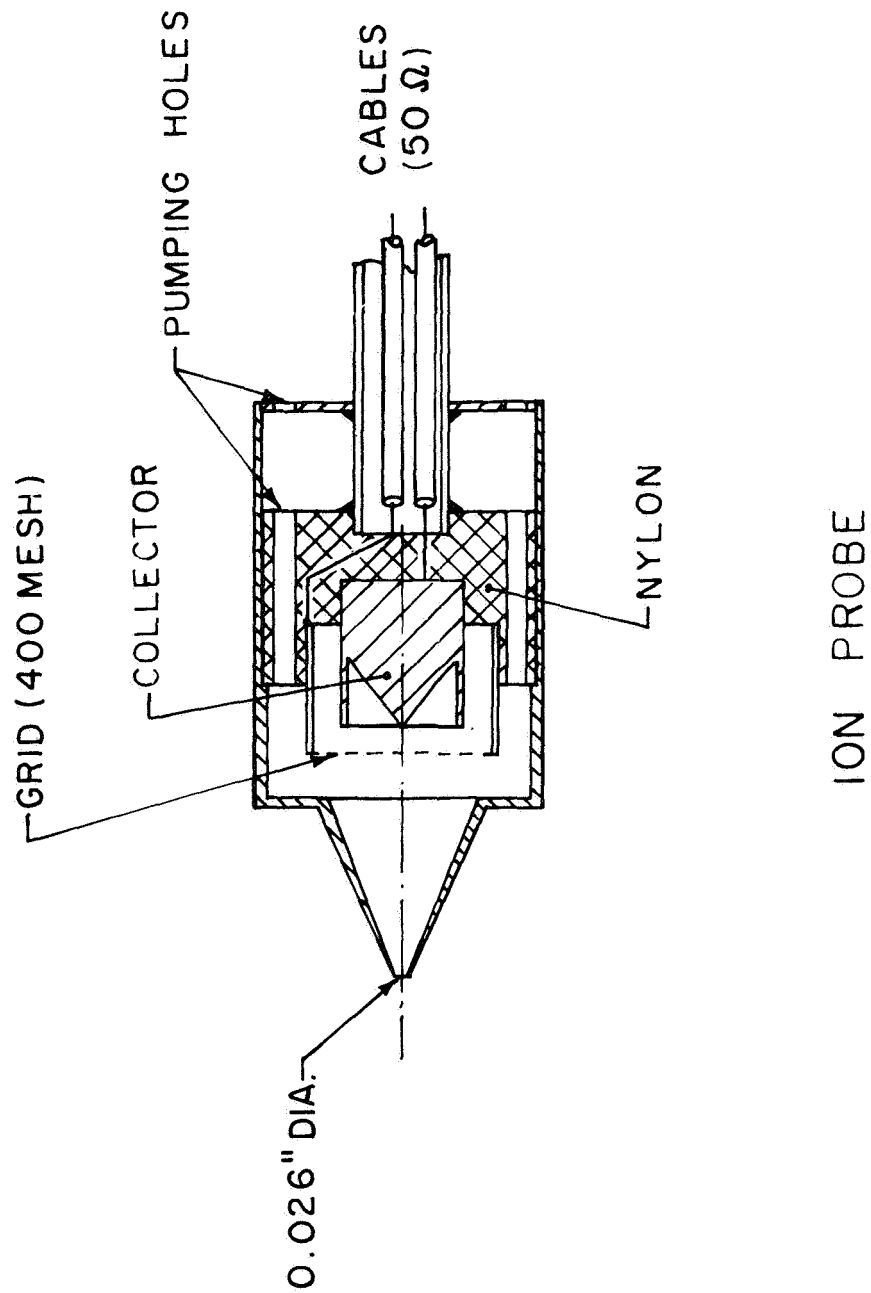
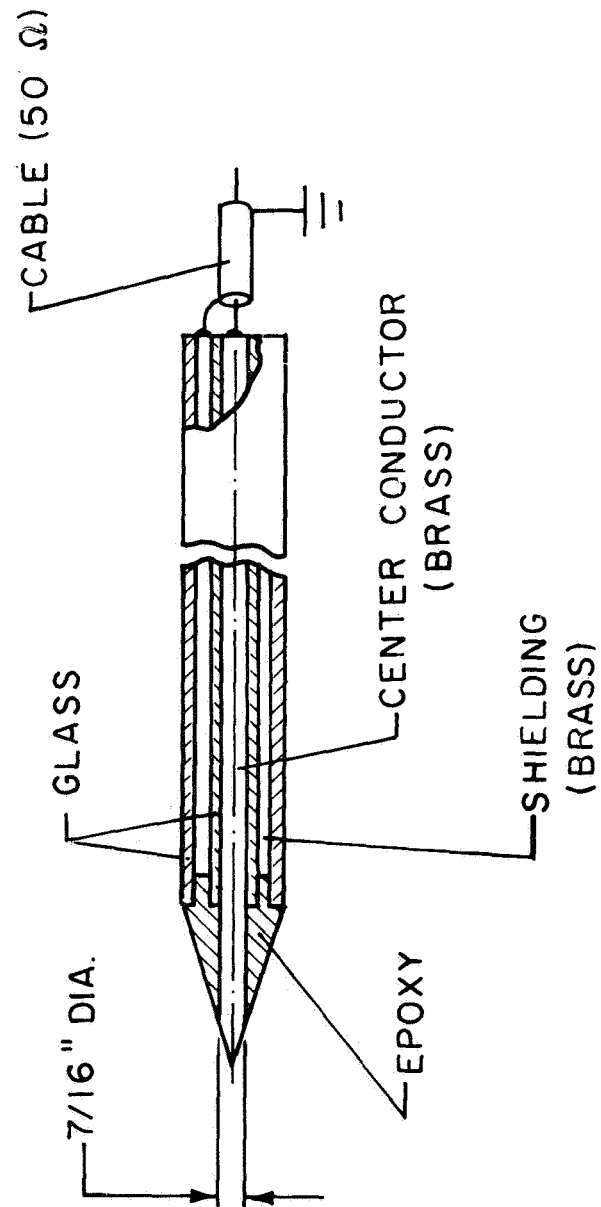


FIGURE 8  
AP 25 · 4549

temperature. Floating potential patterns were determined with the special probe shown in Fig. 9, although in retrospect, the case of the ion probe could serve equally well for this measurement. In our particular accelerator configuration, we find, unlike most discharges, that the floating potential is substantially above the cathode potential, say -40 V compared to -180 V for the cathode. This appears to result from the very large surface area of our anode, compared to the cathode, and is related to the anode fall phenomena discussed in Sec. III.

The circuit employed with the ion probe is shown in Fig. 10. The grid and the case are at floating potential which is connected to ground through a  $10^8$  ohm resistor. After charging the capacitor, the double switch disconnects the biasing circuit from the measuring circuit in order to avoid noise pickup during the measurement. The voltage drop across the 100 ohm resistor due to the electron current flowing to the collector surface is recorded. The transformer serves to isolate the probe from the oscilloscope. The probe circuit was calibrated with a square wave generator and test circuit, and found to yield a linear output voltage response to probe current.

Total ion current measurements were carried out at different axial positions on the center line and 1 in. off the center line. It was found that a range of bias voltages from -20 V to -50 V with respect to the floating potential was required to collect the entire ion current at different positions. A typical series of probe responses for different bias voltages taken 9 in. from the anode plane is shown in Fig. 11. The trace in Fig. 11a may be interpreted as the collection of the fast electron component ahead of the steady state phase. With a bias of -2 V with



FLOATING POTENTIAL PROBE

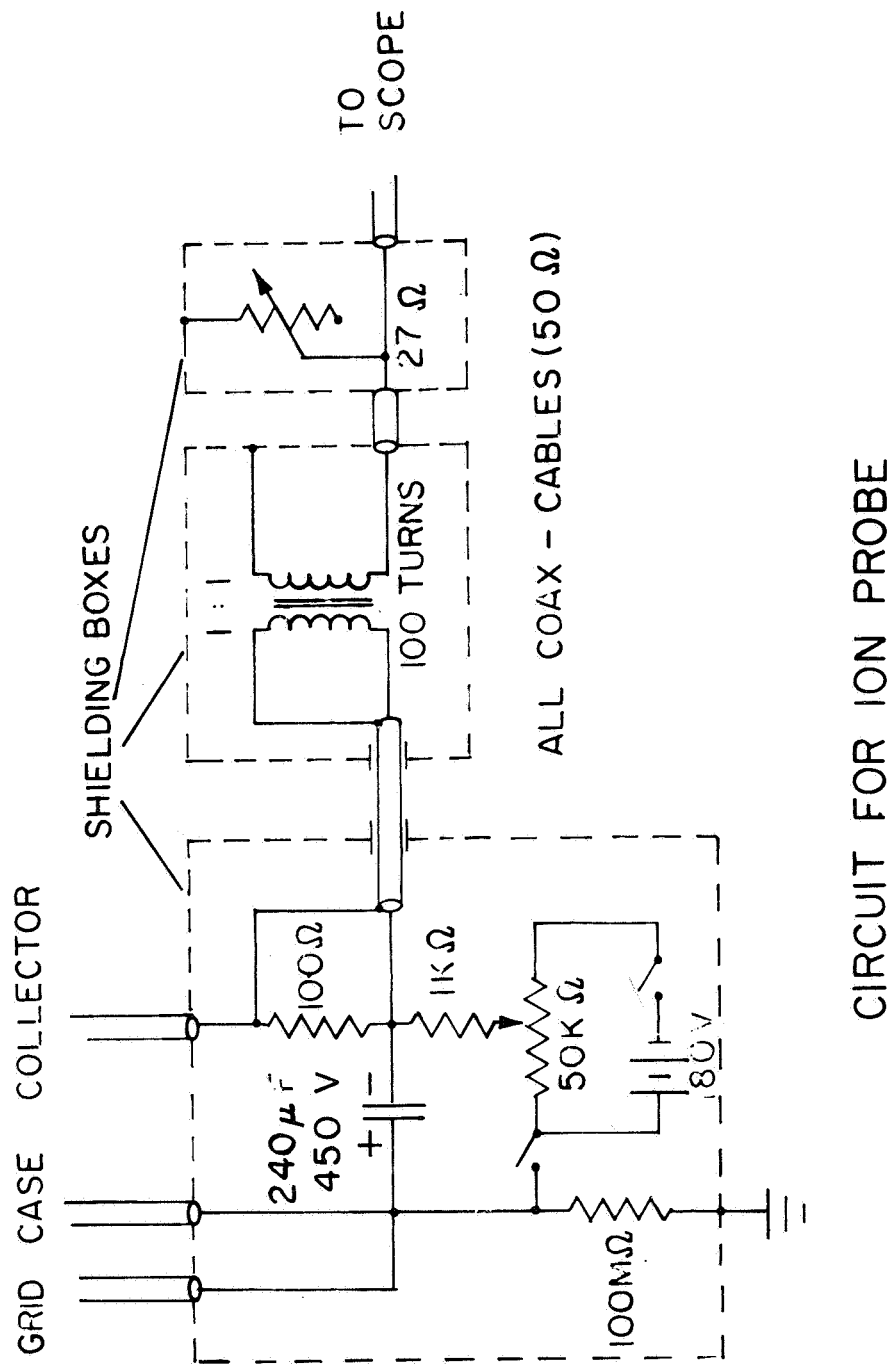
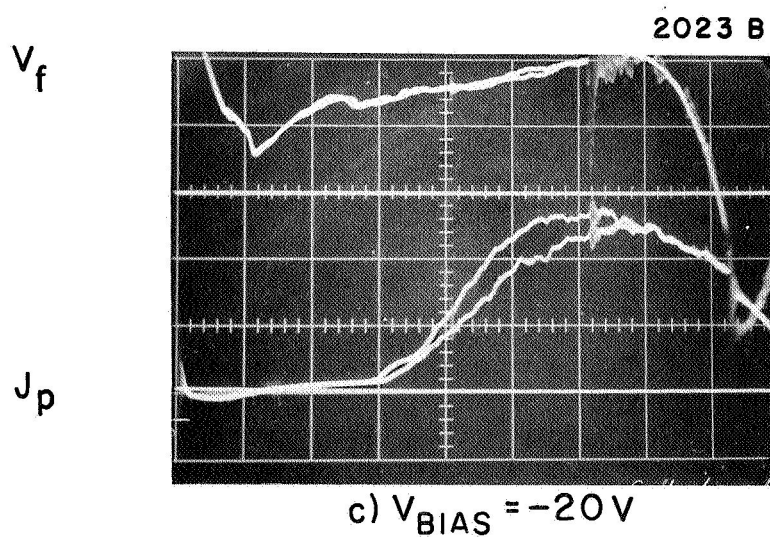
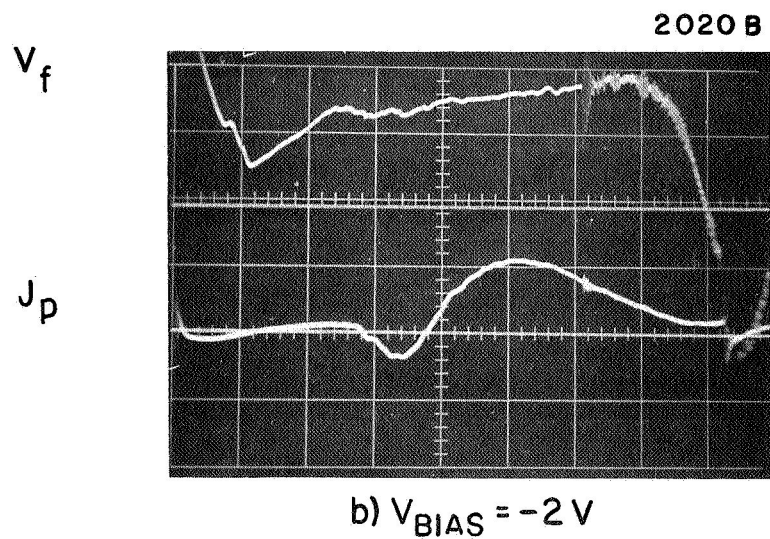
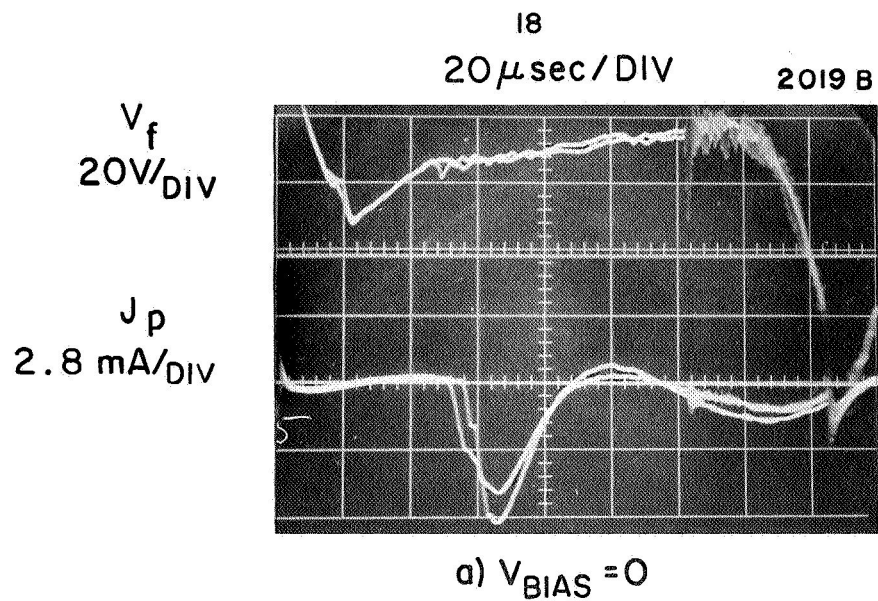


FIGURE 10  
AP 25 · 4547



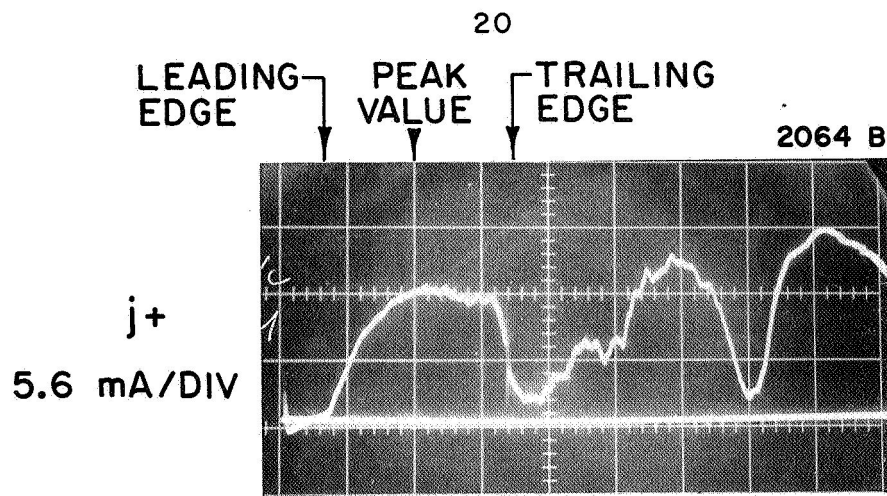
COLLECTOR CURRENT  $j_p$  AT 9" FROM  
ANODE 1" OFF  $\phi$

FIGURE 11  
AP25 P307

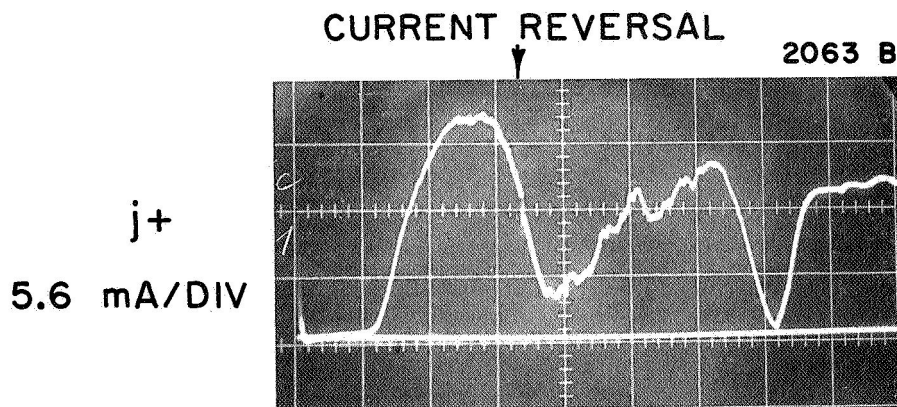
respect to the floating potential (Fig. 11b), the electron component is considerably reduced so that the net current to the collector becomes positive a short time later. At -20 V bias (Fig. 11c) all electrons are repelled and only ions are collected. Further decrease of the bias voltage yields no further increase of the net current. Therefore, this signature is taken to represent the total ion flux.

An interesting aspect of the flow development is displayed in Fig. 12, where the ion current signature is recorded over a time period of nearly three half cycles of the arc current waveform. Looking only at the first half cycle, three characteristic portions of the trace can be distinguished. First, the leading edge is seen to arrive at successively later times at these three axial positions. Second, the quasi-steady phase represented by the flat portion of the trace shortens and disappears going to further downstream positions. Third, the trailing edge moves faster than the leading edge, "eating" into the slower portions of the accelerated plasma, just as observed in the biased double probe studies of the previous section. Note also that the maximum ion current is larger at 6 in. from the anode than at either the upstream or downstream positions. Data of this sort are summarized in the t-x graph of Fig. 13. The trajectories confirm that the trailing edge and later, quasi-steady portion of the flow are propagating more rapidly than the initial "snowplow" burst and early, transition flow, so that the former actually telescope into the latter, shortening the plasma sample as it proceeds downstream.

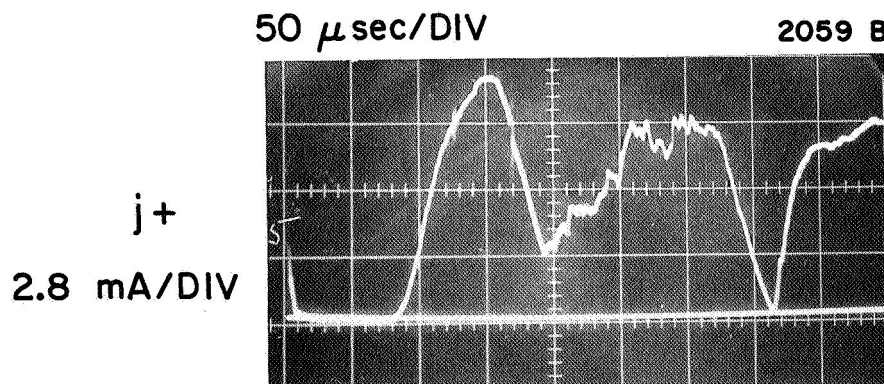
In Fig. 14 are plotted the maximum ion current, corrected for the transmissivity of the probe grid, as a function of axial position along the center line, and the corresponding ion density. The latter was calculated using



a) 3 INCHES FROM ANODE

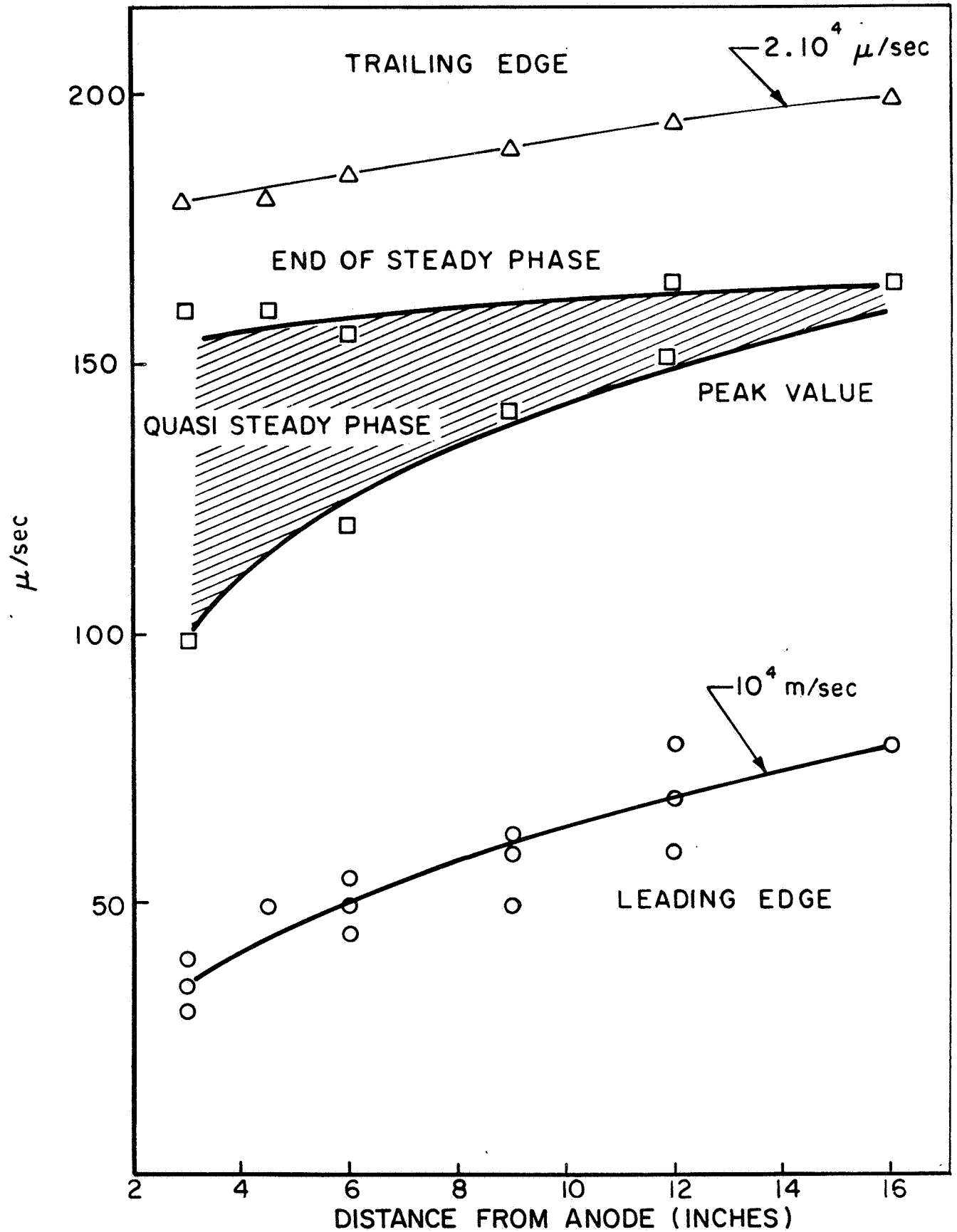


b) 6 INCHES FROM ANODE



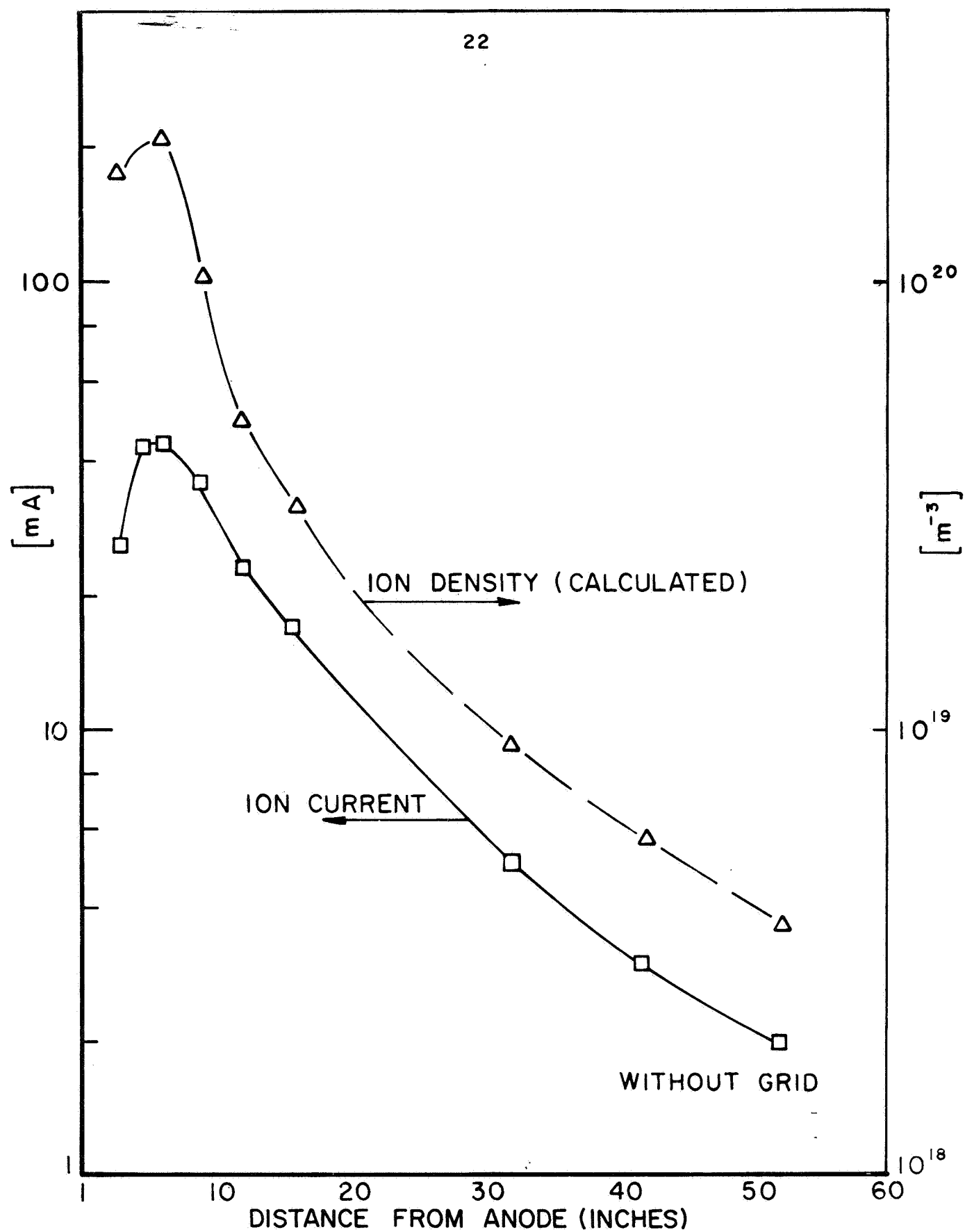
c) 12 INCHES FROM ANODE

ION CURRENT  $j+$  AT DIFFERENT AXIAL POSITIONS



TRAJECTORIES OF ION CURRENT SIGNATURES





MAX. ION CURRENT AND ION DENSITY ON  $\mathcal{E}$

FIGURE 14

AD 25-4554

the velocity profile of the maximum ion current portion of the flow sample (Fig. 13) and the orifice area of the probe. Note that the ion density also reaches a maximum about 6 in. downstream of the anode plane, indicative of a focusing effect of the ejected plasma in this region. This focusing is also suggested by Kerr-cell photographs taken in this same region.

Beyond this point the plasma spreads again with a corresponding reduction in ion density. If one assumes this spreading is dominated by the random thermal motion of the ions, it is possible to estimate ion temperature from the observed axial density gradient. For our data, this calculation yields a ratio of ion thermal velocity to streaming velocity of about 1:8, indicative of an ion temperature of about 2 eV.

A more sophisticated gridded probe is now being tested which will expand the collected flow sufficiently to allow proper functioning of the inter-electrode fields for energy discrimination of the ion flux.

### C. $\vec{u} \times \vec{B}$ Probes - Cory

If a local magnetic field of sufficient intensity can be imposed upon the streaming plasma, an interior electric field will arise from the charge separation of ions and electrons oppositely deflected in the magnetic field. The magnitude and direction of this induced electric field are given by the vector relation

$$\vec{E} = q(\vec{v} \times \vec{B})$$

and the measurable voltage signal thus depends on the size and orientation of any sensing element. Unfortunately, the

same effect which yields the desired signal tends to exclude plasma from the region of magnetic field, by virtue of the small gyro radius of the electrons, and any experiment of this sort involves a delicate compromise between adequate signal-to-noise ratio and tolerable disturbance to the plasma stream under study.

Our first series of experiments with this concept have not successfully reconciled these constraints. An unbiased double probe with 1.6 cm electrode separation was fixed in the tank on the center line. A permanent magnet was mounted on a movable platform which allowed the applied magnetic field at the probe to be varied from  $\sim 5$  gauss to  $\sim 1,000$  gauss between the pole pieces by changing the magnet position. Oscilloscope photographs showed the time resolved potential across the double probes. With low applied magnetic fields, shot-to-shot variations in the observed probe potential were of the order of 50 V/m, and these obscured any  $\vec{u} \times \vec{B}$  effect, even when the magnetic field direction was reversed for comparison. With larger magnetic fields, the observed peak potentials were appreciably larger (reached 120 V/m) but frequently reversed direction, indicating strong interaction between the plasma stream and the applied magnetic fields. Further, the observed potentials indicated plasma velocities far lower than the other velocity measurements, suggesting that the stream was not successfully penetrating the field region.

A second round of experiments of this class are now underway, in the hope of finding a probe configuration which is more adaptable to this particular plasma flow.

### III. ANODE PROCESSES IN HIGH-CURRENT DISCHARGES — OBERTH

In this section we shall briefly review earlier observations of anode phenomena, suggest certain interpretations of this data, and present recent results which are consistent with these interpretations.

Recall our earlier observations of current sheet behavior in an 8-in. diameter pinch discharge for various gas pressures and driving-current waveforms.<sup>75</sup> In general, we observed, both photographically and electrically, that the sheet attaches to the cathode in a narrow well-defined ring whereas the anode attachment is broad, diffuse and sometimes divided into two or more high-current density regions. Figure 15, showing Kerr-cell photographs taken through the sidewall of the pinch chamber, illustrates this configuration. This type of anode-cathode asymmetry is the basis for our more detailed studies of anode processes.

In another experiment various portions of the anode and cathode surfaces were selectively insulated, and the results further emphasized and marked differences between anode and cathode mechanisms. The resistive drop was measured by a voltage tap inserted through the center of the pinch chamber, while a 7-in. diameter circular piece of mylar insulation was alternatively attached to the anode and cathode surfaces. Figure 16 shows typical results from this experiment for 100  $\mu$  argon ambient fill and the driving-current waveform shown on the oscillograms. Figure 16a shows the voltage signature for the normal all-metal electrode situation. The portion of the signature of

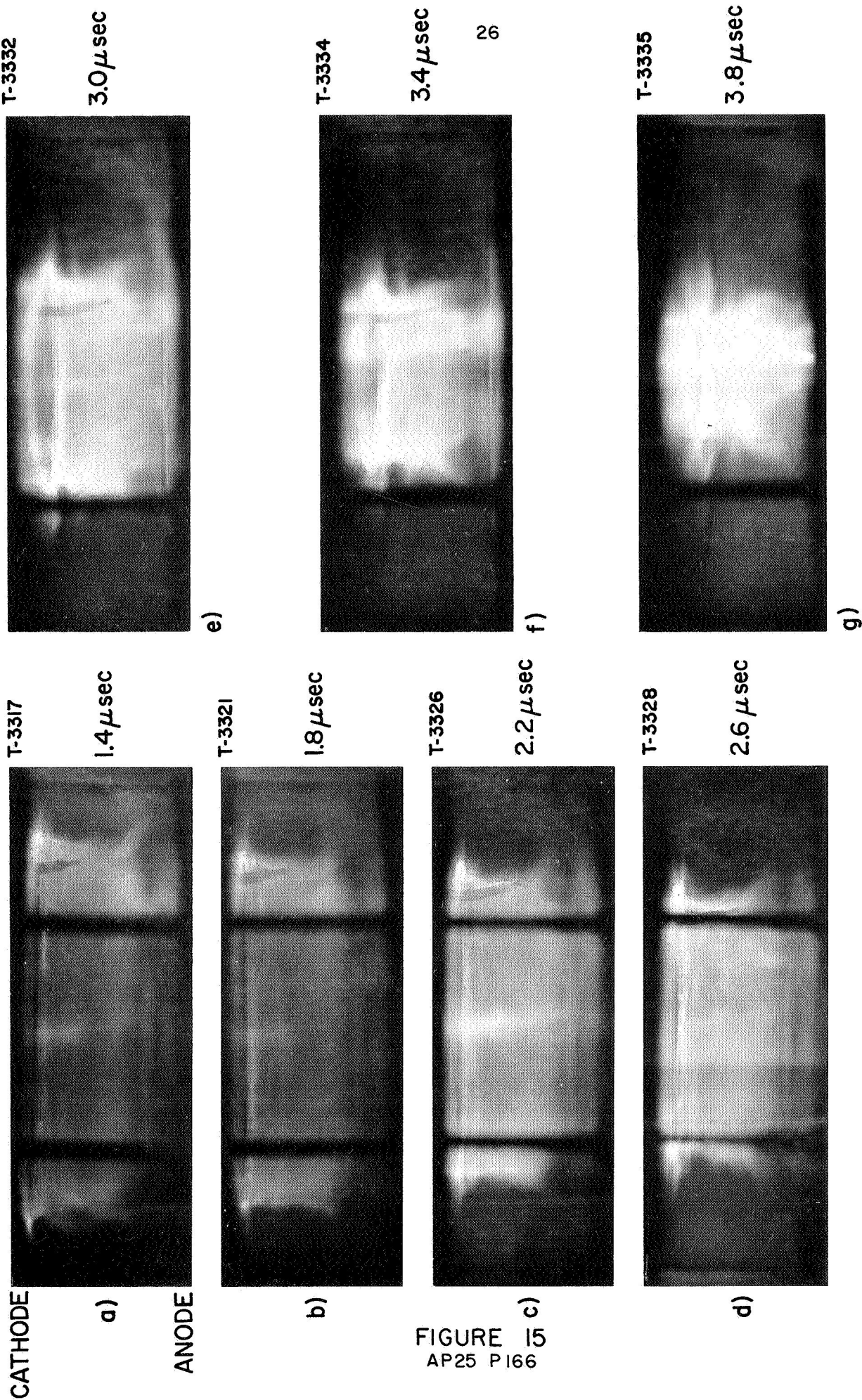
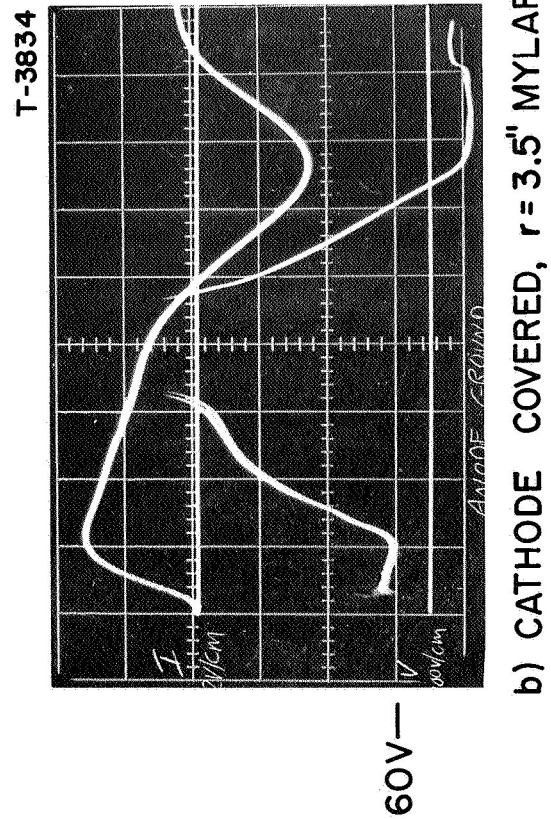
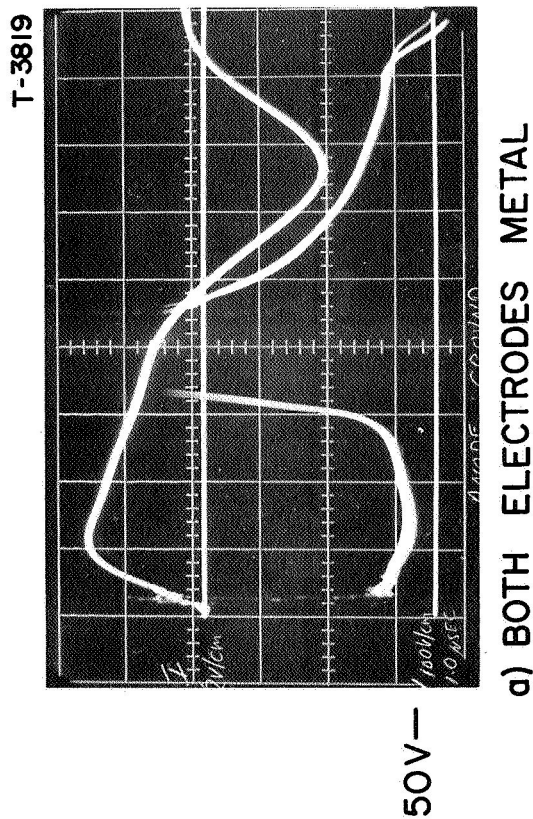
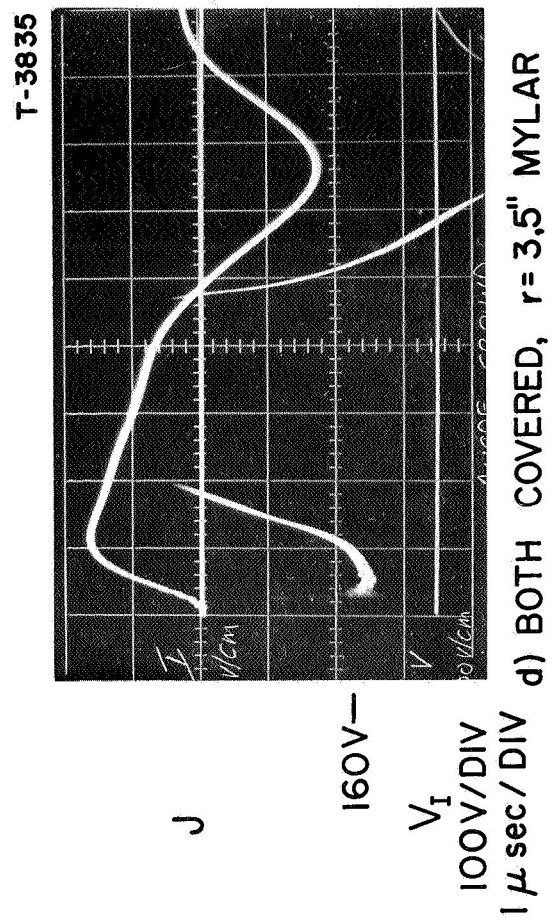
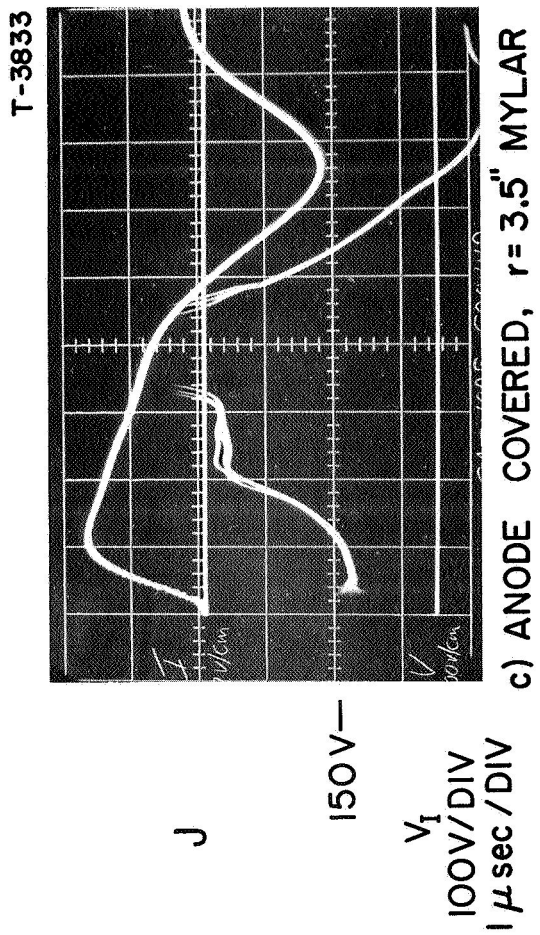


FIGURE 15  
AP25 P166

PROGRESS OF BIFURCATING CURRENT SHEET IN 100  $\mu$  ARGON



OSCILLOGRAMS OF CURRENT WAVE FORM

FIGURE 16  
AP 25 P184

primary interest lies between 0.5 and 3.0  $\mu\text{sec}$ , i.e., well before the arrival of the current sheet at the center tap. The large signal following at 4  $\mu\text{sec}$  is caused by magnetic flux linkage in the measuring circuit after the current sheet collapses at the chamber center. Figures 16b and 16c demonstrate the different effects on the resistive arc voltage caused by cathode and anode insulation, respectively. Figure 16b is interpreted as follows: during the first 1.0  $\mu\text{sec}$  after breakdown the narrow cathode attachment has not yet contacted the insulation and, therefore, the arc voltage closely approximates the all-metal case over this time period. At 1.0  $\mu\text{sec}$  the cathode attachment reaches the insulation and is arrested there while the bulk of the current sheet runs inward, bending back along the insulation to maintain contact with the exposed cathode. The large voltage rise between 1  $\mu\text{sec}$  and 3  $\mu\text{sec}$  may thus be due to the increasing arc length as the current pattern moves inward, or to some other dissipative effect associated with this distortion of the cathode attachment pattern.

When this experiment is repeated with the anode, rather than cathode insulated (Fig. 16c), the voltage is substantially higher at the earliest observable time, say 0.5  $\mu\text{sec}$ , indicating that the broader anode attachment has already been distorted by the insulating layer.

From this time, the voltage continues to rise monotonically as the main portion of the current sheet passes the insulation edge and propagates toward the chamber center. This failure of the arc voltage to attain the "all metal" voltage, even at the earliest times, is indicative of an involvement of a major portion of the entire anode surface in the early phases of the normal discharges.

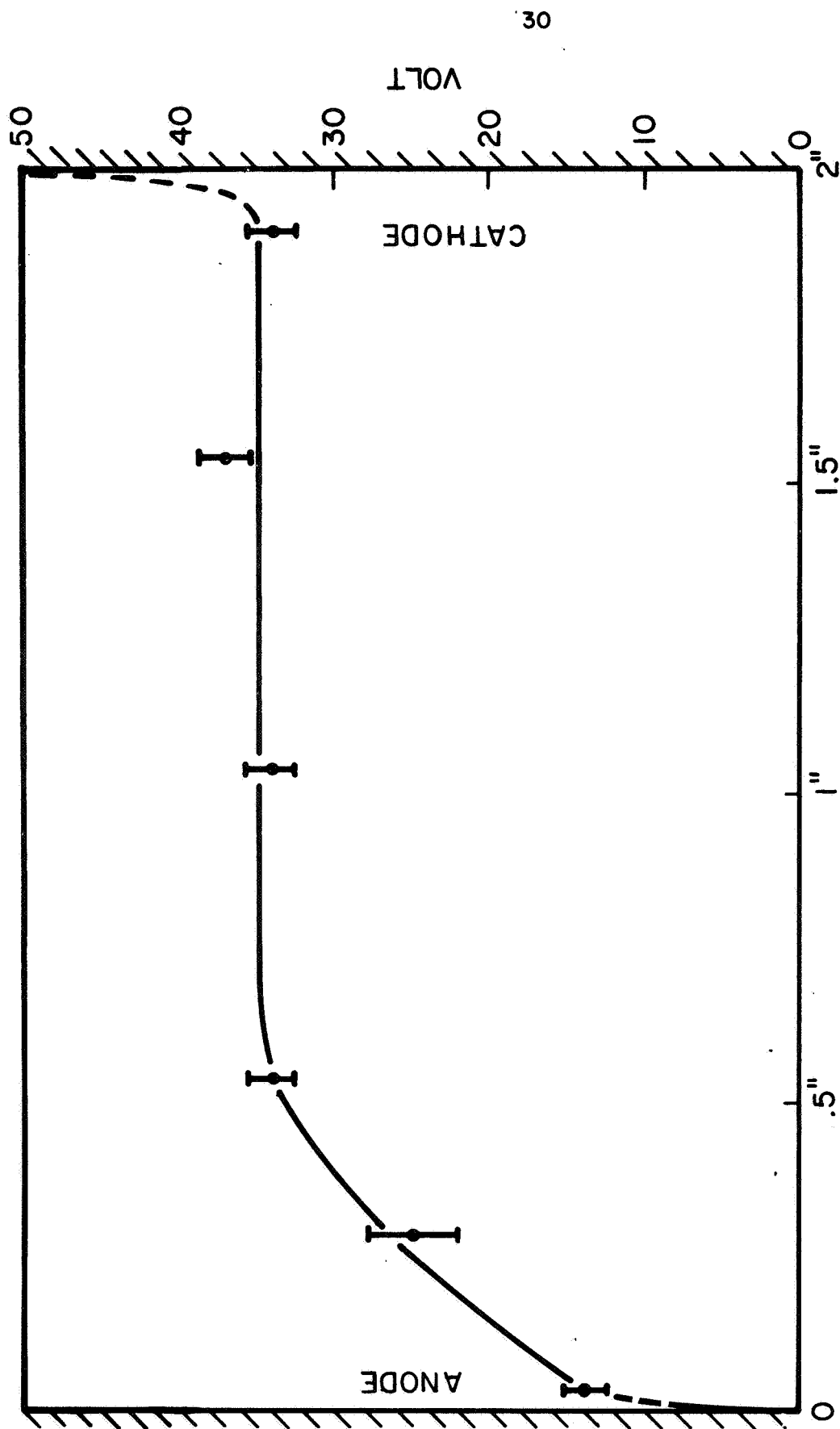
To test this hypothesis various measurements were made of the local properties of the slightly ionized plasma which exists in the region ahead of the propagating current sheet. For example, sensitive magnetic induction coils were inserted to search for possible central chamber current densities ahead of the sheet. These experiments proved inconclusive because of leakage magnetic fields from current sheet asymmetries, and because of an inherent irreproducibility in these precursor current patterns under study.

A single tip electrostatic probe was then inserted to map the plasma potential throughout the pinch chamber. The probe tip diameter was  $1/32$  in. and was formed such that it could be placed very close to the top electrode of the chamber. The measuring circuit had a very high resistance forcing the probe tip to float at plasma potential less a small sheath drop associated with the electron temperature.

In its first application the probe was used to determine the potential distribution between the pinch electrodes at a radius of 1 in. at the time the current sheet reached a radius of about 3 inches. This distribution of potential for all-metal electrodes, shown in Fig. 17, shows that most of the voltage drop occurs within  $1/2$ -in. of the anode, with a much smaller drop near the cathode.

This result may relate to the markedly different arc voltage signatures obtained for substantial insulation of anode and cathode, discussed above. The existence of a large voltage gradient near the anode in the region well ahead of the current sheet suggests that current conduction of some sort is occurring in this part of the chamber. The





VOLTAGE DISTRIBUTION ACROSS CHAMBER AT 1 INCH RADIUS

$t = 1 \mu \text{ sec}$   
CURRENT SHEET AT  $R = 3''$

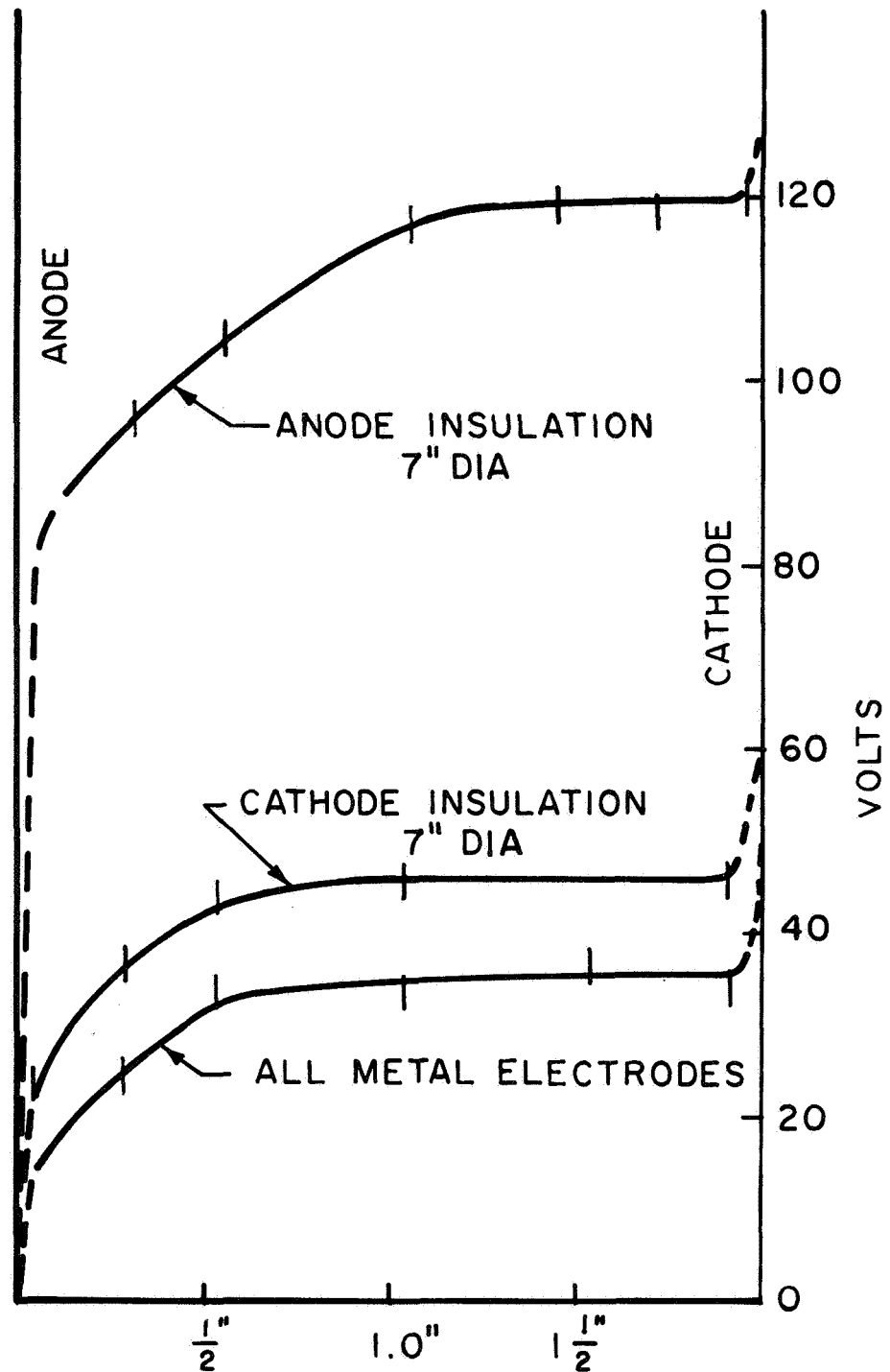
FIGURE 17  
AP 25-4492

placement of insulation on the central portions of the anode must inhibit this part of the current conduction pattern, and the arc may respond to this disruption by increasing its total voltage. Conversely, the absence of precursor cathode conduction is consistent with the minimal effect of cathode insulation on the arc voltage.

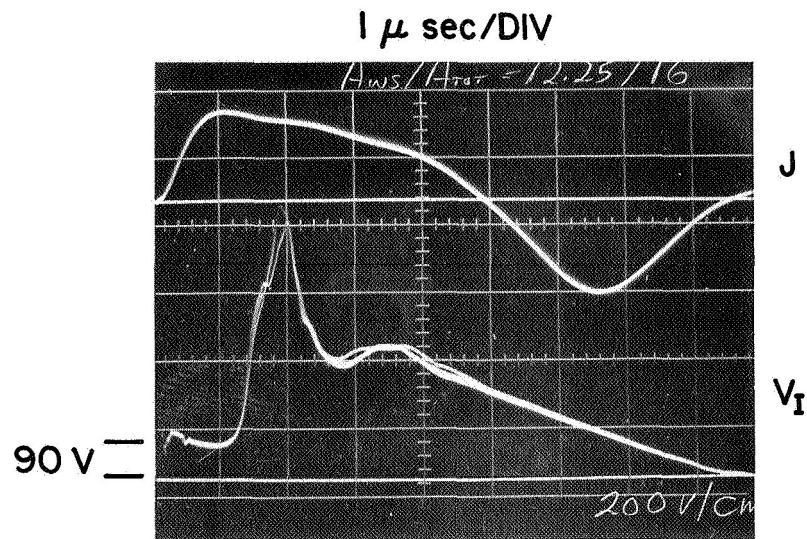
It is instructive to repeat the electrostatic probe measurements of plasma potentials at the same radius of 1 in., but with a 7-in. diameter mylar disc placed alternatively on the anode and cathode. Figure 18 shows these potential distributions in comparison with that of the all-metal case. For both types of insulation the potential distribution retains a similar form except for a somewhat larger anode fall in the case of cathode insulation and a much larger anode fall when the anode is insulated.

To further demonstrate the importance of the precursor anode conduction to overall arc voltage, the anode was fitted with an annular disc of mylar, extending from the outer wall,  $r = 4.0$ " to an inner radius of 2.65 in., and the central voltage tap again established. Figure 19a compares the response to this configuration, with that obtained with the earlier 7-in. diameter insulating disc (Fig. 19b). Now the voltage drops to about 90 V, compared to 150 V for the equal area central disc, before increasing rapidly when the current sheet collapses at the chamber center. It thus appears that the availability of the central anode surface considerably reduces the impedance of the total discharge. The value of 90 V is somewhat higher than the all-metal value, 50 V, probably because the discharge is forced to break down along a longer,

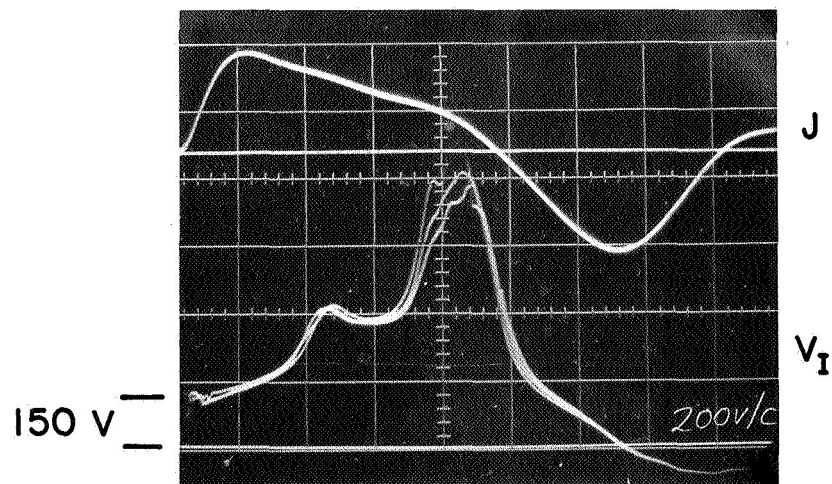
CURRENT SHEET AT  $r > 3''$   
 $t = 1 \mu \text{ sec}$



POTENTIAL DISTRIBUTIONS ACROSS  
DISCHARGE CHAMBER AT  $R = 1$  INCH



a) PERIPHERAL INSULATION  
OF ANODE



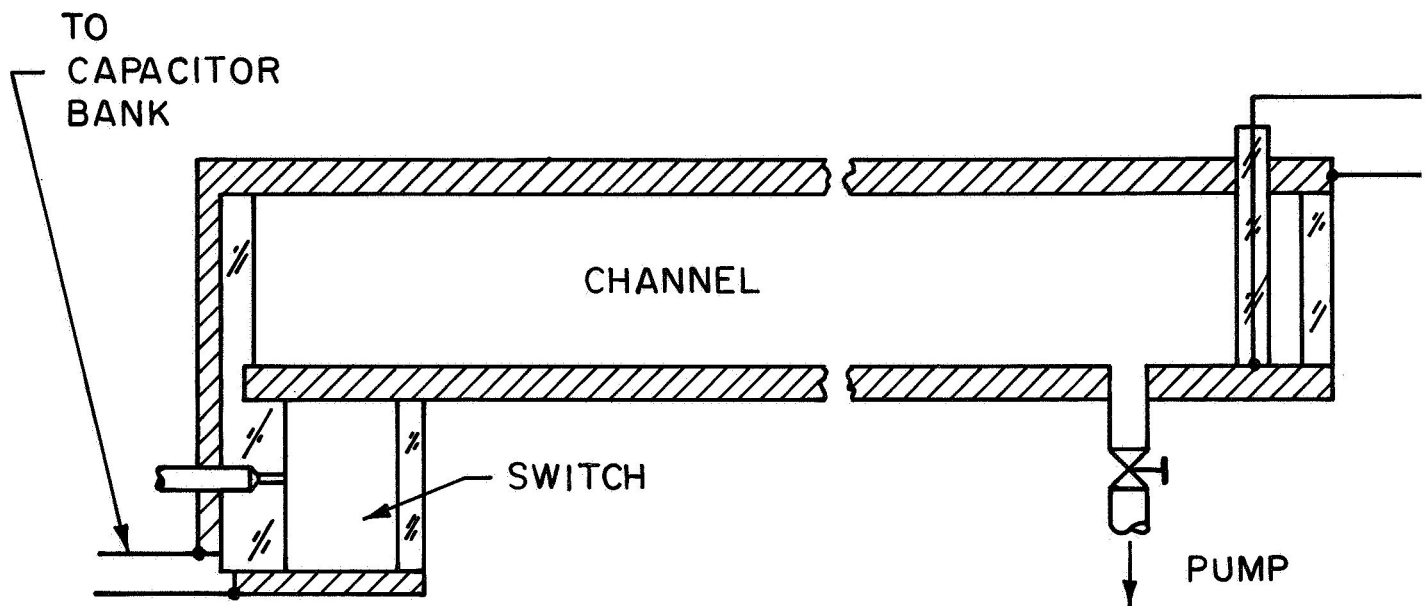
b) INSULATION OF CENTRAL  
PORTION OF ANODE

ARC VOLTAGES FOR DIFFERENT ANODE INSULATION

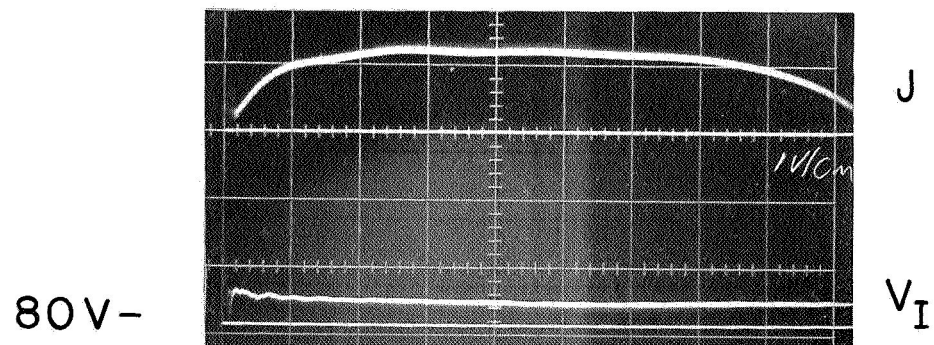
higher inductance path in this case. Note also that the voltage maximum related to sheet pinch occurs much earlier, indicating that the discharge arose at a smaller initial radius.

During the present reporting period, the anode phenomena studies have been extended to our parallel-plate accelerator,<sup>67</sup> to determine which of the above effects persist in this geometry, and which are modified by it. In these experiments, the discharge is driven into a 100  $\mu$  argon ambient fill by a 120,000 A current pulse lasting for 20  $\mu$ sec. A voltage tap is located at the downstream end of the machine, in which position it responds only to resistive voltage drop across the electrodes. Figure 20a shows a schematic of the accelerator and measuring circuit, while Fig. 20b displays the driving-current waveform and a typical response of the voltage tap for a current sheet propagating along the full length of the electrodes. Note that the arc voltage for this all-metal case is virtually constant at a value of 80 V.

The same measurements have been repeated with varying portions of the anode and cathode insulated by mylar. Typical oscillograms for anode insulation are shown in Fig. 21. Figure 21a, for 5 1/4 in. of anode exposed, again shows an elevated voltage, 170 V in this case, immediately after breakdown followed by an increasing signal as the anode attachment encounters the insulation and the arc length begins to increase. Figures 21b,c,d for increasing lengths of uninsulated anode display the same general characteristics, but with successively lower initial voltages and later onset of voltage increase. Figure 22 summarizes the dependence of voltage minimum on exposed anode length when the anode attachment reaches the insulated portion.



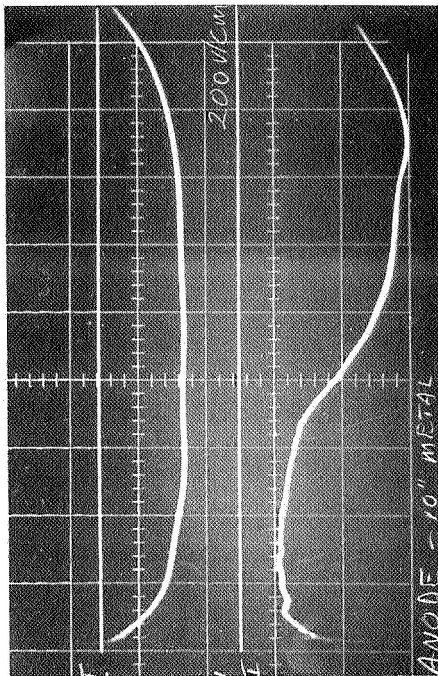
a) SCHEMATIC OF PARALLEL PLATE ACCELERATOR



b) ARC VOLTAGE FOR ALL METAL ELECTRODES

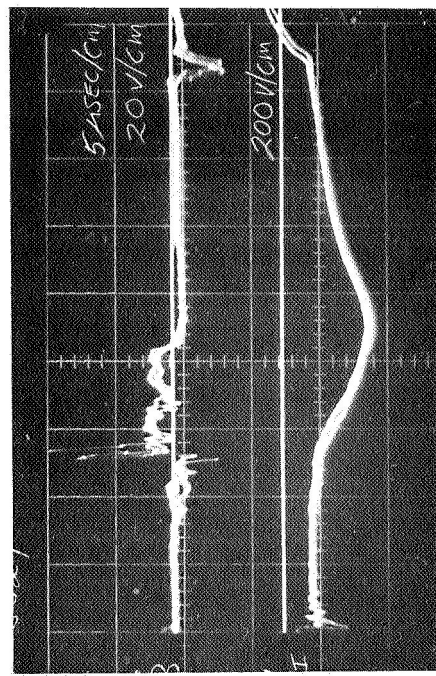
## PARALLEL PLATE ACCELERATOR

A - 3315



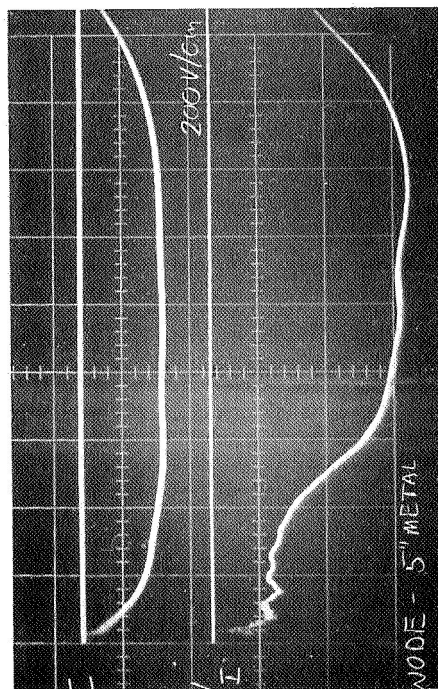
b) 10" ANODE LENGTH

A - 3324



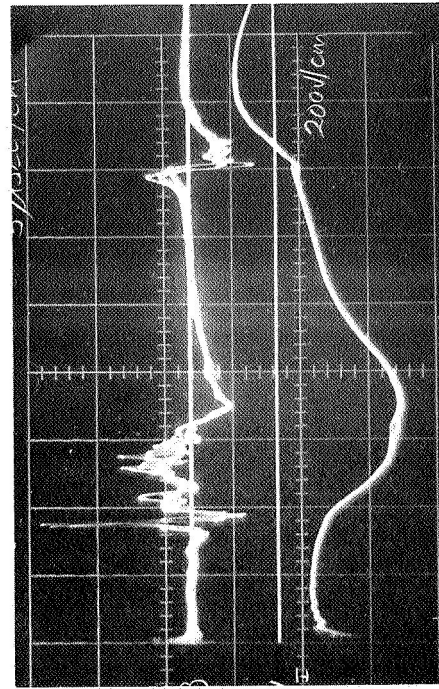
d) 21" ANODE LENGTH

A - 3310



a) 5 1/4" ANODE LENGTH

A - 3338



c) 14 1/2" ANODE LENGTH

INNER DIVIDER RECORDS FOR ANODE INSULATION

FIGURE 21  
AP 25 • P 296

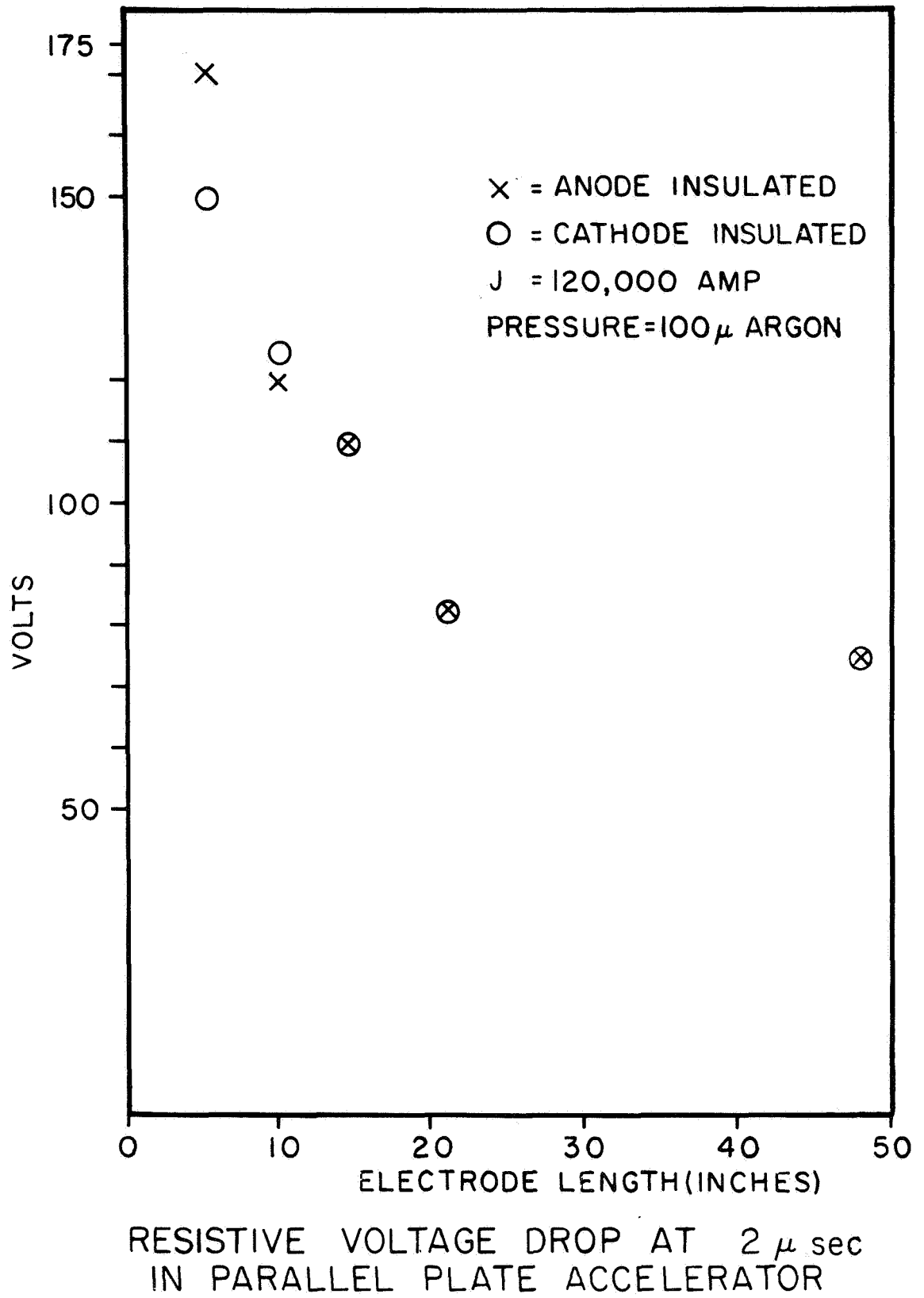
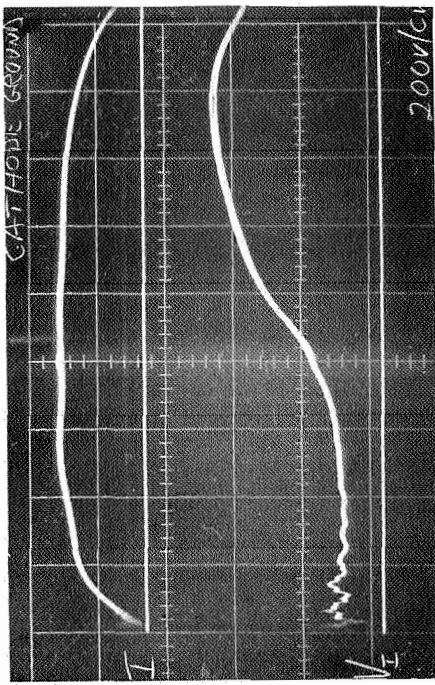


FIGURE 22  
AP 25 - 4544

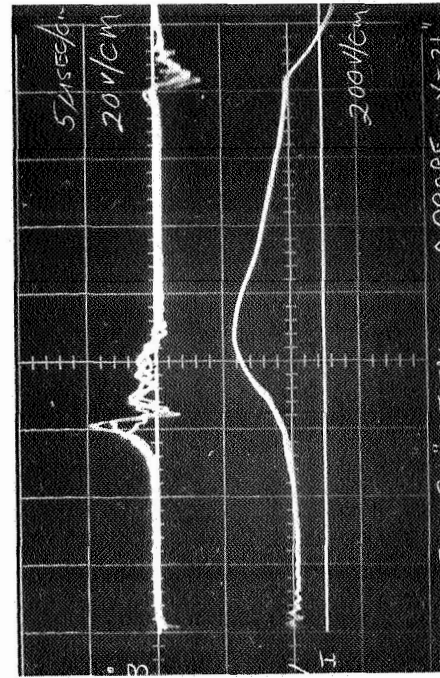


In order to correlate the arrival time of the anode attachment at the insulation interface with the beginning of the voltage signal increase, a magnetic induction coil was inserted at the point where insulation begins adjacent to the anode. The responses of such magnetic probes are shown in the upper traces of Figs. 21c,d for 14 1/2 in. and 21 in. of exposed anode. Observe that the voltage signal begins to rise when the leading edge of the "anode foot" contacts the insulation and then continues to increase until the lagging parts of the "foot" have passed. It is not clear whether this voltage increase is caused by constriction of the previously broad and diffuse anode attachment at the insulator edge, or whether it is related to the onset of quasi-steady mhd gas acceleration in this region, as discussed in Ref. 67. In either case it appears to be distinct from the precursor conduction mechanisms which were responsible for the higher voltages observed at the beginning of the discharge.

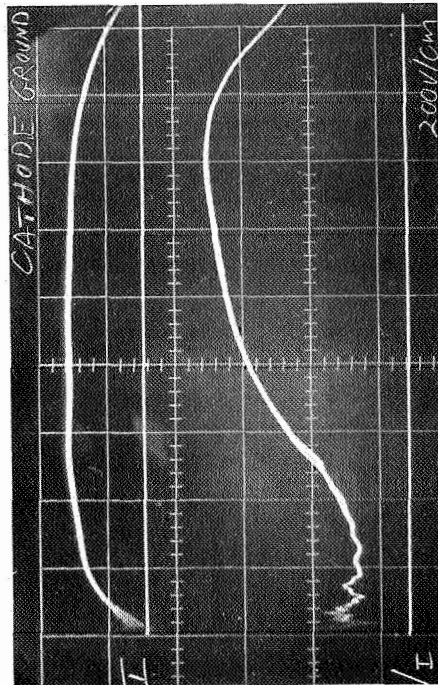
A significant departure from the pinch geometry behavior is observed when the same measurements are repeated on the cathode. With the machine polarity reversed so that the cathode now becomes the insulated electrode the voltage traces obtained for the four different lengths of cathode insulation (Fig. 23) are unexpectedly similar to those for corresponding anode insulation (Fig. 21). Once again we have the elevated voltage readings at the beginning of the discharge followed by increasing voltage when the cathode attachment meets the insulation. In each case the initial voltage is almost the same as that for comparable anode insulation, contrasted with the 8-in. pinch data which showed a marked difference between anode and cathode insulation. This seems to imply that the downstream current conduction processes are of comparable importance at anode



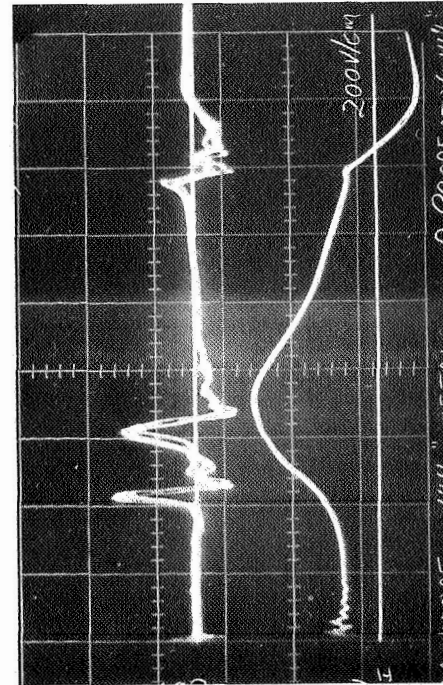
b) 10 " CATHODE LENGTH



d) 21" CATHODE LENGTH



a) 5 1/4" CATHODE LENGTH



c) 14 1/2" CATHODE LENGTH

and cathode, unlike those in the pinch discharge where the downstream anode currents appear more critical.

The response of the magnetic probe, located on the cathode surface at the insulation interface, are shown in Figs. 23c,d along with the accompanying voltage traces. These signatures show that the cathode attachment trails the leading part of the "anode foot" somewhat, and that it also has a structure which is broad and divided. Again, the foot arrival times correlate well with the first indications of a voltage increase.

The appearance of a substantial "cathode foot" in these experiments in contrast to the relatively sharp cathode attachment in the pinch discharge may reflect the substantially longer streamwise dimension available for the current sheet to propagate in the former, compared with the 4-in. radial dimension of the latter. That is, the cathode foot may grow more slowly than the anode foot, and simply not be adequately developed to observe in the pinch experiments. One cannot assign the entire discrepancy to this factor, however, for as noted above, the cathode attachment in the parallel-plate geometry is well aware of the insulation at the earliest times, even when the body of the sheet is 4 or 5 in. upstream of the discontinuity, whereas in the pinch geometry, cathode insulation to within 1/2 in. of the outer wall has little effect on early discharge voltage.

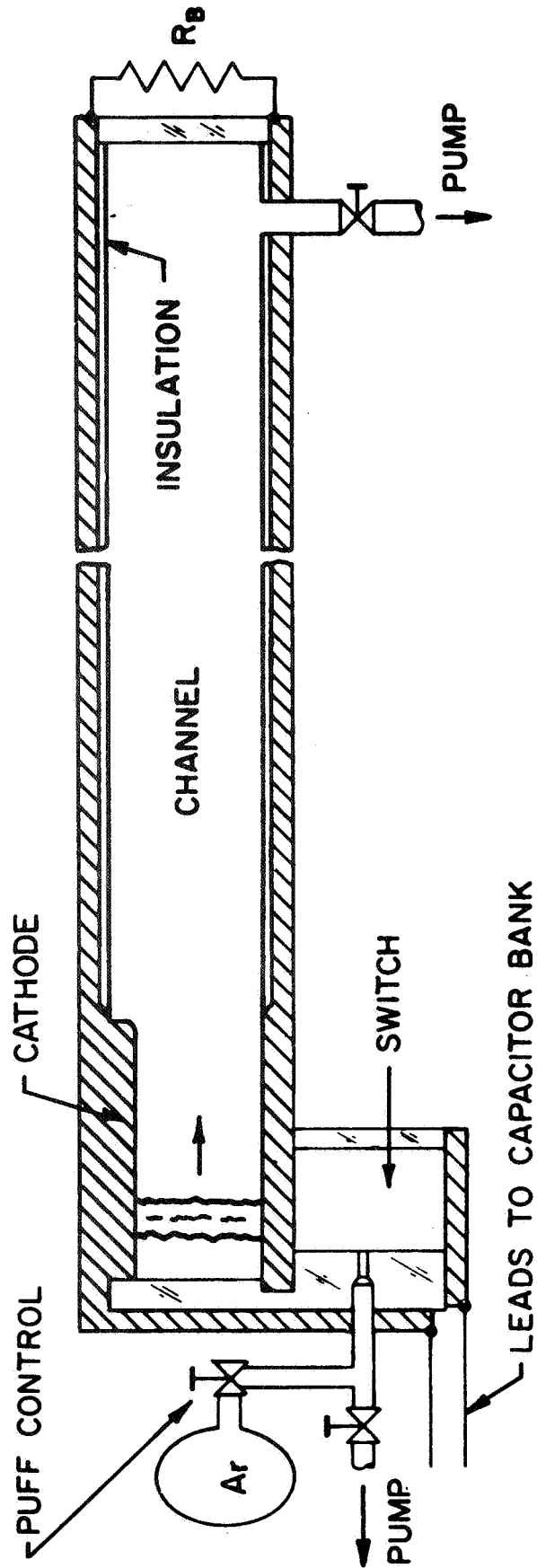
Clearly, more phenomenological experiments of this kind are needed further to localize the important parameters affecting the electrode attachment processes before more sophisticated experiments and analytical models can profitably be pursued. Such data are currently being accumulated.

#### IV. CATHODE JET STUDIES IN A PARALLEL- PLATE GEOMETRY — TURCHI

Preliminary studies of the cathode jet in a quasi-steady plasma accelerator described earlier<sup>75</sup> have been continued in greater detail and with other diagnostic techniques. The goals of the experiments to be discussed are to verify that a reasonably uniform cathode jet exists, to observe the dependence of the appearance of the jet on pressure and current level, and to examine the structure of the jet by means of interior diagnostics, both to obtain some ideas as to the magnitudes of the quantities of interest and to evaluate various possible diagnostic techniques.

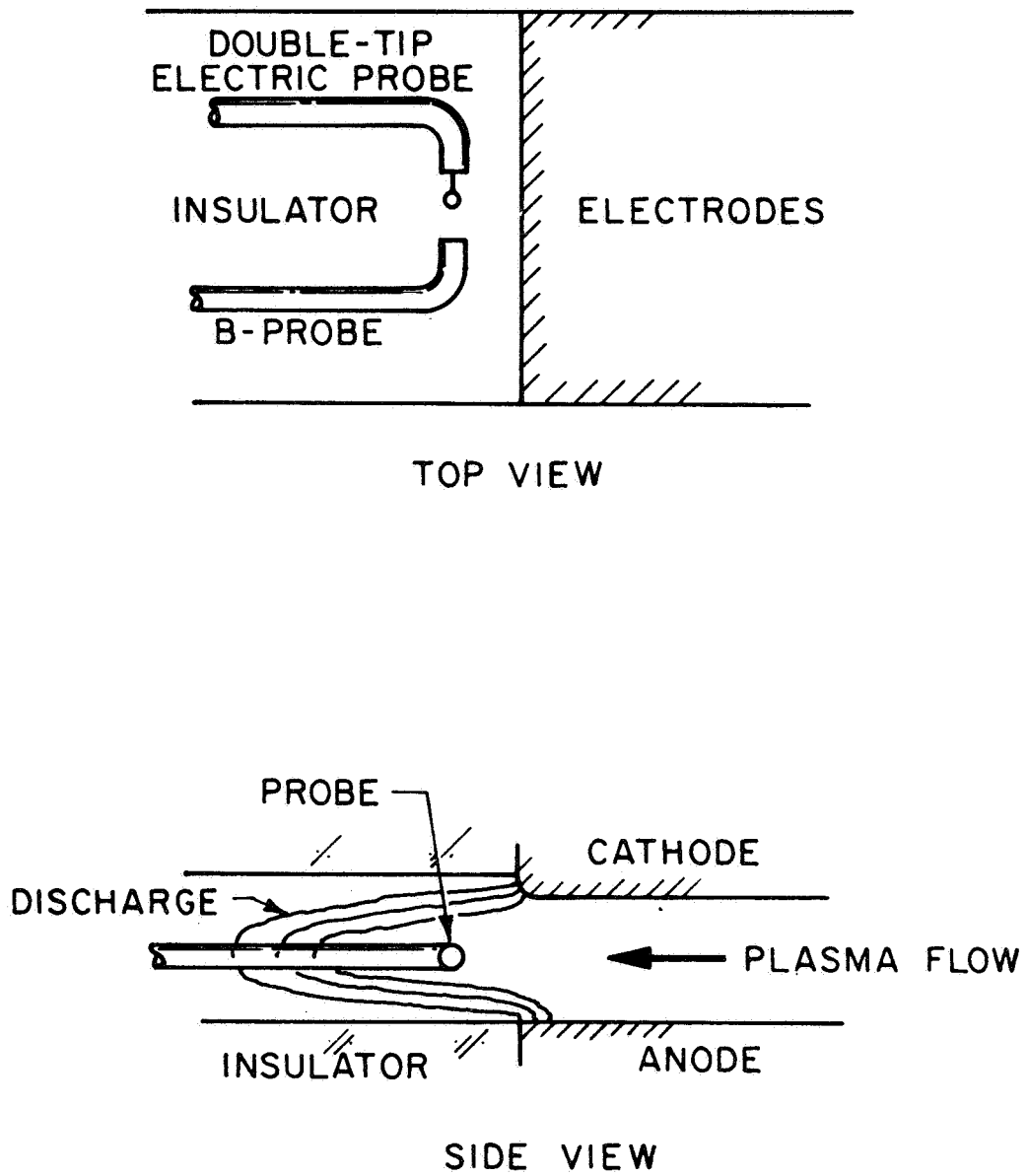
To maintain geometrical simplicity and optimize access to the region of interest, the experiments were performed in the modified parallel-plate facility, shown in Fig. 24. The modification consists of an additional section on the cathode which allows the jet to initiate away from the insulator interface. Figure 25 shows the arrangement of the diagnostic probes in the discharge chamber. Once the probes are positioned with respect to the channel width, they can be moved continuously in both the transverse (vertical) and streamwise directions.

The first series of experiments examined the discharge uniformity with respect to the channel width. Magnetic probes were placed at the center line and half way to the channel wall, at the same transverse and streamwise positions. The B-field records obtained at various streamwise positions were then compared to see if any major current concentrations were present. Such comparisons indicated



SCHEMATIC DIAGRAM OF PARALLEL PLATE ACCELERATOR  
MODIFIED FOR CATHODE JET STUDIES

FIGURE 24  
AP 25 . 4319 E



## PROBE POSITIONING

FIGURE 25  
AP 25 4556

that the current density was uniform to about 30 percent along the width of the channel in the region and time of interest. Visual investigation of the electrode and insulator surfaces after many discharges also indicated that, while some sort of boundary region existed near the channel walls, the central portion of the discharge, some 2 in. of the 6-in. channel width, was essentially uniform. These tests were conducted at both 17,000 A and 42,000 A total current and at initial pressures of argon of 50  $\mu$  and 100  $\mu$ . It was found that the cathode jet extended further downstream for the higher currents and lower pressures, consistent with the convection and diffusion of a magnetic field in a finite resistivity plasma flow. Thus, to optimize the dimensions of the jet, we chose to continue the more detailed stages of our work at a current level of 42,000 A and a pressure of 50  $\mu$ .

The electromagnetic structure of the cathode jet was investigated by a combination of magnetic and electric field probes, of the usual design.<sup>61</sup> In Fig. 25, the probe positioning is shown, with the probes stationed at the same transverse and streamwise positions but symmetrically on either side of the channel axis, in the uniform region mentioned earlier. Measurements of the magnetic field at over a hundred points within the discharge allowed mapping of the magnetic field distribution and, from this, determination of the current density distribution and direction. In a sense, the discharge and the electrodes may be considered as a one-loop, finite-length solenoid, and as expected, the magnetic field changes direction within the discharge pattern. This finite solenoid effect is important since the assumption of an infinite solenoid would lead to the conclusion that negative currents or eddies are present at the downstream edge of the discharge.

Contours of constant magnetic field strength are shown in Fig. 26. The dot-dashed line represents an arbitrary definition of the cathode jet as the region over which current streamlines from the cathode have a downstream component. In this case this jet extends a few inches downstream of the cathode and is confined to about a 1/2-in. thick region. Note that some 70 percent of the total current travels downstream within the cathode jet.

In Fig. 27 we present the corresponding transverse current density,  $j_y$ , as a function of streamwise position for a typical distance off the cathode surface,  $h = 1/4$ ". Note that current enters the jet rather uniformly for a few inches downstream of the cathode. This may be an indication of a "virtual cathode" effect. In Fig. 28 the streamwise component of the current density,  $j_x$ , is shown as a function of streamwise position for two transverse positions:  $h = 0$  (even with the cathode surface), and  $h = -1/4$ ". We see that the streamwise current density is rather uniform with respect to transverse position in the jet and decreases with distance from the cathode. Figure 29 compares the streamwise and transverse current densities for  $h = 0$ ; note that the streamwise current component is much greater than the transverse one for a few inches away from the cathode. The magnitudes of the current densities involved,  $10^6 - 10^7$  amps/m<sup>2</sup>, are comparable with those observed in the coaxial MPD arcjets.

The transverse electric field component was obtained during the same survey using a double-floating tip electric probe. The probe tips were both spherical with diameters of 1 mm and were separated so that the voltage difference between them indicated the electric field in the transverse



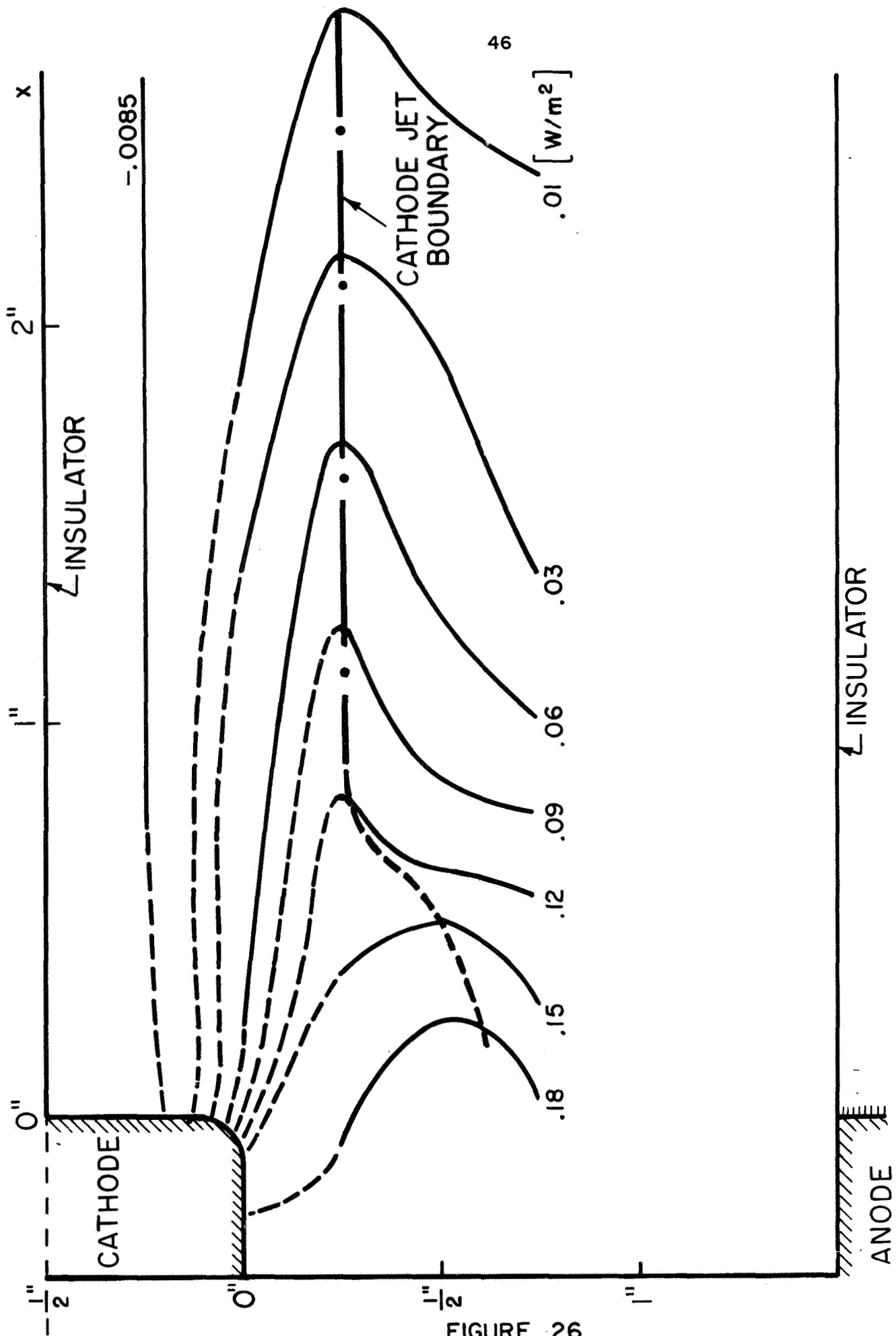


FIGURE 26  
AP 25-4500

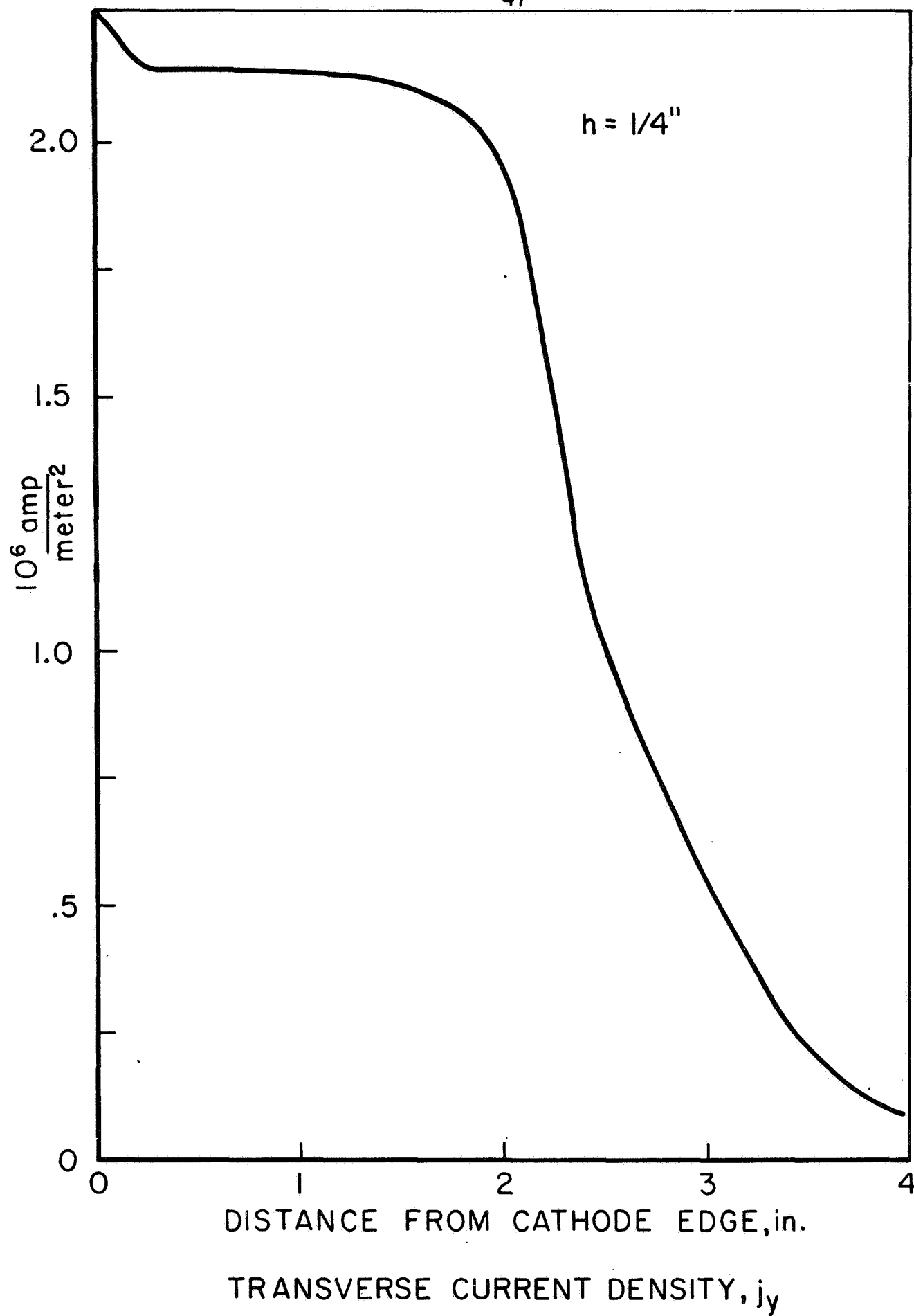
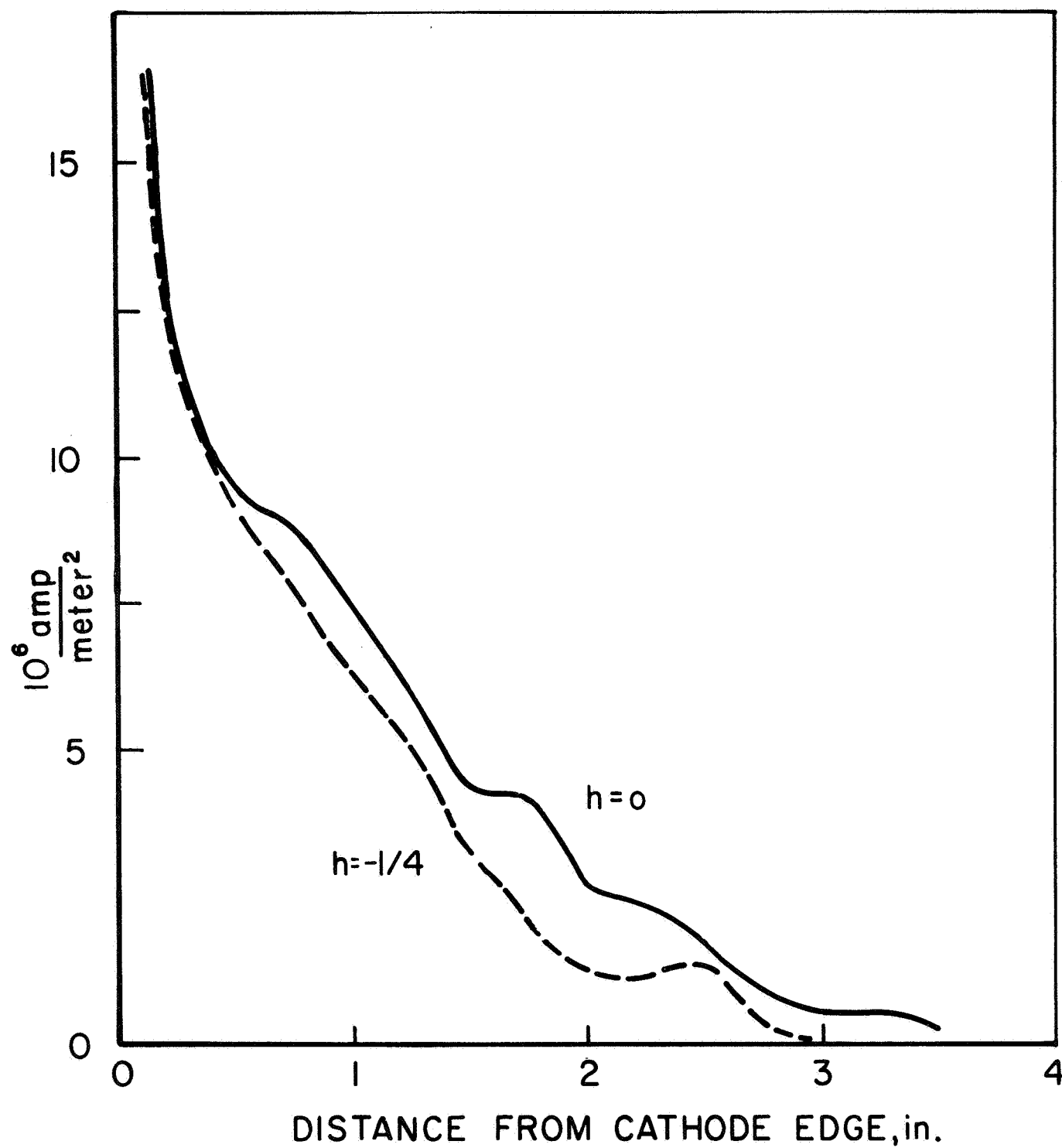
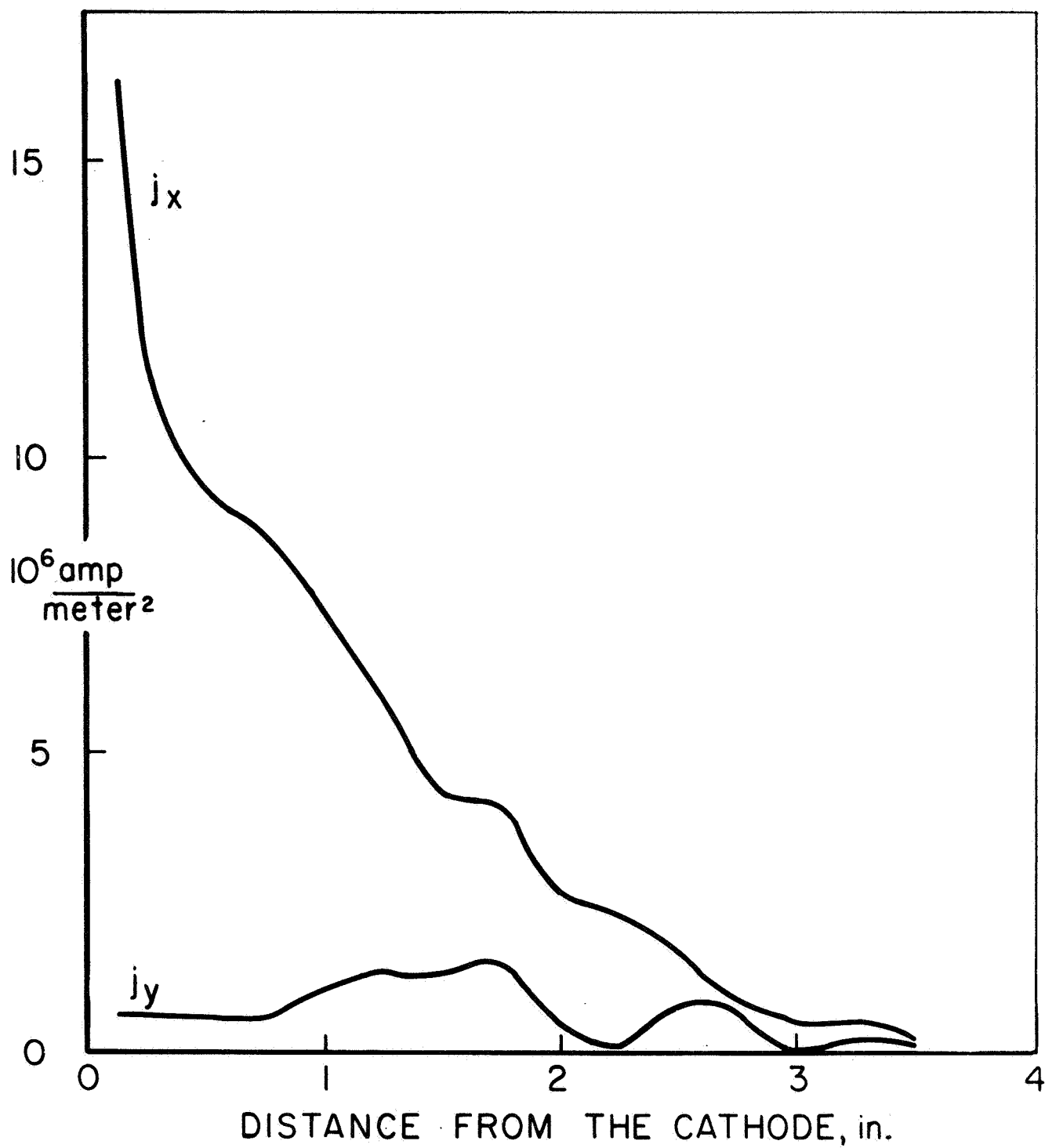


FIGURE 27  
AP 25 - 4498



STREAMWISE CURRENT DENSITY  $J_x$

FIGURE 28  
AP 25-4494



COMPARISON OF STREAMWISE AND  
TRANSVERSE CURRENT DENSITY

direction. Since the probe actually measures a difference in floating potential, the technique must beware sheath drops at the tips if these are comparable with the measured voltage. For an electron temperature of a few volts, this means that we must be concerned with thermal gradients whenever the measured field is on the order of a few hundred volts per meter or less. This is seen to be the case in Fig. 30 over substantial portions of the jet.

We may combine our information on the field structure and current flow with a generalized Ohm's law to deduce some properties of the plasma flow. The problems and assumptions of such a technique have been discussed previously<sup>56</sup> and are complicated here by the presence of the insulator interface. Briefly, if we make the broad assumption that the electrons are acted on only by the fields we have measured and by collisions with ions, we may obtain the streamwise electron velocity in the cathode jet. The essential point here is that, if the transverse current density in the jet is zero, the electrons are not accelerating with respect to the ions, and therefore the electric field in the transverse direction must be balanced by the Lorentz force on the electrons moving in the magnetic field.

The results of such computations are displayed in Fig. 31. Beyond about an inch from the cathode edge our assumption of zero transverse current density becomes unacceptable, so the calculation is terminated. In the early portion of the cathode jet, we see that the electrons tend to accelerate downstream to velocities on the order of  $10^4$  meters per second. If we assume that the primary current conduction in this region is due to electrons, this

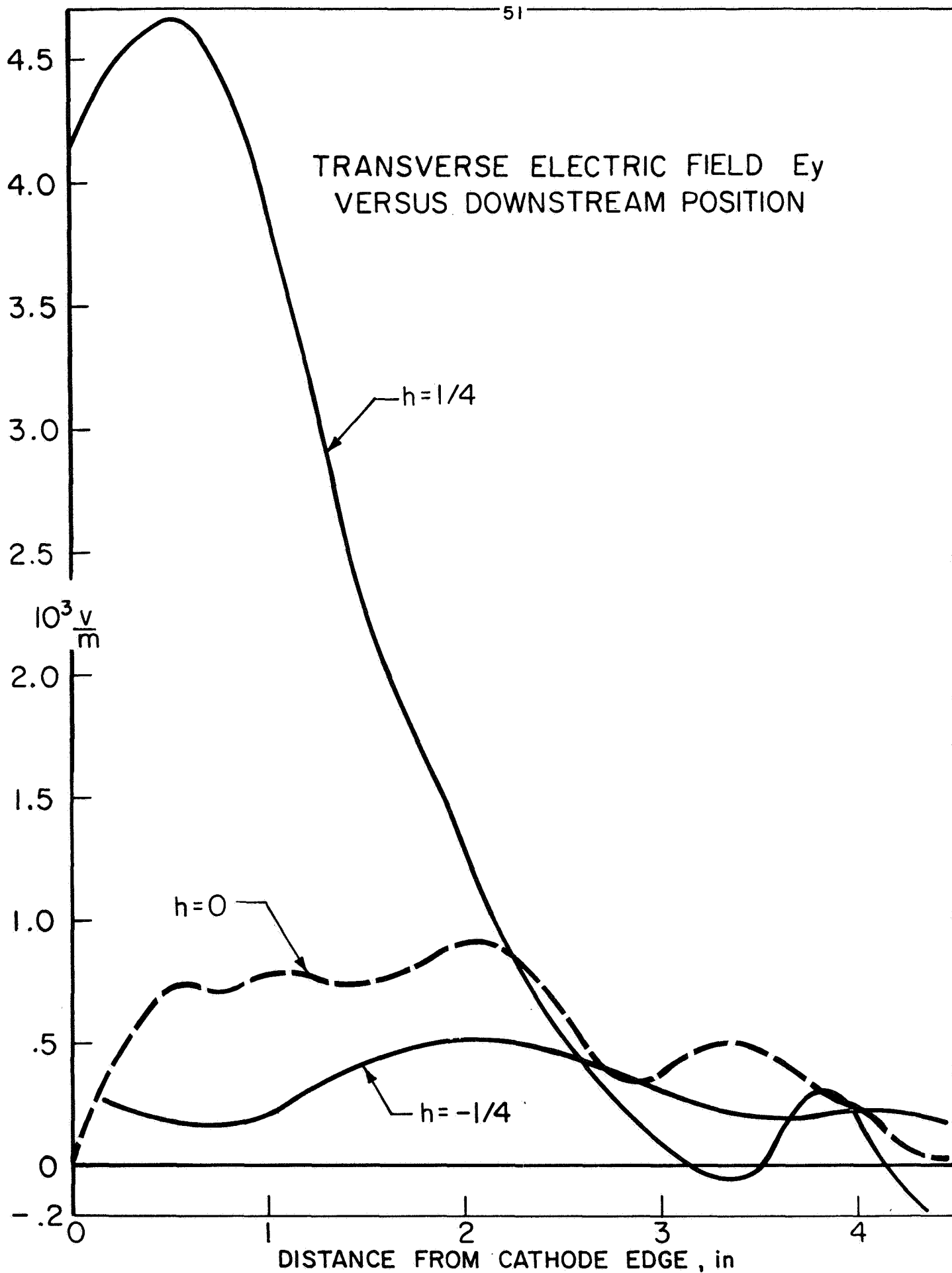


FIGURE 30  
AP 25-4499

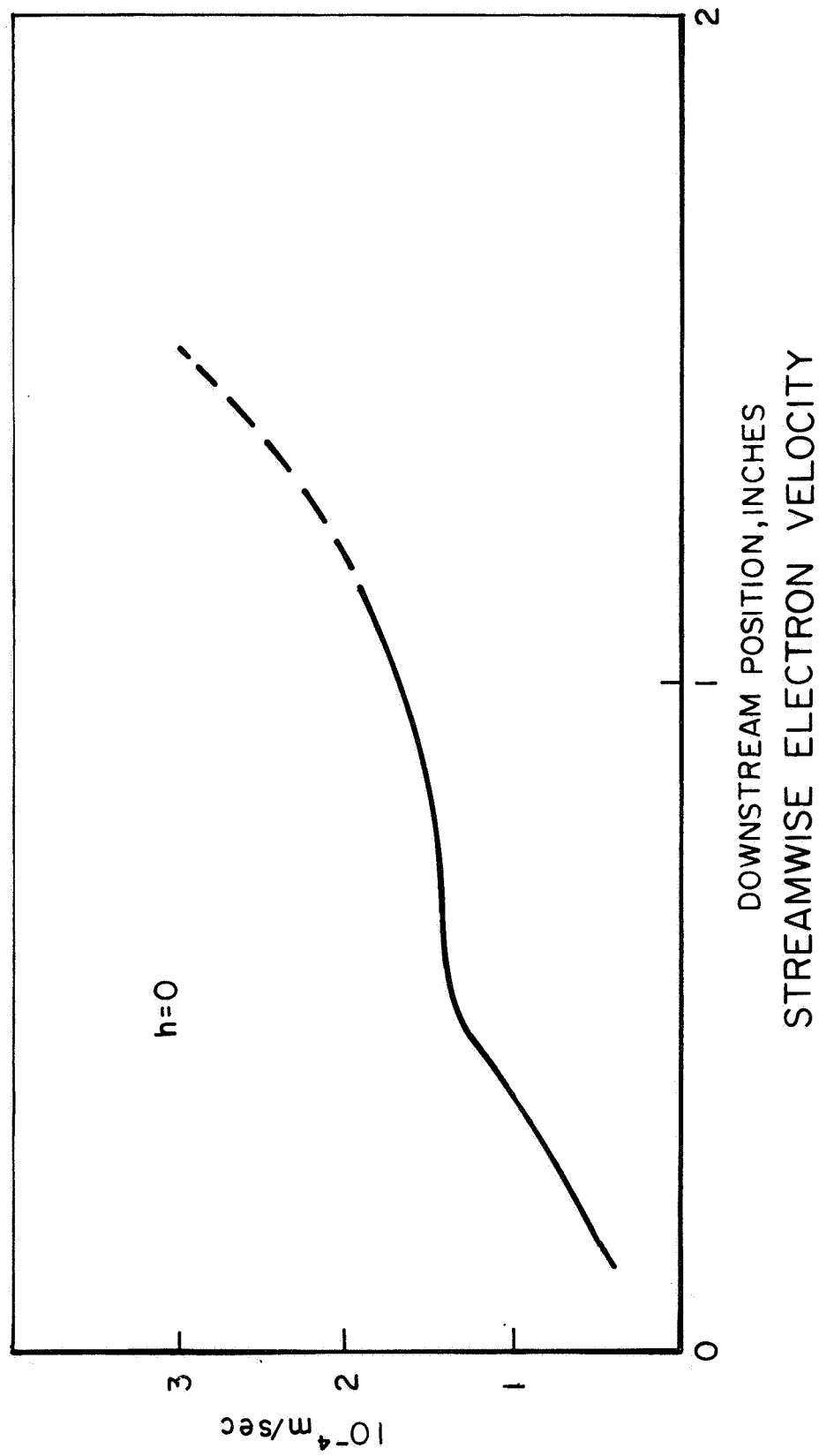


FIGURE 31  
AP 25-4550

implies electron number densities on the order of  $10^{16} \text{ cm}^{-3}$ ; which for an electron temperature of a few volts is about the right level in terms of a high pressure pumped plasma core formed by the magnetic pressure gradient.

Further studies of the cathode jet region of quasi-steady plasma accelerators are in progress, including extension of the above techniques and introduction of other methods into an experimental geometry more appropriate to a thruster.



## V. RADIATIVE PROCESSES IN QUASI-STEADY DISCHARGES — BRUCKNER

Based on information available on MPD arcs and argon-ion lasers, it appears likely that a population inversion in the energy levels of the ionized argon emerging from an MPD accelerator can arise due to the nonequilibrium heating processes existing in the discharge.<sup>A-2,A-3,A-4;75</sup> The implication of this effect to plasma propulsion concerns the associated frozen flow losses for monatomic-ionic species, since a not insignificant fraction of flow energy may be tied up in the relatively high electronic energy levels involved. Further, study of population inversion in the outflows from plasma accelerators can lead to better understanding of the structure of the accelerating zone.

We are currently engaged in a study of this effect in our parallel-plate accelerator operated in the quasi-steady mode with partially insulated electrodes. This device, described fully elsewhere,<sup>67</sup> while simulating many features of the MPD arc, has the advantage of producing an essentially uniform two-dimensional flow. Figure 32 shows typical stabilized enclosed current contours 16  $\mu$ sec after discharge initiation for a 120,000 A x 20  $\mu$ sec current pulse in 100  $\mu$  argon prefill pressure. The bulk of the current across the midplane is conducted within three channel heights downstream of the metal-to-insulation junction. Somewhere in this region occur the processes which may give rise to inverted energy distributions in the first ionic specie of argon. The possible excitation mechanisms are well documented

$p = 100 \text{ m torr}, 120,000 \text{ amp } 20 \mu\text{sec}$

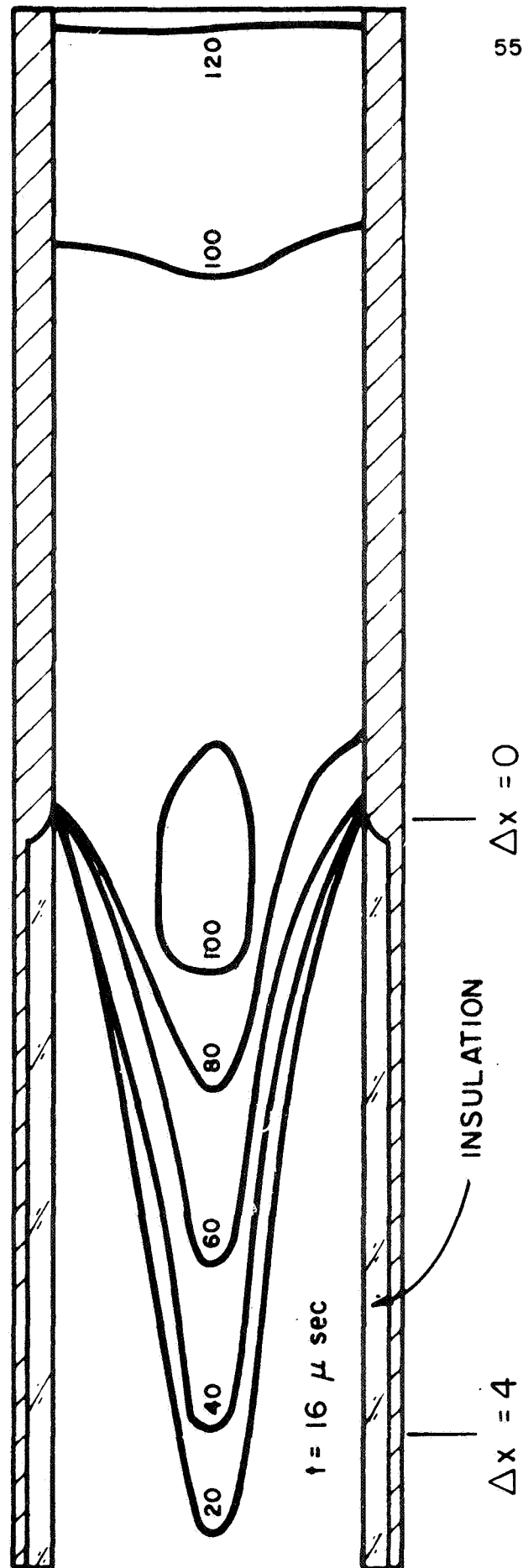


FIGURE 32  
AP 25-4552

ENCLOSED CURRENT CONTOURS IN PARALLEL PLATE ACCELERATOR

in the literature.<sup>A-5 to A-12</sup> The effect, however, may not become observable until farther downstream due to a time delay caused by radiation trapping effects which alter the lifetime of the lower energy levels. Thus, we have begun a systematic probing of the discharge at various positions in and downstream of the stabilized current zone, at various initial pressures and driving currents.

This technique consists of passing through the discharge a beam of radiation of wavelength equal to that of the radiative transition between the levels whose inversion is in question. If the probing radiation is amplified it is evidence of an inverted energy distribution. If, on the other hand, the incident radiation is attenuated we can surmise that a more normal energy distribution exists, possibly even one following Boltzmann statistics. The quantity we are interested in is the fractional amplification (or attenuation) per unit length of plasma, commonly called the gain coefficient,

$\alpha$ . Positive values signify gain, negative values signify absorption.

As the source of the incident radiation we use an argon-ion laser, which radiates power in several spectral lines. For our purposes we have chosen the line at 4880 Å because it has the highest potential gain, typically  $4.0 \times 10^{-3} \text{ cm}^{-1}$  in static laser discharges.<sup>A-9</sup>

Figure 33 shows a schematic diagram of the apparatus. The TRW Model 71-A pulsed laser with pulse width of 40  $\mu\text{sec}$  is placed parallel to the accelerator and its output beam is deflected into the latter by an adjustable first surface mirror. The glass windows, set at Brewster's angle to minimize reflection losses in the plane polarized

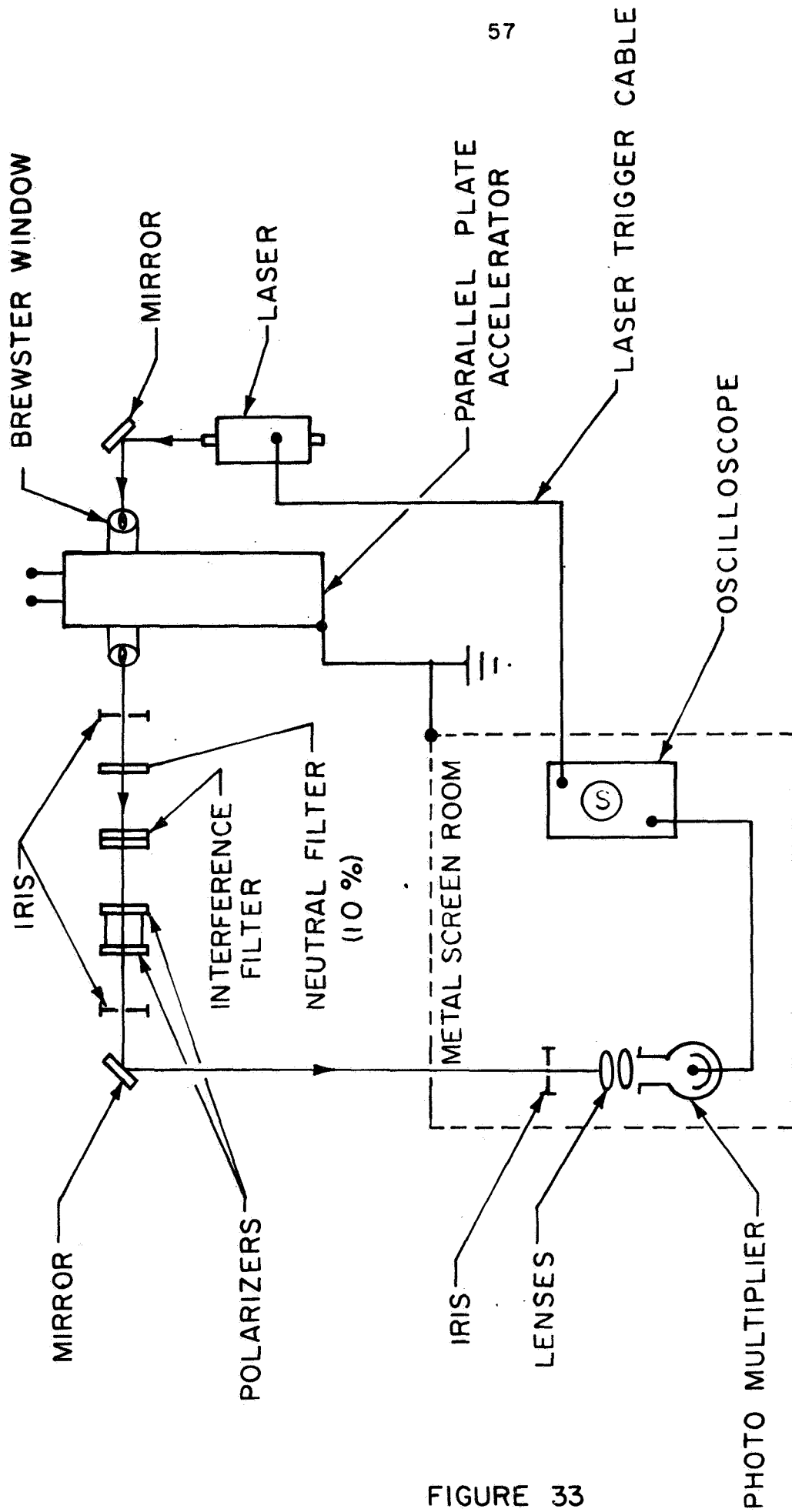


FIGURE 33  
AP 25-4545

SCHEMATIC OF EXPERIMENTAL APPARATUS

laser beam, are mounted on nylon holders which can be inserted into holes drilled into the Plexiglas side-walls at various positions. One pair of holes is located at midplane between the electrodes at  $\Delta x = 4$  in., i.e., 4 in. downstream of the electrode-insulator junction. This location allows probing of the discharge at a point about 1 in. downstream of the location of maximum current density for the 120,000 A pulse. Two other pairs of windows are located at  $\Delta x = 10.5$  in. and  $\Delta x = 17.0$  in., also at midplane.

Upon emerging from the accelerator, the laser beam passes through a 10% neutral density filter, an adjustable iris diaphragm, a 4880 Å, 10.7 Å bandwidth interference filter, and a pair of rotatable polarizers which act as a variable density filter. The light then passes through another iris diaphragm and is reflected into the screen room via another front-surface mirror. The photodetector casing is equipped with an iris diaphragm and a pair of crossed Plexiglas cylindrical lenses which expand the entering beam to cover a significant area of the photocathode of the RCA 1P28 photomultiplier tube. The location of the photomultiplier and its power supply within the screen room is dictated by the severe electrical noise radiated by this parallel-plate geometry discharge.

Two types of experiment have been undertaken with this optical arrangement: (1) monitoring spontaneous 4880 Å emission from the discharge, and (2) measuring the intensity changes inflicted on the laser beam by the discharge. For the spontaneous emission studies the polarizers are adjusted to maximum transparency and the neutral density filter is removed, whereas for the gain measurements the filters are set for near-maximum opacity and the neutral

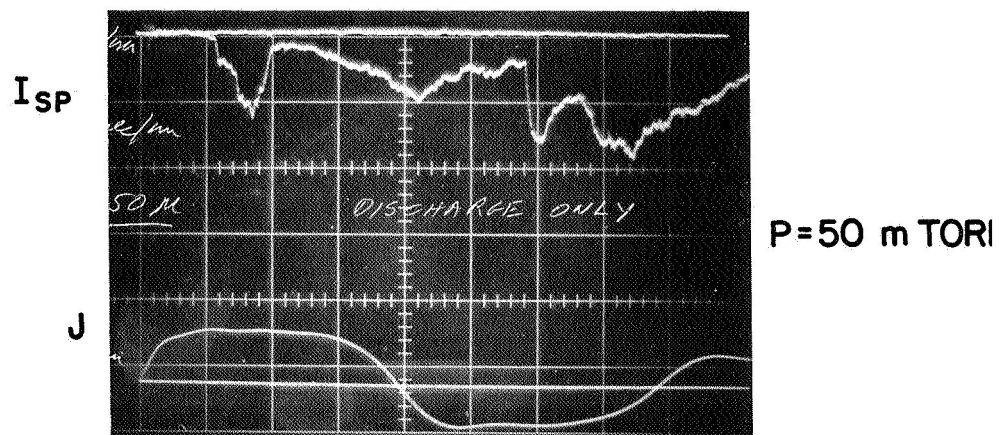
filter is in place. For this latter arrangement the spontaneous emission intensity reaching the phototube was found to be undetectable.

The spontaneous emission was first monitored at 4880 Å at  $\Delta x = 4$  in. for several initial pressures to observe how the line radiation intensity develops in time as the propagating current stabilizes. In Fig. 34 are shown the results for 50  $\mu$ , 100  $\mu$ , and 200  $\mu$ . In each case there is a sharp burst of light followed by radiation of lower intensity and slower variation. Then there is a sudden second jump in intensity, occurring about 30  $\mu$ sec after breakdown. It is postulated that in each case the first spike of light comes from the initially snowplowed plasma swept up by the current sheet prior to stabilization. The following 15 to 20  $\mu$ sec of slowly varying emission can be attributed to the period of quasi-steady operation. (Note that this time period decreases with increasing pressure.) The second sharp rise in intensity may be due to the passage of a current sheet created by a secondary breakdown initiated by current reversal in the external driving circuit, a possibility yet to be verified by magnetic probing.

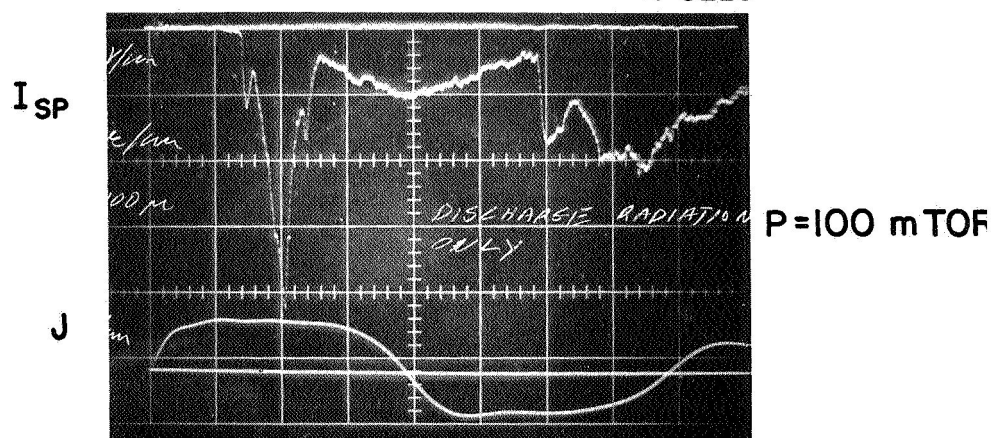
As expected, the intensity of the spontaneous emission increases with pressure. Since the photomultiplier has not been calibrated against a standard source, we cannot at this time determine absolute intensities of spontaneous emission, which would allow calculation of the population density of the upper level of the transition.<sup>A-9</sup>

Gain coefficient measurements have been undertaken at the same location in the discharge. Figure 35 shows the results for various ambient pressures. The oscillograms on the left are records of the laser output only,  $I_0$ ,

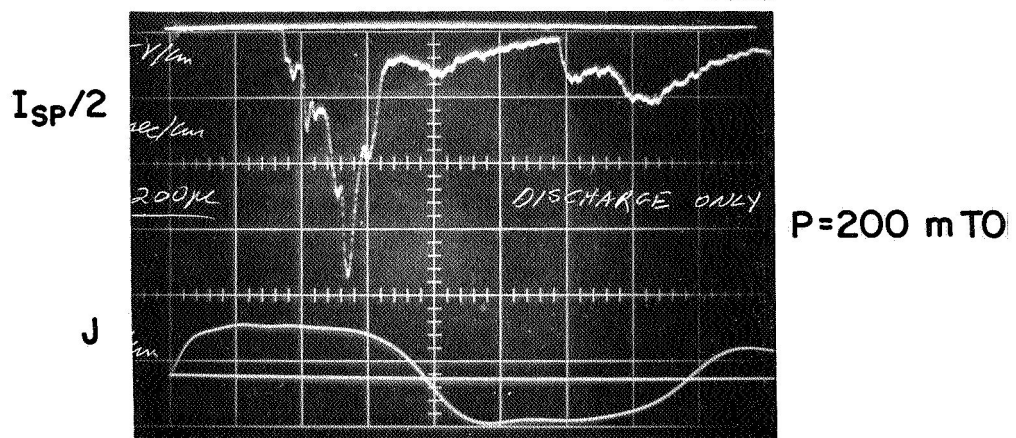
A-3236



A-3226

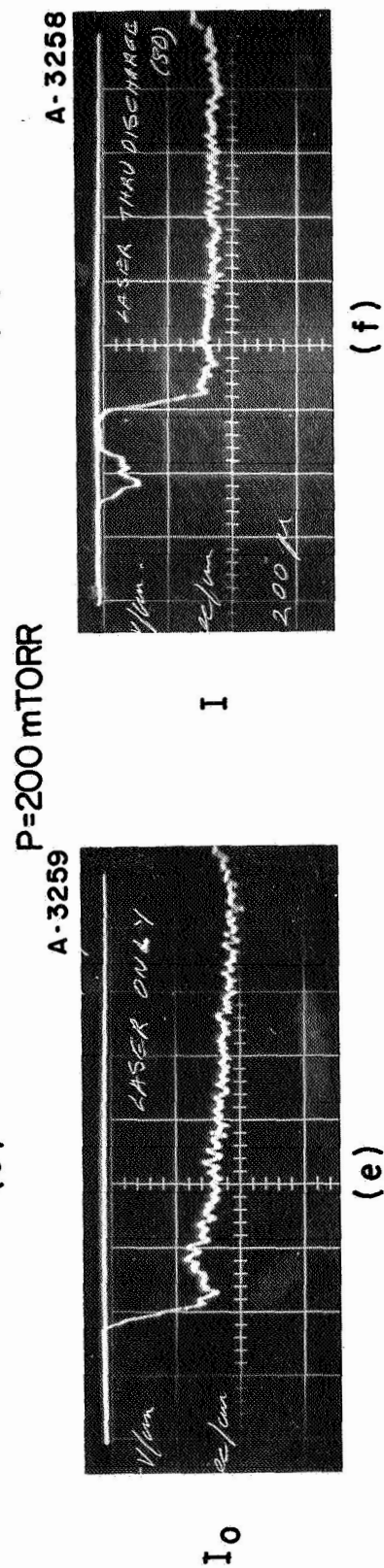
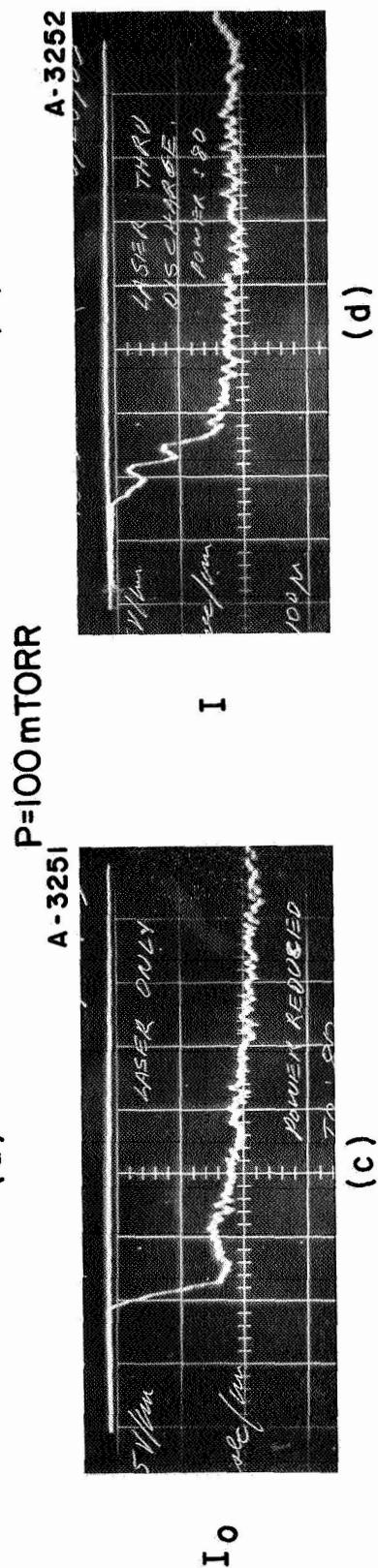
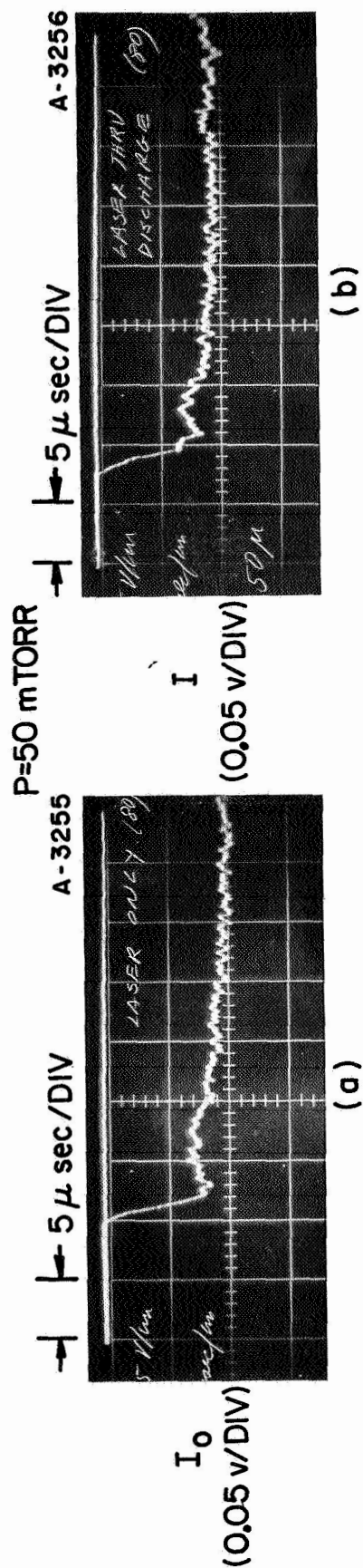


A-3233



→ | ← 5  $\mu$  sec/DIV

INTENSITY OF SPONTANEOUS EMISSION  $I_{SP}$   
AT 4880 Å



LASER INTENSITIES  
MODIFIED BY DISCHARGE

FIGURE 35  
AP 25 · P 297



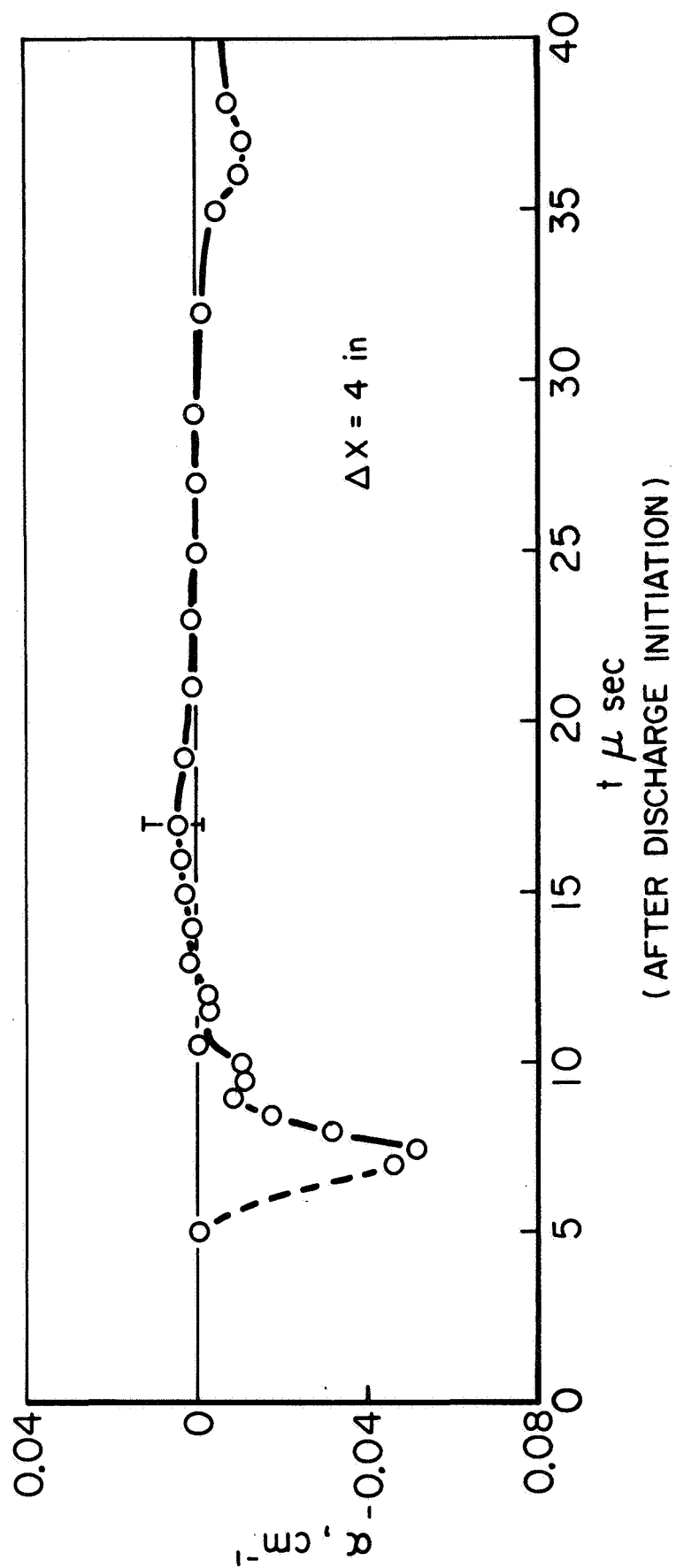
taken either before or after each firing of the accelerator. The pictures on the right are records of the discharge modified laser output, I.

Laser triggering during the discharge was accomplished by the signal from the Rogowski coil used to monitor the total current through the discharge. The approximately 7  $\mu$ sec delay between discharge initiation and the beginning of the laser pulse is a property of the laser discharge itself.<sup>A-14</sup>

Note the region of attenuation shown in each case of Fig. 35. It is slight for the 50  $\mu$  case, increasing in depth and duration with increasing initial pressure. No regions of amplification are immediately obvious. A comparison of these oscillograms with those of Fig. 34 shows that the regions of major attenuation of the laser beam correspond to the initial spike of light which we have attributed to the passage of the snowplowed plasma sheet. The time variation of gain coefficient  $\alpha$  is obtained by using the measured  $I_0$  and I values in the relation

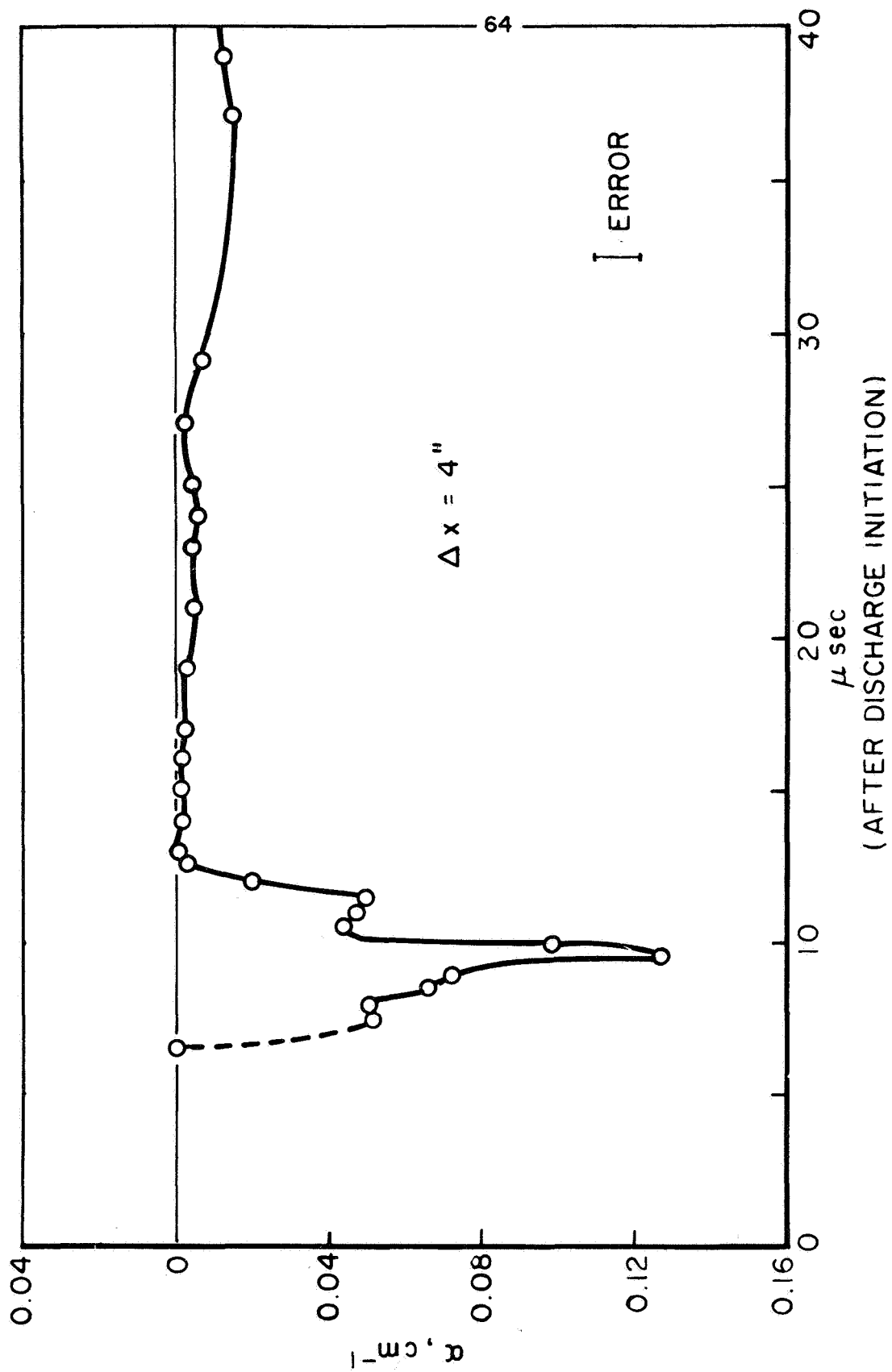
$$\alpha = \frac{1}{L} \ln \frac{I}{I_0}$$

derived from a simple one-dimensional analysis of radiative transfer which neglects spontaneous emission effects.<sup>A-13</sup> The results of this data reduction are presented in Figs. 36, 37, and 38 where the gain,  $\alpha$ , is plotted against time for various initial fill pressures. The gain is found to be negative at all times except for a slight positive excursion in the 50  $\mu$  case, beginning about 13  $\mu$ sec after breakdown and lasting approximately 10  $\mu$ sec. For all three pressures,  $\alpha$  exhibits the expected sharp negative spike



GAIN COEFFICIENT  $\alpha$  FOR 50 mT AMBIENT ARGON

FIGURE 36  
AP 25 · 4541



GAIN COEFFICIENT  $\alpha$  FOR 100 mTorr AMBIENT ARGON

FIGURE 37  
AP 25 · 4542

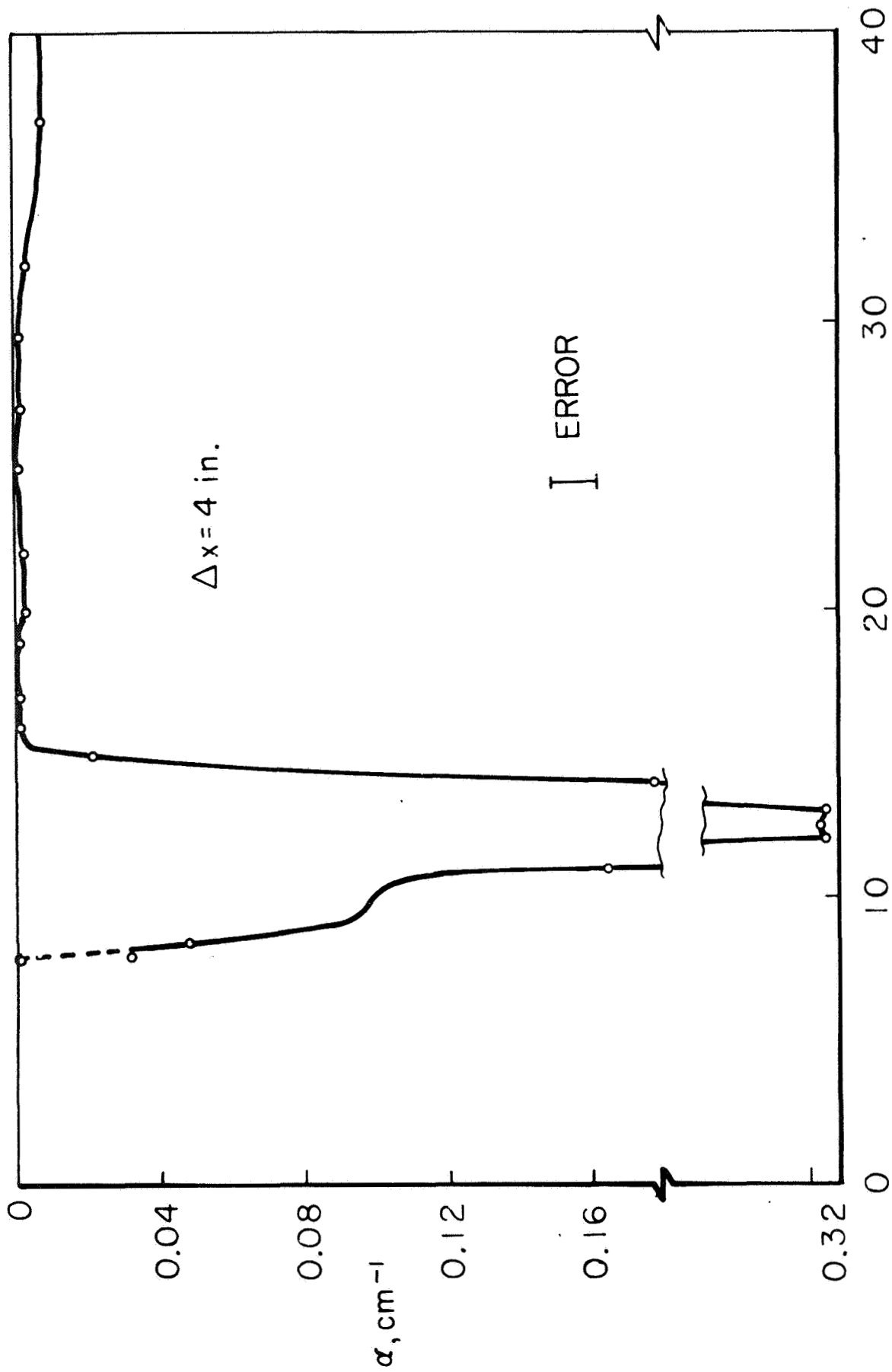


FIGURE 38  
AP 25 · 4551

GAIN COEFFICIENT  $\alpha$  FOR 200 m torr AMBIENT ARGON  
AFTER DISCHARGE INITIATION  
 $t \mu\text{sec}$

associated with the passage of the snowplowed plasma sheet. Its peak value is  $-0.052 \text{ cm}^{-1}$  for  $50 \mu$ ,  $-0.129 \text{ cm}^{-1}$  for  $100 \mu$ , and  $-0.325 \text{ cm}^{-1}$  for  $200 \mu$ . Tests have also been carried out at higher pressures up to 2 mm. In general, the width and magnitude of the negative  $\alpha$  spike increases with pressure.

The dotted portion of each curve is an extrapolation necessitated by the delay between laser triggering and laser output. For both the  $50 \mu$  and  $100 \mu$  cases the snowplowed plasma reached the laser beam location before the laser pulse began. The extrapolation was based on the arrival of the plasma sheet deduced from the spontaneous emission data.

At this stage in the study, the positive value of  $\alpha$  in the  $50 \mu$  case is not beyond doubt because its magnitude is within the experimental error. The error arises not only in reading the oscillograms, but also because the  $I$  and  $I_0$  records are not taken simultaneously. However, the laser amplitude is reproducible from shot-to-shot to within the width of the oscilloscope trace with the superimposed photodetector thermal noise, and the result may well be real. The corresponding peak positive value of  $\alpha$  is  $4.8 \times 10^{-3} \text{ cm}^{-1}$  corresponding to  $\sim 7$  percent amplification through the discharge which agrees with typical static discharge data.<sup>A-9</sup> At the least, our data indicate that the tendency for  $\alpha$  to be positive (i.e., existence of population inversion) increases with decreasing initial pressure at this location in the flow.

The gain coefficient is related to the atomic parameters of the discharge through the following equation:<sup>A-9, A-11</sup>

$$\alpha = \frac{A_{21} \lambda_o^2 \sqrt{\ln 2}}{4 \pi^{3/2} \Delta \nu_o} \left( N_2 - \frac{g_2}{g_1} N_1 \right)$$

where  $N_2, N_1$  are the population number densities of the upper and lower energy levels, respectively of the radiative transition

$g_2, g_1$  are the corresponding energy level degeneracies

$A_{21}$  is the transition probability for spontaneous emission from the upper to the lower level

$\lambda_0$  is the wavelength of the transition

$\Delta\nu_0$  is the full half width of the Doppler

$$\text{broadened line} = \frac{2\nu_0}{c} \sqrt{\frac{2kT}{m}} \ln 2 \text{ sec}^{-1}$$

In a nonequilibrium state, such as during population inversion ( $\alpha > 0$ ), we must determine separately one of the level populations, in addition to  $\alpha$ , in order to calculate the other level population. For example, the value of  $N_2$  could be determined from absolute line intensity measurements of the spontaneous radiation. On the other hand, if there is local thermodynamic equilibrium (LTE), in which case  $\alpha < 0$ , the value of  $\alpha$  is directly proportional to the lower level number density,  $N_1$ . In such a case the knowledge of  $\alpha$  is enough to establish not only the lower level population but also the total number densities of all species present in the discharge plasma, by means of the Boltzmann and Saha equilibrium relations. It is doubtful that LTE exists anywhere in the discharge. First, the electron density in the current stabilized zone is too low for LTE,<sup>A-13,A-15</sup> and snowplowed plasma sheets have been shown to be in a nonequilibrium state.<sup>69</sup> However, on the basis of the high negative values of  $\alpha$  encountered

in the snowplowed plasma sheet we may assume LTE as a first order rough approximation. Making this assumption, the peak number densities of various species in the plasma sheet were calculated for the 100  $\mu$  case. An equilibrium temperature of 3 eV was assumed<sup>69</sup> neutral density was neglected, but species up to the triple ion included. Partition function data were obtained from Refs. A-16 and A-17. The following numerical results were obtained:

$$\begin{array}{lll}
 N_1 & = & 1.40 \times 10^{11} \text{ cm}^{-3} \quad (\text{1st ion lower level}) \\
 N_e & = & 6.45 \times 10^{16} \text{ cm}^{-3} \quad (\text{electrons}) \\
 N_+ & = & 2.72 \times 10^{15} \text{ cm}^{-3} \quad (\text{1st ions}) \\
 N_{++} & = & 2.39 \times 10^{16} \text{ cm}^{-3} \quad (\text{2nd ions}) \\
 N_{+++} & = & 4.71 \times 10^{15} \text{ cm}^{-3} \quad (\text{3rd ions})
 \end{array}$$

These figures are based on the maximum negative observed value of  $\alpha$  at 100  $\mu$ , and thus reflect conditions approximately at the center of the snowplowed plasma sheet at  $\Delta x = 4$  in. and  $t = 9.5$   $\mu$ sec. We see that under our assumptions the main heavy particle component is doubly ionized argon. Furthermore, the concentration of the triply ionized specie is somewhat greater than that of the singly ionized one. If these are accurate reflections of actual conditions in the sheet, they signify that a nonnegligible fraction of discharge energy may be tied up in producing these higher order ionized species. Whether any of this energy is recovered as directed motion when the current sheet stabilizes is not known at this stage.

This snowplowed portion of the flow is not the major

interest in quasi-steady acceleration, but it is the only region for which our present data justifies such a calculation. Once our intensity resolution is improved, a similar procedure should yield the excitation population of the quasi-steady regime.

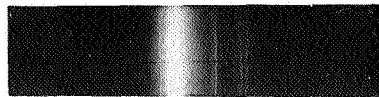
For supplementary information, spectra of the discharge have been taken at  $\Delta x = 4$  in., in the neighborhood of  $4880 \text{ \AA}$ , with a Bausch and Lomb monochromator placed with its entrance slit 2 in. from the Brewster window. The exit slit, opened to its maximum size to reveal approximately a  $150 \text{ \AA}$  bandwidth, is imaged on the focal plane of a 4x5 Polaroid-Graflex camera. The results for these ambient pressures can be seen in Fig. 39. Although these spectra are not time resolved, interesting information may be gleaned from them. Note the bright hydrogen Balmer ( $H_\beta$ ) line at  $4861 \text{ \AA}$  which exhibits the typical Stark broadening effect.<sup>A-13, A-15</sup> Its long wavelength wing overlaps the  $4880 \text{ \AA}$  ArII line to a small extent. Strictly speaking, then, our gain coefficient measurements contain the effect of this  $H_\beta$  overlap. The presence of hydrogen in the discharge tends to increase somewhat the absorptivity of the plasma at  $4880 \text{ \AA}$ , so that if the positive excursion of  $\alpha$  in the  $50 \mu$  case is real, in actual fact the population inversion may be more pronounced than the measured value of  $\alpha$  would indicate.

If we assume that the maximum emission of the  $H_\beta$  line occurs during passage of the snowplowed plasma sheet past the location of the monochromator slit, we can estimate the peak electron density in the sheet by measuring the width of the Stark broadened line. This width was found to be approximately  $26 \pm 5 \text{ \AA}$  for all three initial pressures. Thus, the peak value of  $N_e$  in the discharge,



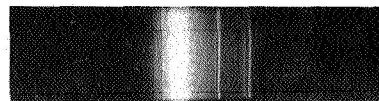
MIDPLANE, SIDE-ON,  $\Delta x = 4''$   
 $5\frac{1}{4}''$  ELECTRODE LENGTH

A 3291



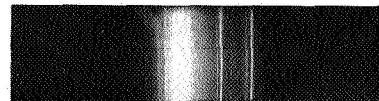
a) P = 50 m TORR

A 3287



b) P = 100 mTORR

A 3294



c) P = 200 mTORR

$4880 \text{ \AA} (\text{Ar II})$  —┐  
 $4861 \text{ \AA} (\text{H}\beta \text{ II})$  —┐  $4765 \text{ \AA} (\text{Ar II})$   
 $4806 \text{ \AA} (\text{Ar II})$  —┐

SPECTROGRAMS OF  $120 \text{ KA} \times 20 \mu\text{sec}$  DISCHARGE

in each case, is about  $4.3 \pm 1.0 \times 10^{16} \text{ cm}^{-3}$ , A-15 which compares favorably with  $N_e = 6.45 \times 10^{16} \text{ cm}^{-3}$  found for the 100  $\mu$  case based on the measured value of  $\alpha$ .

In the future it is planned to perform time resolved measurements on the  $H_\beta$  line to determine whether its intensity indeed reaches a maximum at the same time as the 4880 Å ArII line. The magnitude of the interference of the  $H_\beta$  line on the latter must be determined in order for the measured values of gain coefficient to be meaningful. More reliable values of  $\alpha$  will also become available when the measurements of  $I$  and  $I_0$  are made simultaneously. This will be done by means of a balanced two beam optical method. These techniques will then be applied to the other locations in the discharge and at different initial conditions.

# VI. A 160-KILOJOULE PULSE-FORMING NETWORK FOR QUASI-STEADY PLASMA ACCELERATORS — DI CAPUA

The general characteristics of a power supply for a quasi-steady plasma accelerator were discussed in the previous semi-annual report.<sup>75</sup> Briefly, in a device of useful dimensions, flow stabilization requires a current pulse with a duration of hundreds of microseconds while vigorous electromagnetic acceleration predicates current levels in the order of 100 kA.

A pulse-forming network which stores a charge of 32 coulombs at 10 kV is currently under construction. It consists of four LC ladder networks each assembled from 30 equal sections composed of 500 nH series inductors and 27.1  $\mu$ F shunt capacitors as shown in Fig. 40. Each network, when charged to 10 kV, will deliver into a load, equal to the characteristic impedance of the network, a 37 kA current pulse for 200  $\mu$ sec. The following table summarizes the current pulses available from the networks.

Connection	Current into accelerator	Pulse length
4 lines in series. . . . .	37 kA	880 $\mu$ sec
4 lines in series- parallel . . . . .	74 kA	440 $\mu$ sec
4 lines in parallel. . . . .	148 kA	220 $\mu$ sec

To prevent a voltage reversal in the network due to the mismatch which exists between the network impedance,  $Z_L$ , which ranges from 34 milliohms to 136 milliohms and the accelerator impedance,  $Z_A$ , which is of the order of 6

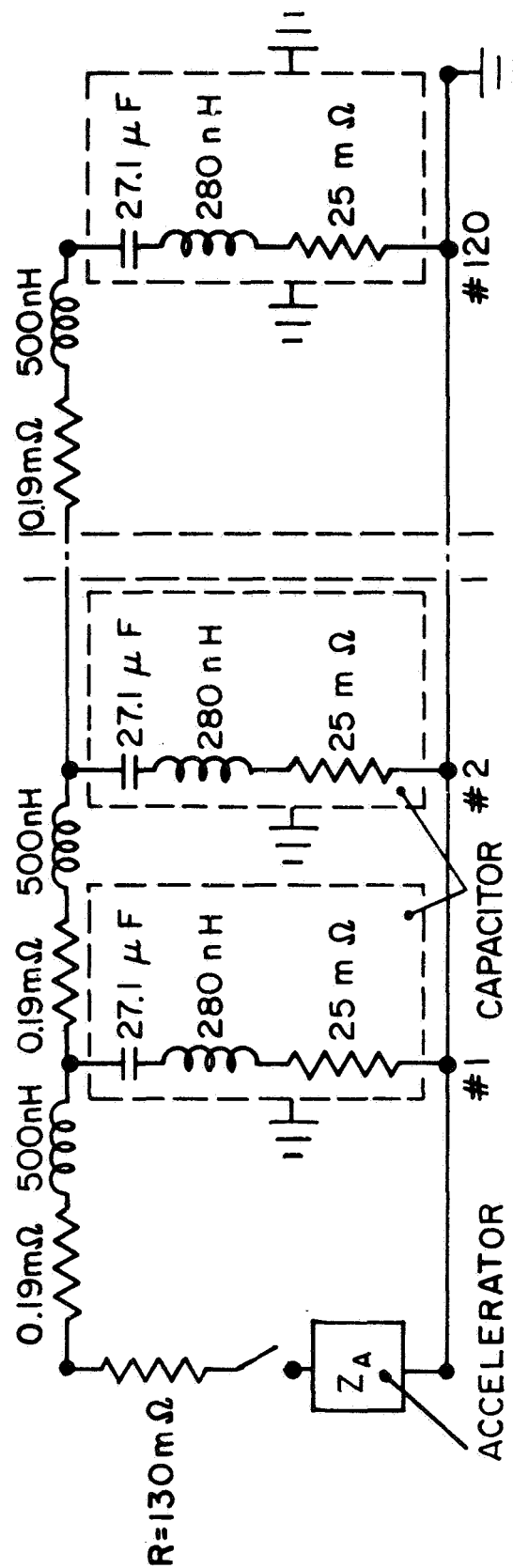


**FIGURE 40**  
**AP 25-4553**

# SCHEMATIC OF PULSE FORMING NETWORK

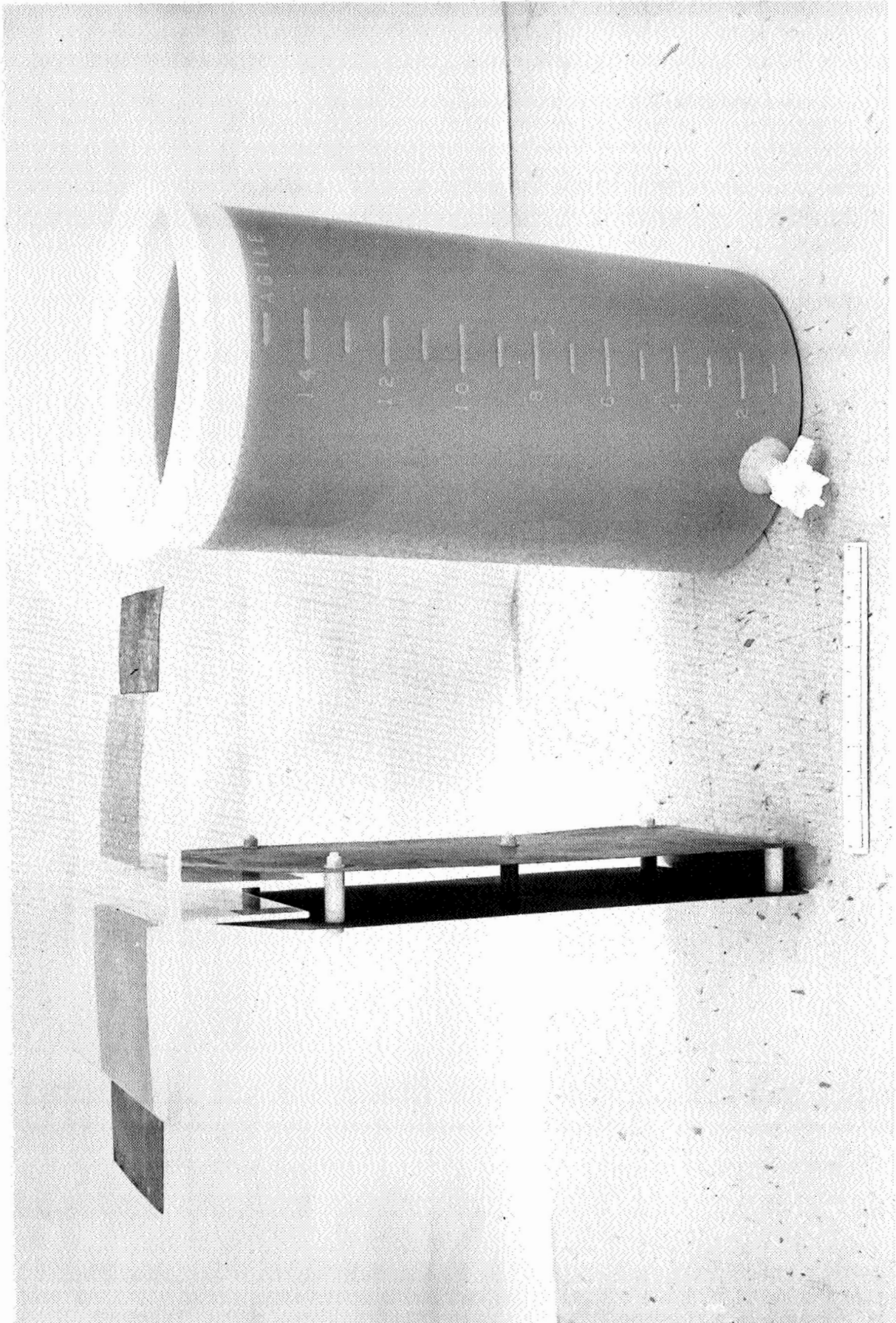
milliohms, a resistor,  $R$ , must be connected in series between the network and the accelerator as shown in Fig. 40. If the value of the resistor is  $R = Z_L - Z_A$  then the load formed by the accelerator and the resistor is effectively matched to the network and no appreciable voltage reversal should occur in the network when it is discharged across the load. This absence of voltage reversal has several benefits. First, the waveform is ideal for the accelerator experiments; second, the capacitors endure considerably less stress; finally, any transients occurring in the network due to a capacitor failure while the network is charged at high voltage will be promptly dissipated in the load resistor, thereby increasing the safety of operation.

Each of the four ladder networks will be equipped with a 130 milliohm electrolytic resistor<sup>A-18</sup> which will be connected between the high-voltage lead of the network and the high-voltage terminal of the accelerator as shown in Fig. 41. The resistor consists of two copper plates 1/32-in. thick, approximately 13" x 25", with a separation of 2 in. suspended in a polyethylene tub filled with 16 gallons of electrolyte. The electrolyte is a 0.26 molar aqueous cupric sulphate solution with a resistivity of 110 ohms-cm at 25 °C. A prototype, shown in Fig. 42, has performed adequately when tested at full voltage (10 kV) with one of the smaller capacitor banks. Besides its simplicity of operation and small initial cost, this type of resistor is particularly advantageous for this application due to the enormous energy absorption capacity of the liquid. It is estimated that the temperature of the solution will rise 0.6 °C during the 37 kA x 880  $\mu$ sec pulse. Since the series-parallel connection of the lines will involve two resistors, while



FIGURE 41  
AP25 P303





VIEW OF 130  $\Omega$  ELECTROLYTIC RESISTOR

the parallel connection will involve four, their temperature rise will be correspondingly less.

The capacitor bank will be loaded with a three-phase, voltage-doubler power supply which is being built to our specifications by DEL Electronics Inc. of Mt. Vernon, New York. This power supply will automatically load the bank to 10 kV in approximately one minute. The high-voltage section will be located adjacent to the network, thereby avoiding any proximity of the operator to high-voltage elements.

A flexible low inductance connection between the resistors and the accelerator switch will be made with five parallel RG 14-A/U coaxial cables. The switch will be of the gas-triggered variety,<sup>18</sup> similar to that currently utilized in the 8-in. pinch machines.

Delivery of the power supply is expected late in July, at which time the pulse-forming network will be completed and testing will begin.



## PROJECT REFERENCES

1. Proposed Studies of the Formation and Stability of an Electromagnetic Boundary in a Pinch, proposal for NASA Research Grant NsG-306-63, Princeton University, 5 March 1962.
2. Pulsed Electromagnetic Gas Acceleration, 1st semi-annual progress report for the period 1 July 1962 to 31 December 1962, Princeton University Aeronautical Engineering Report No. 634, January 1963.
3. Jahn, R. G. and W. F. von Jaskowsky, "The Plasma Pinch as a Gas Accelerator," A.I.A.A. Electric Propulsion Conference, Colorado Springs, Colo., 11-13 March 1963, A.I.A.A. Preprint 63013.
4. Pulsed Electromagnetic Gas Acceleration, 2nd semi-annual progress report for the period 1 January 1963 to 30 June 1963, Princeton University Aeronautical Engineering Report No. 634a, June 1963.
5. Jahn, R. G. and W. F. von Jaskowsky, "Structure of a Large-radius Pinch Discharge," A.I.A.A. Journal 1, 8, 1809-1814 (1963).
6. Jahn, R. G., W. F. von Jaskowsky, and A. L. Casini, "Gas-triggered Inverse Pinch Switch," The Review of Scientific Instruments 34, 12, 1439-1440 (1963).
7. Jahn, R. G., W. F. von Jaskowsky, and A. L. Casini, "A Gas-triggered Inverse Pinch Switch," technical note, Princeton University Aeronautical Engineering Report No. 660, August 1963.
8. Jahn, R. G. and W. F. von Jaskowsky, "Pulsed Electromagnetic Gas Acceleration," 4th NASA Intercenter Conference on Plasma Physics, Washington, D. C., 2-4 December 1963, Paper No. II, 8.
9. Pulsed Electromagnetic Gas Acceleration, 3rd semi-annual progress report for the period 1 July 1963 to 31 December 1963, Princeton University Aeronautical Engineering Report No. 634b, December 1963.
10. Jahn, R. G. and W. F. von Jaskowsky, "Current Distributions in Large-radius Pinch Discharges," A.I.A.A. Aerospace Sciences Meeting, New York, 20-22 January 1964, A.I.A.A. Preprint 64-25.

## PROJECT REFERENCES-contd.

11. Jahn, R. G. and W. F. von Jaskowsky, "Current Distributions in Large-radius Pinch Discharges," A.I.A.A. Bulletin 1, 1, 12 (1964).
12. Jahn, R. G. and W. F. von Jaskowsky, "Current Distributions in Large-radius Pinch Discharges," A.I.A.A. Journal 2, 10, 1749-1753 (1964).
13. Pulsed Electromagnetic Gas Acceleration, renewal proposal for 15-months extension of NASA Research Grant NsG-306-63, Princeton University, 15 January 1964.
14. Pulsed Electromagnetic Gas Acceleration, 4th semi-annual progress report for the period 1 January 1964 to 30 June 1964, Princeton University Aerospace and Mechanical Sciences Report No. 634c, July 1964.
15. Jahn, R. G., W. F. von Jaskowsky, and A. L. Casini, "Gas-triggered Pinch Discharge Switch," Princeton University Aerospace and Mechanical Sciences Technical Note No. 101, July 1964.
16. Corr, J. M., "Double Probe Studies in an 8" Pinch Discharge," M.S.E. thesis, Department of Aerospace and Mechanical Sciences, Princeton University, Princeton, N. J., 1964.
17. Jahn, R. G. and W. F. von Jaskowsky, "Exhaust of a Pinched Plasma From an Axial Orifice," A.I.A.A. Bulletin 1, 10, 570 (1964).
18. Jahn, R. G., W. F. von Jaskowsky, and A. L. Casini, "Gas-triggered Pinch Discharge Switch," The Review of Scientific Instruments 36, 1, 101-102 (1965).
19. Jahn, R. G. and W. F. von Jaskowsky, "Exhaust of a Pinched Plasma From an Axial Orifice," A.I.A.A. 2nd Aerospace Sciences Meeting, New York, 25-27 January 1965, A.I.A.A. Paper 65-92.
20. Jahn, R. G., W. F. von Jaskowsky, and R. L. Burton, "Ejection of a Pinched Plasma From an Axial Orifice," A.I.A.A. Journal 3, 10, 1862-1866 (1965).
21. Pulsed Electromagnetic Gas Acceleration, 5th semi-annual progress report for the period 1 July 1964 to 31 December 1964, Princeton University Aerospace and Mechanical Sciences Report No. 634d, January 1965.

## PROJECT REFERENCES-contd.

22. Jahn, R. G. and N. A. Black, "On the Dynamic Efficiency of Pulsed Plasma Accelerators," A.I.A.A. Journal 3, 6, 1209-1210 (1965).
23. Black, N. A., "Linear Pinch Driven by a High-current Pulse-forming Network," A.I.A.A. Bulletin 2, 6, 309 (1965).
24. Wright, E. S., "The Design and Development of Rogowski Coil Probes for Measurement of Current Density Distribution in a Plasma Pinch," M.S.E. thesis, Department of Aerospace and Mechanical Sciences, Princeton University, Princeton, N. J., 1965.
25. Wright, E. S. and R. G. Jahn, "The Design and Development of Rogowski Coil Probes for Measurement of Current Density Distribution in a Plasma Pinch," Princeton University Aerospace and Mechanical Sciences Report No. 740, June 1965.
26. Pulsed Electromagnetic Gas Acceleration, renewal proposal for 12-months extension of NASA Research Grant NsG-306-63, Princeton University, 7 June 1965.
27. Black, N. A., "Linear Pinch Driven by a High-current Pulse-forming Network," A.I.A.A. 2nd Annual Meeting, San Francisco, Calif., 26-29 July 1965, A.I.A.A. Paper 65-336.
28. Jahn, R. G. and E. S. Wright, "Miniature Rogowski Coil Probes for Direct Measurement of Current Density Distribution in Transient Plasmas," The Review of Scientific Instruments 36, 12, 1891-1892 (1965).
29. Pulsed Electromagnetic Gas Acceleration, 6th semi-annual progress report for the period 1 January 1965 to 30 June 1965, Princeton University Aerospace and Mechanical Sciences Report No. 634e, July 1965.
30. Jahn, R. G. and A. C. Ducati, "Design and Development of a Thermo-ionic Electric Thrustor," 5QS 085-968 Interim Report, NASA Contract NASw-968, Giannini Scientific Corporation, August 1965.
31. Rowell, G. A., "Cylindrical Shock Model of the Plasma Pinch," M.S.E. thesis, Department of Aerospace and Mechanical Sciences, Princeton University, Princeton, N. J., 1966.

## PROJECT REFERENCES-contd.

32. Pulsed Electromagnetic Gas Acceleration, 7th semi-annual progress report for the period 1 July 1965 to 31 December 1965, Princeton University Aerospace and Mechanical Sciences Report No. 634f, January 1966.
33. Rowell, G. A. and R. G. Jahn, "Cylindrical Shock Model of the Plasma Pinch," Princeton University Aerospace and Mechanical Sciences Report No. 742, February 1966.
34. Burton, R. L. and R. G. Jahn, "Electric and Magnetic Field Distributions in a Propagating Current Sheet," A.I.A.A. Bulletin 3, 1, 35 (1966).
35. Burton, R. L. and R. G. Jahn, "Electric and Magnetic Field Distributions in a Propagating Current Sheet," A.I.A.A. 5th Electric Propulsion Conference, San Diego, Calif., 7-9 March 1966, A.I.A.A. Paper 66-200.
36. Black, N. A., "Pulse-forming Networks for Propulsion Research," Proceedings of the 7th Symposium on Engineering Aspects of Magnetohydrodynamics, Princeton University, Princeton, N. J., March 30-April 1, 1966, pp. 10-11.
37. Black, N. A., "Dynamics of a Pinch Discharge Driven by a High-current Pulse-forming Network," Ph.D. thesis, Department of Aerospace and Mechanical Sciences, Princeton University, Princeton, N. J., 1966.
38. Black, N. A. and R. G. Jahn, "Dynamics of a Pinch Discharge Driven by a High-current Pulse-forming Network," Princeton University Aerospace and Mechanical Sciences Report No. 778, May 1966.
39. Jahn, R. G., "Pulsed Plasma Propulsion," Proceedings of the 5th NASA Intercenter and Contractors Conference on Plasma Physics, Washington, D. C., 24-26 May 1966, part V, pp. 75-81.
40. Pulsed Electromagnetic Gas Acceleration, renewal proposal for 24-months extension of NASA Research Grant NsG-306-63, Princeton University, 25 May 1966.
41. Ducati, A. C., R. G. Jahn, E. Muehlberger, and R. P. Treat, "Design and Development of a Thermo-ionic Electric Thrustor," FR-056-968 Final Report, NASA CR-54703, Giannini Scientific Corporation, May 1966.
42. Jahn, R. G. and K. E. Clark, "A Large Dielectric Vacuum Facility," A.I.A.A. Journal 4, 6, 1135 (1966).

## PROJECT REFERENCES-contd.

43. Burton, R. L., "Structure of the Current Sheet in a Pinch Discharge," Ph.D. thesis, Department of Aerospace and Mechanical Sciences, Princeton University, Princeton, N. J., 1966.
44. Burton, R. L. and R. G. Jahn, "Structure of the Current Sheet in a Pinch Discharge," Princeton University Aerospace and Mechanical Sciences Report No. 783, September 1966.
45. Pulsed Electromagnetic Gas Acceleration, 8th semi-annual progress report for the period 1 January 1966 to 30 June 1966, Princeton University Aerospace and Mechanical Sciences Report No. 634g, July 1966.
46. Jahn, R. G., "Electromagnetic Propulsion," *Astronautics and Aeronautics* 4, 69 (1966).
47. John, R. R., S. Bennett, and R. G. Jahn, "Current Status of Plasma Propulsion," A.I.A.A. 2nd Propulsion Joint Specialist Conference, Colorado Springs, Colo., 13-17 June 1966, A.I.A.A. Paper 66-565.
48. Ellis, W. R., Jr., "An Investigation of Current Sheet Structure in a Cylindrical Z-Pinch," Ph.D. thesis, Department of Aerospace and Mechanical Sciences, Princeton University, Princeton, N. J., 1967.
49. Pulsed Electromagnetic Gas Acceleration, 9th semi-annual progress report for the period 1 July 1966 to 31 December 1966, Princeton University Aerospace and Mechanical Sciences Report No. 634h, January 1967.
50. Pulsed Electromagnetic Gas Acceleration, 10th semi-annual progress report for the period 1 January 1967 to 30 June 1967, Princeton University Aerospace and Mechanical Sciences Report No. 634i, July 1967.
51. Ellis, W. R., Jr. and R. G. Jahn, "An Investigation of Current Sheet Structure in a Cylindrical Z-Pinch," Princeton University Aerospace and Mechanical Sciences Report No. 805, July 1967.
52. Clark, K. E. and R. G. Jahn, "The Magnetoplasma-dynamic Arc," *Astronautica Acta* 13, 4, 315-325 (1967).
53. Jahn, R. G., "The MPD Arc," NASA Contract NASw-1513, Giannini Scientific Corporation, August 1967.

## PROJECT REFERENCES-contd.

54. Eckbreth, A. C., K. E. Clark, and R. G. Jahn, "Current Pattern Stabilization in Pulsed Plasma Accelerators," A.I.A.A. Bulletin 4, 9, 433 (1967).
55. Clark, K. E., A. C. Eckbreth, and R. G. Jahn, "Current Pattern Stabilization in Pulsed Plasma Accelerators," A.I.A.A. Electric Propulsion and Plasmadynamics Conference, Colorado Springs, Colo., 11-13 September 1967, A.I.A.A. Paper 67-656.
56. Pulsed Electromagnetic Gas Acceleration, 11th semi-annual progress report for the period 1 July 1967 to 31 December 1967, Princeton University Aerospace and Mechanical Sciences Report No. 634j, January 1968.
57. Ducati, A. C., R. G. Jahn, E. Muehlberger, and R. P. Treat, "Exploratory Electromagnetic Thruster Research," TR 117-1513 Annual Report, NASA CR 62047, Giannini Scientific Corporation, February 1968.
58. Jahn, R. G., Physics of Electric Propulsion (McGraw-Hill Book Company, New York, 1968).
59. Burton, R. L. and R. G. Jahn, "Acceleration of Plasma by a Propagating Current Sheet," The Physics of Fluids 11, 6, 1231-1237 (1968).
60. Pulsed Electromagnetic Gas Acceleration, renewal proposal for step-funding of NASA Grant NGR 31-001-005 for the period 1 October 1968 to 30 September 1971, Princeton University, 1 June 1968.
61. Pulsed Electromagnetic Gas Acceleration, 12th semi-annual progress report for the period 1 January 1968 to 30 June 1968, Princeton University Aerospace and Mechanical Sciences Report No. 634k, July 1968.
62. Wilbur, P. J., "Energy Transfer From a Pulse Network to a Propagating Current Sheet," Ph.D. thesis, Department of Aerospace and Mechanical Sciences, Princeton University, Princeton, N. J., 1968.
63. Wilbur, P. J. and R. G. Jahn, "Energy Transfer From a Pulse Network to a Propagating Current Sheet," Princeton University Aerospace and Mechanical Sciences Report No. 846, September 1968.
64. Ducati, A. C., R. G. Jahn, E. Muehlberger, and R. P. Treat, "Exploratory Electromagnetic Thruster Research, Phase II," 2SS108-1513 Interim Report, NASA Contract NASw-1513, Giannini Scientific Corporation, October 1968.

## PROJECT REFERENCES-contd.

65. Eckbreth, A. C., K. E. Clark, and R. G. Jahn, "Current Pattern Stabilization in Pulsed Plasma Accelerators," A.I.A.A. Journal 6, 11, 2125-2132 (1968).
66. Eckbreth, A. C., "Current Pattern and Gas Flow Stabilization in Pulsed Plasma Accelerators," Ph.D. thesis, Department of Aerospace and Mechanical Sciences, Princeton University, Princeton, N. J., 1968.
67. Eckbreth, A. C. and R. G. Jahn, "Current Pattern and Gas Flow Stabilization in Pulsed Plasma Accelerators," Princeton University Aerospace and Mechanical Sciences Report No. 857, December 1968.
68. York, T. M., "Pressure Distribution in the Structure of a Propagating Current Sheet," Ph.D. thesis, Department of Aerospace and Mechanical Sciences, Princeton University, Princeton, N. J., 1968.
69. York, T. M. and R. G. Jahn, "Pressure Distribution in the Structure of a Propagating Current Sheet," Princeton University Aerospace and Mechanical Sciences Report No. 853, December 1968.
70. Eckbreth, A. C. and R. G. Jahn, "Current Pattern and Gas Flow Stabilization in Pulsed Plasma Accelerators," A.I.A.A. Bulletin 5, 12, 730 (1968).
71. Wilbur, P. J. and R. G. Jahn, "Energy Transfer from a Pulse Network to a Propagating Current Sheet," A.I.A.A. Bulletin 5, 12, 730 (1968).
72. Ellis, W. R. and R. G. Jahn, "Ion Density and Current Distributions in a Propagating Current Sheet, Determined by Microwave Reflection Technique," Report No. CLM-P-187, Culham Laboratory, Abingdon, Berkshire, Great Britain, December 1968.
73. Eckbreth, A. C. and R. G. Jahn, "Current Pattern and Gas Flow Stabilization in Pulsed Plasma Accelerators," A.I.A.A. 7th Aerospace Sciences Meeting, New York, 20-22 January 1969, A.I.A.A. Paper 69-112.
74. Wilbur, P. J. and R. G. Jahn, "Energy Transfer from a Pulse Network to a Propagating Current Sheet," A.I.A.A. 7th Aerospace Sciences Meeting, New York, 20-22 January 1969, A.I.A.A. Paper 69-113.

## PROJECT REFERENCES-contd.

75. Pulsed Electromagnetic Gas Acceleration, 13th semi-annual progress report for the period 1 July 1968 to 31 December 1968, Princeton University Aerospace and Mechanical Sciences Report No. 634~~8~~, January 1969.
76. Clark, K. E., "Quasi-steady Plasma Acceleration," Ph.D. thesis, Department of Aerospace and Mechanical Sciences, Princeton University, Princeton, N. J., 1969.
77. York, T. M. and R. G. Jahn, "Pressure Distribution in the Structure of a Propagating Current Sheet," A.I.A.A. Bulletin 6, 2, 75 (1969).
78. Clark, K. E. and R. G. Jahn, "Quasi-steady Plasma Acceleration," A.I.A.A. Bulletin 6, 2, 75 (1969).
79. York, T. M. and R. G. Jahn, "Pressure Distribution in the Structure of a Propagating Current Sheet," A.I.A.A. 7th Electric Propulsion Conference, Williamsburg, Va., 3-5 March 1969, A.I.A.A. Paper 69-264.
80. Clark, K. E. and R. G. Jahn, "Quasi-steady Plasma Acceleration," A.I.A.A. 7th Electric Propulsion Conference, Williamsburg, Va., 3-5 March 1969, A.I.A.A. Paper 69-267.
81. Jahn, R. G. and W. R. Mickelsen, "Electric Propulsion Notebook," A.I.A.A. Professional Study Series, Williamsburg, Va., 1-2 March 1969.
82. Boyle, M. J., "Plasma Velocity Measurements with Electric Probes," B.S.E. thesis, Department of Aerospace and Mechanical Sciences, Princeton University, Princeton, N. J., April 1969.
83. Boyle, M. J., "Plasma Velocity Measurements with Electric Probes," A.I.A.A. Northeastern Regional Student Conference, Princeton University, Princeton, N. J., 9-10 May 1969, Paper No. 4.
84. Mickelsen, W. R. and R. G. Jahn, "Status of Electric Propulsion," A.I.A.A. Bulletin 6, 6, 257 (1969)
85. Mickelsen, W. R. and R. G. Jahn, "Status of Electric Propulsion," A.I.A.A. 5th Propulsion Joint Specialist Conference, AF Academy, Colo., 9-13 June 1969, A.I.A.A. Paper 69-497.



## PROJECT REFERENCES-contd.

86. Ducati, A. C. and R. G. Jahn, "Electron Beam from a Magnetoplasmadynamic Arc," The Physics of Fluids 12, 6, 1177-1181 (1969).

## GENERAL REFERENCES

- A-1. Liebing, A.: "Probe for the Measurement of Ion Velocity Distributions in Low Density Plasma Beams," A.I.A.A. Electric Propulsion and Plasmadynamics Conference, Colorado Springs, Colo., September 1967, A.I.A.A. Paper 67-706.
- A-2. Leonard, L. R. and A. Hertzberg: "Plasma Lasers Utilizing the MPD Arc," Conf. on Gas Lasers, NASA Headquarters, Washington, D. C., Summer 1968.
- A-3. Russel, G. R. and K. G. Harstad: "Feasibility of Magnetogasdynamic Lasers Utilizing Faraday Generators and Accelerators," Conf. on Gas Lasers, NASA Headquarters, Washington, D. C., Summer 1968.
- A-4. Wilson, J.: "Nitrogen Laser Action in a Supersonic Flow," Appl. Phys. Let. 8, 7 (1966).
- A-5. Demtröder, W.: "Excitation Mechanisms of Pulsed Argon Ion Lasers at 4880 Å," Phys. Let. 22, 4, 436-438, Sept. 1, 1966.
- A-6. Gordon, E. F. et al.: "Excitation Mechanisms of the Argon-Ion Laser," Physics of Quantum Electronics, (McGraw-Hill Book Company, New York, 1966), p. 664.
- A-7. Statz, H., F. A. Horrigan, et al.: "Transition Probabilities, Lifetimes, and Related Considerations in Ionized Argon Lasers," Physics of Quantum Electronics, Kelley, P. L., Lax, B., and Tannenwald, P. E. (eds.), (McGraw-Hill Book Company, New York, 1966).
- A-8. Koozekanani, S. H.: "An Excitation Mechanism for the  $A^+$  Laser," Appl. Phys. Let. 11, 3, Aug. 1, 1967.
- A-9. Rudko, R. I.: "Excitation Mechanisms in the Ionized Argon Laser," Ph.D. thesis, Cornell University, 1967.
- A-10. Husain, S. A.: "Resonance-Radiation-Trapping Effects in a Pulsed-Ion Laser," Electronics Let. 4, 12, June 14, 1968.
- A-11. Herziger, G. and W. Seelig: "Berechnung der Besetzungsdichte und Ausgangsleistung von Ionenlasern," Z. Physik 215, 437-465 (1968).

## GENERAL REFERENCES-contd.

- A-12. Smith, A. L. S. and M. H. Dunn: "Time-resolved Spectra of High-current Pulsed Argon Lasers," I.E.E.E. J. of Quantum Electronics, Vol. QE-4, No. 11, Nov. 1968.
- A-13. McWhirter: "Spectral Intensities," Plasma Diagnostic Techniques, Huddleston, R. H. and Leonard, S. L. (eds.), (Academic Press, New York, 1965).
- A-14. Meserve, E.: Private communication, TRW Systems, El Segundo, Calif.
- A-15. Griem, H. R.: Plasma Spectroscopy, (McGraw-Hill Book Company, New York, 1964).
- A-16. Drellishak, K. S., D. P. Aeschliman, and A. B. Cambel: "Tables of Thermodynamic Properties of Argon, Nitrogen, and Oxygen Plasmas," Arnold Engineering Development Center, Rept. No. AEDC-TKR-64-12, Jan. 1964.
- A-17. Drellishak, K. S.: "Partition Functions and Thermodynamic Properties of High Temperature Gases," Arnold Engineering Development Center, Rept. No. AEDC-TDR-64-22.
- A-18. Bishop, A. E., and G. D. Edwards: "Electrolytic Resistors in Plasma Physics Research," J. Nucl. Energy 7, part C, p. 423 (1965).

## APPENDIX A.

NASA NGL 31-001-005  
PULSED ELECTROMAGNETIC GAS ACCELERATION

Semi-annual Statement of Expenditures

1 January 1969 - 30 June 1969

Direct Costs

I.	Salaries and Wages		
	A. Professional	\$14,661	
	B. Students	3,603	
	C. Technicians	8,745	
	D. Supporting Staff	<u>6,218</u>	
			\$ 33,227
II.	Employee Benefits (19%)		5,629
III.	Equipment, Materials, and Services		12,668
IV.	Travel	<u>1,207</u>	
	Total Direct Costs		\$ 52,731

Indirect Costs

V.	Overhead (68% of I)	<u>22,594</u>
	Total Costs	\$ <u><u>75,325</u></u>